ELECTROCHEMICAL FORMATION OF Al-Sc ALLOY IN MOLTEN SALT

A THESIS SUBMITTED TO
THE GRADUATE SCHOOL OF NATURAL AND APPLIED SCIENCES
OF
MIDDLE EAST TECHNICAL UNIVERSITY

BY

ÇAĞLAR POLAT

IN PARTIAL FULFILLMENT OF THE REQUIREMENTS
FOR
THE DEGREE OF MASTER OF SCIENCE
IN
METALLURGICAL AND MATERIALS ENGINEERING

SEPTEMBER 2019

Approval of the thesis:

ELECTROCHEMICAL FORMATION OF Al-Sc ALLOY IN MOLTEN SALT

submitted by **ÇAĞLAR POLAT** in partial fulfillment of the requirements for the degree of **Master of Science in Metallurgical and Materials Engineering Department, Middle East Technical University** by,

Prof. Dr. Halil Kalıpçılar
Dean, Graduate School of **Natural and Applied Sciences** _____

Prof. Dr. Cemil Hakan Gür
Head of Department, **Met. and Mat. Eng.** _____

Prof. Dr. İshak Karakaya
Supervisor, **Met .and Mat. Eng., METU** _____

Assist. Prof. Dr. Metehan Erdoğan
Co-Supervisor, **Met. and Mat. Eng., AYBU** _____

Examining Committee Members:

Prof. Dr. Kadri Aydınol
Met. and Mat. Eng., METU _____

Prof. Dr. İshak Karakaya
Met. and Mat. Eng., METU _____

Assist. Prof. Dr. Metehan Erdoğan
Met. and Mat. Eng., AYBU _____

Assist. Prof. Dr. Erkan Konca
Met. and Mat. Eng., Atılım University _____

Assist. Prof. Dr. Batur Ercan
Met. and Mat. Eng., METU _____

Date: 05.09.2019

I hereby declare that all information in this document has been obtained and presented in accordance with academic rules and ethical conduct. I also declare that, as required by these rules and conduct, I have fully cited and referenced all material and results that are not original to this work.

Name, Surname: Çağlar Polat

Signature :

ABSTRACT

ELECTROCHEMICAL FORMATION OF Al-Sc ALLOY IN MOLTEN SALT

Polat, Çağlar
Master of Science, Metallurgical and Materials Engineering
Supervisor: Prof. Dr. İshak Karakaya
Co-Supervisor: Assist. Prof. Dr. Metehan Erdoğan

September 2019, 121 pages

Al-Sc alloys have better mechanical properties in comparison to commercial aluminum alloys. The aim was to produce Al-Sc alloys containing at least 2wt % scandium by electrochemical reduction of the byproducts such as ScF_3 or the alternative compounds obtained from hydrometallurgical processing of low grade lateritic nickel in this thesis.

Electrochemical production of Al-Sc alloy in pure molten $CaCl_2$ and $CaCl_2$-NaCl mixtures was studied for this purpose. The graphite-liquid aluminum-$CaCl_2$ or $CaCl_2$-NaCl interaction, the effect of voltage and duration of the electrolysis on Sc recovery rate, the coalescence behavior of the electrolytic Al-Sc alloy in molten $CaCl_2$ and $CaCl_2$-NaCl mixtures, the effect of CaO left from the dehydration process on the purity of Al-Sc alloy and the effect of NaCl addition into the electrolyte were investigated. In addition, solubility behavior of ScF_3 in pure molten $CaCl_2$ and $CaCl_2$-NaCl mixtures and utilization of different cathode materials and ceramic membranes were examined.

According to the results of the optical microscopy, SEM-EDS and XRD analyses, Al-Sc alloys were produced successfully by electrochemical reduction of domestic scandium bearing powder containing ScF_3, $NaScF_4$ and Na_3ScF_6 phases. Alloying in-

situ with liquid aluminum in both molten $CaCl_2$ and $CaCl_2$-NaCl salt mixtures with molten salt electrolysis method was possible.

Keywords: Lateritic Nickel Ore, Al-Sc Alloy, Electrochemical Reduction, Molten Salt, Electrolysis

ÖZ

ERİMİŞ TUZ İÇERİSİNDE ELEKTROKİMYASAL YÖNTEMLE Al-Sc ALAŞIMI OLUŞTURULMASI

Polat, Çağlar
Yüksek Lisans, Metalurji ve Malzeme Mühendisliği
Tez Danışmanı: Prof. Dr. İshak Karakaya
Ortak Tez Danışmanı: Dr. Öğr. Üyesi Metehan Erdoğan

Eylül 2019, 121 sayfa

Al-Sc alaşımları ticari olarak satılan alüminyum alaşımlarına kıyasla daha iyi mekanik özelliklere sahiptir. Bu tez çalışmasında, düşük tenörlü lateritik nikel cevherinin hidrometalurjik işlem sonucu yan ürün olarak elde edilen ScF_3 veya alternatif bileşikleri, elektrokimyasal olarak indirgeyip ağırlıkça en az %2 skandiyum içeren Al-Sc alaşımları üretilmesi hedeflenmiştir.

Bu amaçla, Al-Sc alaşımlarının elektrokimyasal üretimi saf $CaCl_2$ ve $CaCl_2$-NaCl karışımları içerisinde çalışılmıştır. Bu çalışmalarda, grafit-sıvı alüminyum- $CaCl_2$ veya $CaCl_2$-NaCl etkileşimi, voltaj ve elektroliz süresinin Sc kazanım oranına etkisi, elektrolitik Al-Sc alaşımlarının $CaCl_2$ ve $CaCl_2$-NaCl karışımları içindeki birleşme davranışları, su giderme işleminden kalan CaO'in Al-Sc alaşımının saflığına etkisi ve elektrolite eklenen NaCl'nin etkisi araştırılmıştır. Bunlara ek olarak, ScF_3'ün $CaCl_2$ ve $CaCl_2$-NaCl karışımlarındaki çözünürlük davranışları ve farklı katot malzemeleri ve seramik membran kullanımı üzerinde durulmuştur.

Optik mikroskop, SEM-EDS ve XRD analizlerinin sonuçlarına göre Al-Sc alaşımları, saf $CaCl_2$ ve $CaCl_2$-NaCl tuz karışımları içerisinde, erimiş tuz elektrolizi yöntemiyle, ScF_3, $NaScF_4$ ve Na_3ScF_6 fazlarını içeren yerli skandiyum tozunun elektrokimyasal olarak indirgenip sıvı alüminyumla yerinde alaşımlanarak başarıyla üretilmiştir

Anahtar Kelimeler: Lateritik Nikel Cevheri, Al-Sc Alaşımı, Elektrokimyasal İndirgeme, Erimiş Tuz, Elektroliz

To My Family

ACKNOWLEDGMENTS

First and foremost, I would like to extend my deepest gratitude to my advisor Prof. Dr. İshak Karakaya for his support, guidance, constant encouragement and patience during my thesis work. I would also want to thank my co-advisor Assist. Prof. Dr. Metehan Erdoğan for his motivation, support and valuable discussions and suggestions during and after my thesis writing process.

I would like to express my sincere thanks to Prof. Dr. Naci Sevinç, Assist. Prof. Dr. Kazım Tur and Assist. Prof. Dr. Erkan Konca for their valuable contribution during my undergraduate studies and in terms of my professional progress, also for making me like my major.

I would like to thank the technicians of our department, Atalay Özdemir and Cemal Yanardağ for helping me benefit from the machine shop facilities and their technical support, Serkan Yılmaz, Nilüfer Özel and Yusuf Yıldırım for their support in materials characterization

I would like to thank my former and current lab mates, especially, Mustafa Serdal Aras, Bilgehan Çetinöz, Olgun Yılmaz, Rauf Aksu, Uğurhan Demirci, Berkay Çağan, Esra Karakaya and Atalay Balta for their friendship and support.

Lastly, to my family who raised me to be who I am today and provided constant support all my life and always standed by my side for all, thank you Mom, Dad and my big sister a million for your love, understanding, patience and trust. To my sister in particular, thank you so much for your diligance and endless help all my life and for always thinking the best for me even better than myself. I could not have completed this thesis study without you.

This work was financially supported by the Scientific Research Projects (BAP) with project number of YLT-308-2018-3537 and MİNERTEK company.

TABLE OF CONTENTS

LIST OF TABLES

TABLES

LIST OF FIGURES

FIGURES

CHAPTER 1

INTRODUCTION

1.1. The Rare Earth Elements

In the periodic table, there is an element group involving of 15 elements. These elements, called as the lanthanides, have atomic numbers that differ from 57 up to 71. These 15 lanthanides along with scandium and yttrium (atomic numbers of 21 and 39, respectively) constitute a new set of elements known as the rare earths (RE) or the rare earth elements (REE) [1]. Since scandium and yttrium have three valence electrons as the lanthanides, they have similar electron configuration which leads Sc and Y to be chemically coherent with the lanthanides. Thus, these two elements are also accepted as the rare earth elements. Due to having similar chemical properties, rare earth elements have tendency to occur within the same ore body which makes the extraction or separation of individual rare earth element tedious [2].

The term ‘rare’ may be misleading as the abundancy of REE is considered. When the crustal abundance of rare earth elements is compared with the well-known metals like silver, gold, copper, lead and tin, most of REE is more abundant than especially the precious metals such as Au and Ag [1] as shown in Figure 1.1.

REE have astonishing properties due to their unique electron configuration. Therefore, they turn out to be an important part of the high technology and are used in various applications such as strong magnets, rechargeable batteries, automobile exhaust catalysts, reinforcement agent for optical materials [3].

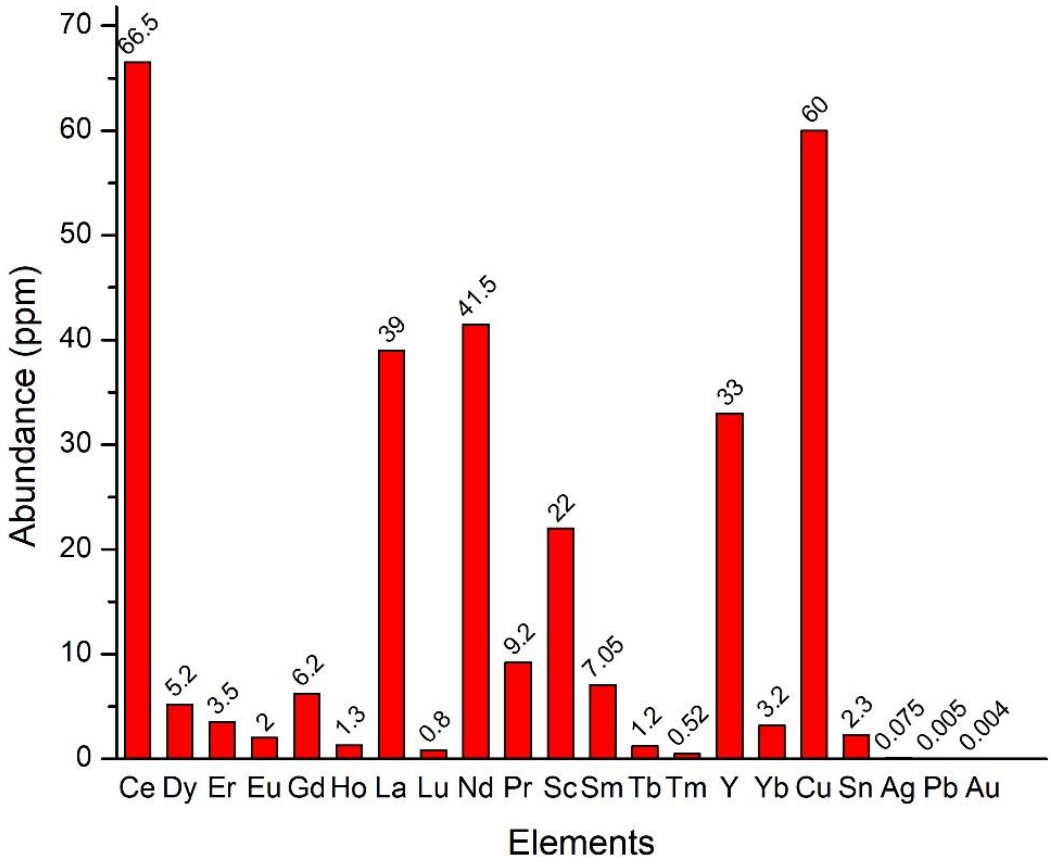

Figure 1.1. The comparison of abundancy of REE in the earth crust with well-known metals [1]

The integration of the high technology in industry has recently been causing an increase in the demand towards REE. In order to balance this need, the global production of REE has needed to increase. From 1990 until now, China is the world REE production leader and controls the supply-demand balance of REE mining [4]. The world REE mine production of the last decade is plotted in Figure 1.2 with the help of the data collected from the annually published 'USGS Mineral Commodity Summaries' [5–14]. Although China is the leader REE producer, there are other countries supplying REE such as Australia, USA, India, Russia, Thailand, Brazil, Malaysia, Vietnam which have also convenient geological conditions for REE mining.

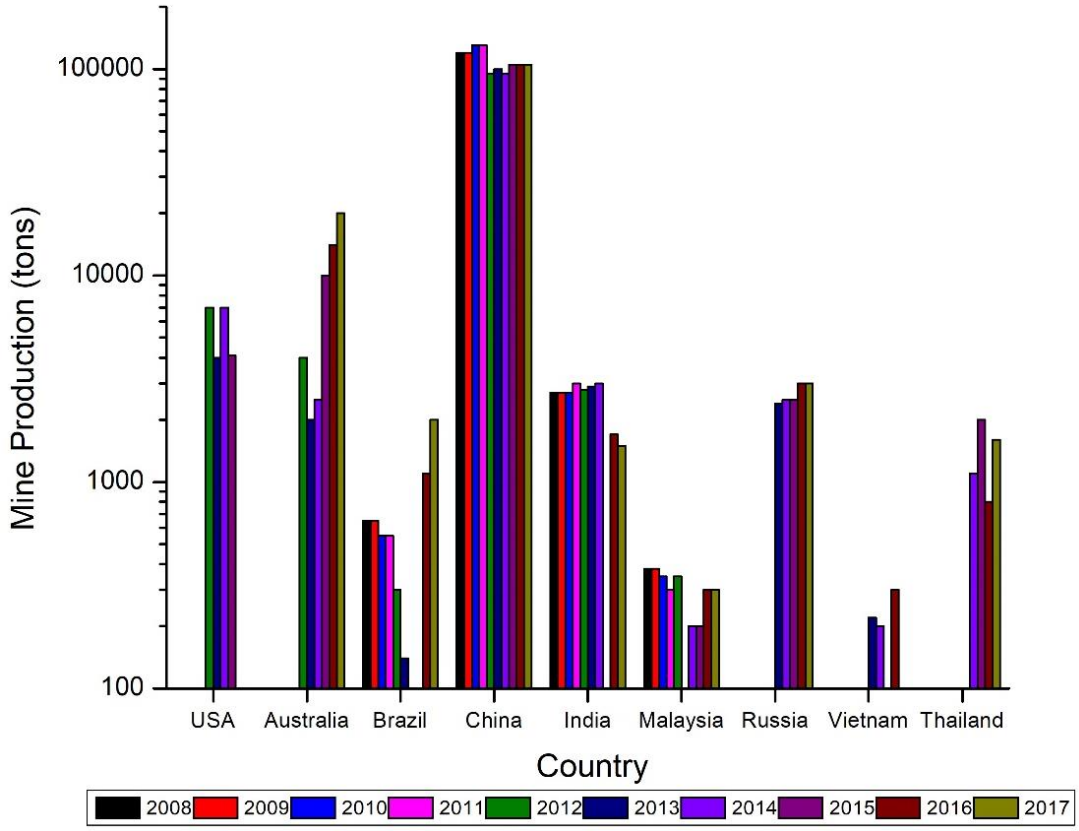

Figure 1.2. The rare earths mine production of major countries in the last decade [5–14]

1.2. Fundamentals and Historical Development of Scandium

Scandium (Sc) is a chemical element placed between Ca and Ti in the periodic table. It has a silvery- white color and is in the form of hexagonal crystal structure. It is the first and the lightest member of transition metals and is also a member of the rare earth elements. It has a melting point (i.e. 1541^{o}C) as high as iron's and a low density like aluminum (i.e. 3 g/cm^{3}) [1]. The combination of a high melting point and a low density makes Sc an attractive element for various applications.

The element scandium was firstly named as ekaboron according to the study of Mendeleev on the periodic table of elements. Mendeleev also used the eka- prefix for some other elements as prototype names with the discovered elements like ekaaluminum, ekasilicon etc. [15]. Subsequent to the publication of his study in 1869,

the missing elements in the periodic table were studied by other scientists. In 1879, a Swedish Chemist, Lars Fredrik Nilson successfully isolated a new rare earth element from gadolinite and euxenite minerals. From these minerals, he obtained a concentrate of 63 g having subject these minerals to subsequent processes. By fractionation and precipitation of the concentrate, 0.35 g of a new element was extracted. However, the amount of the new element prevented Nilson from performing a detailed chemical characterization. In the same year, a researcher called Tobias Robert Thalen conducted a study on spectral analysis of the new element to support the Nilson's work [16]. After Thalen's study, the results of the new element were published in Swedish, German and French Journals [17–19]. Nilson named this new element " scandium " in the honor of Scandinavia where scandium was extracted. Per Theodor Cleve was another scientist who made a contribution to the scandium in 1879. He extracted 1.2 g of scandium oxide from 3 kg keilhauite. Furthermore, he synthesized several compounds of scandium to compare the ekaboron [20]. In 1880, Nilson succeeded in extracting a few grams of high purity scandium oxide from 10 kg euxenite. He calculated the valence number and atomic weight of scandium and supported Cleve's study. In the end, he concluded that scandium and ekaboron represent the same rare earth element [21]. After the studies of Nilson and Cleve on the discovery of scandium, Sir William Crookes (1908-1910) conducted a detailed study for the complete characterization of scandium. He prepared several different compounds of scandium and analyzed each of them by spectroscopic method. He also examined almost all of the attainable rare earth minerals to find their scandium content and he found that some of the rare earth minerals including wiikite (found in Finland) contained considerable amount of scandium [22–24].

In addition to the studies of Crookes (1908-1910), Eberhard (1908) [25] and Fowler (1909) [26], Artini's (1915) [27] spectroscopic studies indicated that there were over eight hundred different minerals containing scandium. In 1908, R.J. Meyer showed that Scandia (Sc_2O_3) could be extracted from wolframite mineral, which is an important tungsten ore, and he then patented this study [28]. In the following years,

Schetelig (1911) defined the first scandium mineral, thortveitite, which was discovered by Thortveit [29].

In 1937, Fischer and his co-workers produced metallic scandium with a purity of 95% for the first time by electrochemically reduced eutectic KCl-LiCl-$ScCl_3$ melt at temperatures gradually increasing from 700 to 800^{o}C [30]. This was the earliest and the only study focusing on the electrochemical production of Sc from scandium compounds.

The following studies related to the production of Sc was focused on the pyrochemical route (a metal production technique involving the reduction of metal compound with a metallic element at considerably high operating temperatures) in which a suitable metallic reducing agent was used to reduce scandium bearing compound. For instance, in the same year with the study of Fischer et.al., a comprehensive study was done to develop a method to produce rare earth metals which would allow to reveal the important physical properties such as crystal structure and density. This process was as such that the anhydrous rare earth alkali chlorides were reduced with alkali metals (K, Rb, Cs). Then a mixture of metallic rare earth and alkali metal chlorides in the powder form was obtained. The resultant mixture was then analyzed further to reveal the abovementioned properties of the rare earths which were based on the assumptions made by the inventors [31].

In 1941, the method developed by Klemm and Bommer was applied to $ScCl_3$ by choosing potassium as the alkali metal reducing agent. As a result of this study, the crystal structure of scandium was clarified and determined as hexagonal closed packed [32].

Alternative studies were conducted to produce high purity metallic scandium in bulk form. In 1956, Iya conducted several experiments to reduce chloride of scandium by Mg and Ca (with Zn as the flux). Mg-Sc and Zn-Sc alloys were obtained at the end. The alloys were then subjected to vacuum distillation to remove Mg and Zn and to obtain bulk scandium having purity above 99% [33].

In the same year with the study of Iya, the first metallic scandium in compact form was successfully produced by reduction of the halide compounds of scandium ($ScCl_3$ and ScF_3) with Ca by Petru et.al. The resultant alloy was distilled under vacuum to obtain high purity scandium [34,35].

As a result of the study of Petru et.al., the metallic scandium obtained after vacuum distillation had a high purity. However, it was not confirmed by a chemical analysis and they did not characterize the scandium product to investigate its properties. In 1960, researchers from Ames Laboratory, whose group leader was Frank Harold Spedding, carried out the most detailed study on the preparation of high purity metallic scandium and the determination of its properties properly which were uncertain due to lack of characterization. In this study, Sc was prepared with two methods. The first one was the calcitothermic reduction of ScF_3 with the addition of Zn and Li in order to obtain a low melting point metal (Sc-Zn) and slag (CaF_2-LiF) mixture. After that the scandium alloy (Sc-60%Zn-1-2%Ca) was subjected to vacuum refining to remove volatile species and obtained a sponge scandium with 90 % yield. In the second method, scandium fluoride was only reduced with calcium and then subjected to firstly to vacuum melting to remove Ca and then to vacuum distillation for further purification. A purer metallic scandium was obtained with a 95% of process efficiency as compared with the first method. After the synthesis of high purity scandium, the product was analyzed and characterized in detail and the melting and boiling points, lattice constant, electrical resistivity etc. were determined [36]. In the same year, the binary and ternary alloys of scandium were started to be investigated and collected in a book written by Gschneidner [37]. In 1973, Spedding and Croat were succeeded to prepare 99.9% pure metallic scandium by comparing the magnetic susceptibilities of pure scandium and scandium containing impurities in the ppm level [38]. In 1998, an extensive systematic study was published focused on the binary and ternary alloys of scandium, the intermetallic compounds and crystal chemistry and topology of these compounds. It was concluded that 65 out of 97 possible Sc binary systems and 200 Sc ternary systems were known [39].

1.3. Extraction of Scandium

Due to having similar electronic configuration, all rare earth elements (including Sc and Y) have identical chemical characteristics. Thus, they are found in nature as complex compounds. For the case of scandium, it does not have the ability to form a mineral due to its low affinity to mineral forming anions. It is widely spread over the lithosphere and is found in more than a hundred minerals which makes the concentration of scandium from these minerals challenging and costly [40]. As reported in the 'Mineral Commodity Summaries 2018', 10-15 tons of scandium are produced annually in worldwide and the major global scandium mining countries are Australia, China, Kazakhstan, Russia and Ukraine [14].

There are a few ore minerals containing considerable amount of scandium. These are thortveitite ($Sc_2Si_2O_7$), bazzite ($Be_2Sc_2Si_6O_{18}$), kolbeckite ($ScPO_4.2H_2O$), Sc-Ixiolite (Ta, Nb, Sn, Mn, Fe, Sc….)$_2O_4$, Sc-perrierite (Ce, La, Ca)$_4$(Fe^{2+}, Sc) (Ti, Fe^{3+})$_2Ti_2[O_4|Si_2O_7]_2$, Magbasite (K, Ba(Al, Sc)$Fe^{2+}Mg_5F_2Si_6O_{20}$) [40]. Since the minerals listed above are scarce in nature, scandium is commonly extracted or recovered in the form of Sc_2O_3 from the tailings, residues, waste liquors, slags which are obtained as a by-product after processing of ores of primarily uranium, tungsten, zirconium, titanium, tin, tantalum, thorium, aluminum [41].

Due to its unique properties (i.e. low density, high melting point, formation of stable compounds), there is an increase in the demand for scandium, especially, in the aerospace industry (i.e. Al-Sc, Al-Mg-Sc and Al-Mg-Sc-Zr alloys), battery industry (i.e. solid oxide fuel cells), electronic industry (i.e. lasers, lightning). There is a need for a long term, reliable Sc resource to fulfill this demand [14].

Recently, several projects such as EURARE [42], REDMUD [43], SCALE [44] financially supported by EU, were carried out for extraction and recycling of scandium efficiently from the ore, waste or residue present in the EU countries having potential deposits by utilizing hydrometallurgical techniques. REDMUD (which takes its name from the waste formed after hydrometallurgical treatment of alumina), among the

projects listed above, seems to be the most promising one since the world average red mud production each year is estimated to be 140 million tons and red mud may contain 50 to 150 ppm Sc in the form of Sc_2O_3 which makes up roughly 7,300 tons of scandium each year with 80 % yield and average 100 ppm Sc concentration [43].

Another important Sc resource besides red mud is the lateritic nickel ores which constitute 70% of world nickel reserves [14]. Although processing of lateritic nickel ores is more laborious in comparison to that of nickel sulphide ores (the remaining 30% of nickel reserves), it is expected that mining of lateritic nickel ores will compensate the decrease in sulphide reserves and help meet the world nickel demand [45]. The studies conducted starting from 1990s showed that lateritic nickel ores have a big potential for scandium extraction [46,47]. The Sc grade of the ores changes depending on the mineralogical and geochemical nature. Although it is found in trace amount in lateritic nickel ores, Sc can be extracted successfully by high pressure acid leaching with a yield of greater than 90%. Two processes were suggested to extract Sc from lateritic nickel ores: metal sulfide precipitation (MSP) and metal hydroxide precipitation (MHP). In MSP method, scandium is extracted by solvent extraction or ion exchange by removing Ni and Co present in the ore by transforming them into Ni-Co sulphide precipitation. In MHP method, scandium is recovered as hydroxide compound containing impurities before removing Ni and Co in the form of hydroxide. Then, the impure scandium hydroxide precipitate is subjected to re-leaching and solvent extraction or ion exchange techniques for further purification [48].

In Turkey, there is a Ni-Co mining company (META Nickel-Cobalt Company) which has a MHP HPAL (high pressure acid leaching) plant located near nickel reserves in Gördes, Manisa which is close to Çaldağ site. Önal and Topkaya conducted a research study based on the ore sample taken from the Çaldağ site to investigate the possibility of scandium extraction from a domestic resource. They investigated the applicability of HPAL technique for lateritic nickel ore and reported that scandium could be extracted as a by-product with a considerable yield with this technique [49]. As a result of the hydrometallurgical operation of the low grade lateritic nickel ore in Çaldağ site,

several different types of fluoride containing scandium compounds in uncalcined form (with NH_4) as seen in Figure 1.3 [50] and calcined form with (e.g. Na_3ScF_6) or without Na element (ScF_3) could be produced. This proves to be a significant advantage over the companies producing Sc_2O_3 from the same type ore since Sc_2O_3 is a very stable compound and is subjected to high temperature fluorination process to obtain a relatively less stable ScF_3 and to produce Sc or alloys of Sc.

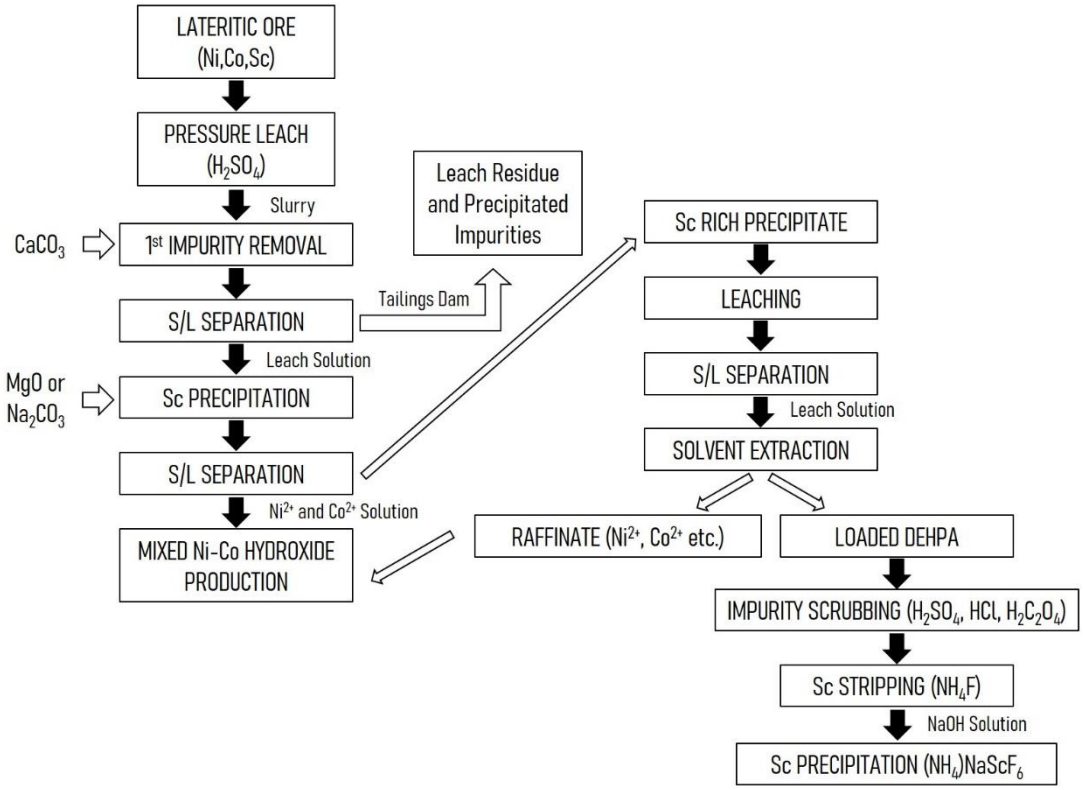

Figure 1.3. Flowsheet of Sc recovery from a lateritic nickel ore [50]

1.4. Scandium as an Alloying Constituent

Due to being both a rare earth element and a transition metal, scandium has a combination of properties such as low density, high melting point and forms chemically stable intermetallics. These make scandium an attractive candidate metal

for several applications especially aerospace and defense industry where light weight and durable materials against different weather conditions are required. In these industries, aluminum alloys are used commonly because of their light weight and formation of stable intermetallics which improve mechanical properties considerably.

The common alloying elements in aluminum alloys are Si, Cu, Mg, Zn. Except from these elements, transition metals (TMs) including Sc are also used as alloying additives which have limited solid solubility in aluminum and form stable trialuminides (in supersaturated solid solution) that improve the properties of aluminum alloys [51]. In 1971, Willey reported that alloying pure aluminum and aluminum alloys (2XXX, 5XXX, 6XXX and 7XXX) with scandium in the range between 0.1 and 1% resulted in improved mechanical properties. Table 1.1 shows the change in the tensile strength and yield strength of the different grade of aluminum alloys upon addition of small amount of scandium. The effect of scandium addition reaches to a greater extent together with mechanical deformation and aging process [52].

Table 1.1. *Effect of scandium addition on mechanical properties of aluminum alloys* [52]

Grade of Aluminum	*Sc addition (wt%)*	*Tensile Strength (MPa)*	*Yield Strength (MPa)*	*Condition of the Alloy*
99.99% Al	0	39.3	20	As Cast
	0.38	72.4	36	
	0	48	15	Aged
	0.38	220	199	
	0	49	14.4	Cold rolled and aged
	0.38	264	240	
	0	34	7.58	Cold rolled, heat treated, water quenched and aged
	0.38	199	199	
Al-1wt%Si	0	159	145	Cold rolled, reheated and cold rolled
	0.3	253	229	
Al-7wt%Zn	0	171	157	Cold rolled, reheated and cold rolled
	0.3	290	278	

The underlying reason of making such an influence on the mechanical properties of Al or Al alloys is related with the formation of Al_3Sc intermetallics which have its unique physical properties such as crystal structure, distribution density, morphology (faceted, globular, script etc.) in comparison to other trialuminides of Al-TM [53,54].

In 1991, a significant development in high strength structural alloys was arose. According to this development, aluminum alloys containing mainly Sc and Zr could be used as a filler material for welding of structural aluminum alloys without hot cracking [55]. In addition to this advance, AlMgSc alloy with small Zr addition was developed to be used as a sheet metal for frames and fuselage parts of an aircraft which could be welded, corrosion resistant and mechanically durable by AIRBUS [56]. This invention would change the nature of joining of structural sheet metals, which was normally riveted to each other due to especially fatigue and corrosion.

1.5. Aim of the Present Study

As stated in the previous sections, Al-Sc alloys is thought to change the future of high strength structural alloys due to the superior properties by the effect of Al_3Sc intermetallics in especially aerospace industry where high performance structural alloys are used. However, the lack of long term, reliable Sc supply is a problematic issue.

Currently, scandium is extracted hydrometallurgically from the tailings and residues of the Sc bearing ores of U, Ta, W, Al, Ti. In addition to these, the production method of nickel has changed from pyrometallurgical to hydrometallurgical and the lateritic nickel ore, which constitutes 70% of world nickel reserves, was started to exploit. The latest researches have indicated that Sc can be recovered as a by-product with nearly 95% yield from the lateritic nickel ores.

In the present study, electrochemical reduction of the domestic scandium product in the form of fluoride extracted from Turkish nickel - cobalt reserve in Gördes, Manisa near Çaldağ site by HPAL in molten $CaCl_2$ and $CaCl_2$-NaCl mixtures and in-situ alloying with liquid aluminum was aimed. The possibility of production of Al-Sc alloy

by using domestic Sc raw material with an environmentally friendly molten salt electrolysis method was investigated in lab-scale electrolysis studies.

CHAPTER 2

LITERATURE REVIEW

2.1. The Importance of Electrical Power in Metal Production

Metals constitute an important part of the daily life. They have a wide variety of application areas such as automotive industry, construction, electrical and electronics industry, aerospace and defense industry. Therefore, the production volume of the metals is quite high and the cost-profit balance of the metal production becomes a critical issue.

The production method of a metal depends on the form of metal in the earth crust. Most metals occur in nature as minerals containing the value metal itself as well as several other elements that form the invaluable part (gangue). For example, the well-known ore mineral for scandium metal is thortveitite ($Sc_2Si_2O_7$). As seen from the chemical formula, Si and O are present in this mineral as impurities and they form a silicate compound. This applies to other metals as well. Therefore, mineral compounds should be decomposed and separated from the impurity part of the ores to obtain the value metal. The amount of the value metal in an ore (tenor) should have a certain value, which needs to be above the crustal abundance of the metal to be produced, for economic processing. The parameters that determine the cost of metal processing can be listed as mining, transportation, labor, fuel cost, electricity cost and the market conditions.

The quality of a metal depends on the application. The most fundamental quality parameter of a metal is its chemical composition. In some cases, the impurity elements in the ore minerals can be tolerated in the final metal product. For example, zinc reduced by carbothermic reduction may contain As and Pb and can be used for

galvanizing. On the other hand, zinc used in special alloys should be as pure as possible; thus, it is electrolytically refined [57] .

In extractive metallurgy, there are three main methods of metal processing: pyrometallurgical, hydrometallurgical and electrometallurgical. According to the ore mineralogy and quality requirements, one method or combination of the two or more methods can be applied. Majority of the metals and alloys are produced by pyrometallurgical method where either carbon, a reducing gas or an active metal is used as the reducing agent. However, this is a high temperature and energy intensive process and it produces CO_2 that has a direct effect on global warming. Hydrometallurgical treatment is based on the aqueous medium (solution of ore mineral and the related solvents). It is generally preferred for the physical or chemical separation of gangue from value metal compound in an ore mineral to obtain a concentrated metal solution and precipitate of the metal compound. Thus, it can be generally accepted as an intermediate process.

When it comes to the high temperature metal extraction process, excluding the hydrometallurgical process, a need for an energy efficient metal production method arises. Electricity (electrons) seems to be an alternative energy source in the metal production. It plays an important role in terms of high process yield and energy consumption in the metal production process, especially of steel and aluminum, which are produced in large tonnages [58,59]. As seen in Figure 2.1, starting from the invention of battery (voltaic pile) by Alessandro Volta and subsequent to the advances in the electricity generation and conversion, the electricity gets more and more available [58].

After Volta, chemists such as H. Davy came up with a battery the poles of which were immersed in water. Then they observed the hydrogen and oxygen evolution from the materials, which would later be named as electrodes by Faraday, having an opposite polarity. Then H. Davy (1807) paved the way for another important development. It

is the isolation of elements like Na, K, Mg from their molten salts by electrolysis in which chemical reactions take place as a result of the applied current [60,61].

In addition to all these findings, Michael Faraday stated after his long-term experimental studies on the relationship between the electricity and the decomposition of metal compounds (during 1930-1940) that the mass of electrolysis product was proportional to the electrical charge passing through the electrochemical cell according to the Faraday's Law of Electrolysis [62]. It was for the first time that metals could be extracted by electrochemical reduction of their compounds in molten state.

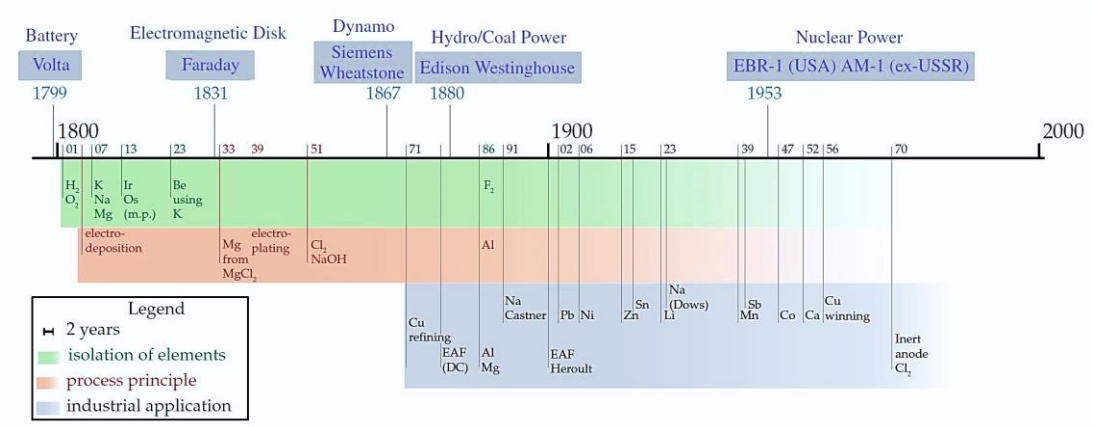

Figure 2.1. Timeline of Advances in Electricity Generation and Its Contribution to the Metal Industry [58]

In 1886, two scientists Hall [63] and Héroult [64], each separately announced that they successfully obtained aluminum as a result of the electrolysis of cryolite melt containing dissolved alumina (Hall-Héroult process). This crucial process in metallurgical industry is called as fused or molten salt electrolysis. Although 0.45 kg carbon/ kg aluminum is consumed and CO and CO_2 is produced, the extraction of aluminum with this process is the only commercially feasible way. In addition to aluminum production, magnesium is also produced heavily by molten salt electrolysis (i.e. Dow and I.G. Farben) [65].

Apart from these two applications, there is also a recently adopted electrochemical production technique which has been studied since 1990's. This technique aims to produce metals or alloys directly by electrochemical reduction of the related metal oxides, which are the most common form of the metals in nature, in molten salts preferentially alkali or alkaline earth chloride salts. The name of this specific technique is FFC Cambridge Process and it was originated from the first letters of the last names of the inventors from Cambridge University. The first element produced lab-scale by this technique was titanium. However, there are also other metals produced by electrodeoxidation such as Nb [66], Zr [67], Cr [68], Ta [69],W [70], Si [71]. It should be noted that during electrodeoxidation of metal oxides, only the anionic species are removed and the cationic impurities present in the metal oxides will end up with the cathodic product. However, this can be turned into advantage to produce alloys by reducing the mixtures of the selected metal oxides. Nb-Ti, Nb-Sn [72], Ti-W [73], Fe-Ti [74], Mg-Ni [75] and Al-Sc [76] alloys can be given as examples of the alloys produced by electrodeoxidation.

2.2. The Choice of Production Method for Al-Sc Alloy

Al-Sc alloys have recently become very attractive and popular due to their excellent properties upon addition of small amount of scandium to pure aluminum or aluminum alloys (e.g. Al-Si, Al-Mg-Si, Al-Li). The combination of featured properties such as low density, hot cracking resistance, specific strength, corrosion resistance and recrystallization resistance makes Al-Sc alloys a new candidate material for several industrial areas from sporting goods to transportation industries where lightweight and structural durability are two important material selection parameters [77]. However, the laborious extraction process of scandium and scarcity of high grade scandium ore minerals such as thortveitite limit the production volume and increase the price of metallic scandium which in turn affect the cost of Al-Sc alloys.

The choice of production method of Al-Sc alloys is critical due to the situation of Sc supply. As the starting material for scandium gets purer, the cost of Al-Sc alloy production increases due to the additional cost coming from purification of Sc. Thus, the starting material for Sc is generally preferred as the Sc compounds (e.g. Sc_2O_3, ScF_3, $ScCl_3$). Due to strong affinity to the oxygen as seen in Figure 2.2., scandium sources are extracted in the form of scandium oxides.

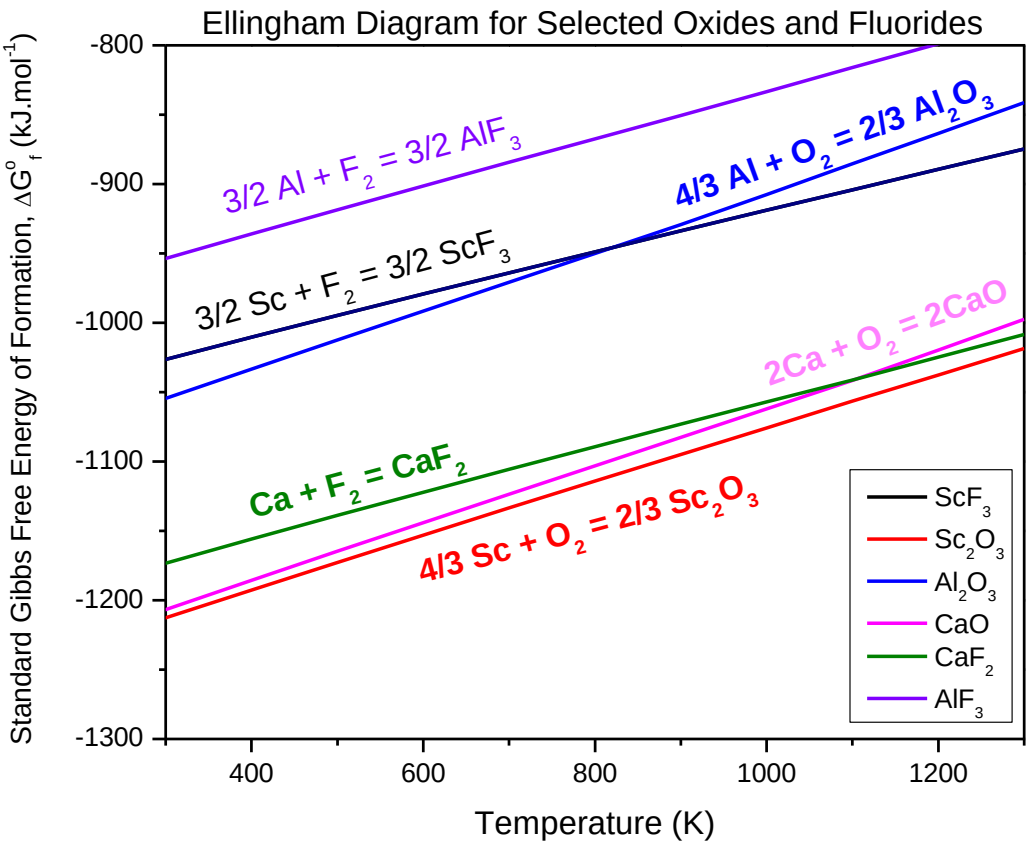

Figure 2.2. Ellingham Diagram for Selected Oxides and Fluorides [78]

Thus, the reduction of its oxide by most commonly used reducing agent carbon and some of the active metals (e.g. Mg, Ca, Na) becomes difficult. Hence, Sc_2O_3 is converted into either ScF_3 or $ScCl_3$ by using suitable compounds. Since the

hygroscopic nature of chloride compounds makes handling and processing difficult, relatively less stable ScF_3 is preferred most of the time as a starting material for scandium in Al-Sc alloy production [79].

There are fundamentally three ways to produce Al-Sc alloys; casting by using metallic Al and Sc, metallothermic reduction with a suitable reducing agent and electrochemical reduction of scandium bearing compounds within a suitable molten salt medium. In all three methods, the aim is to introduce Sc as an alloying element into the aluminum matrix to obtain Al-Sc alloy containing Al_3Sc intermetallics.

2.2.1. Casting

Casting is the most commonly utilized metal or alloy formation method in metallurgical industry. The mechanism in this method is simply melting the matrix metal and adding the alloying element, whose melting point is most of the time higher than the matrix metal, in the solid form (ingot, briquette, powder) that will dissolve and diffuse in the molten metal. After solidification, the desired alloy is obtained.

For the case of Al-Sc alloy, the same procedure is applicable. However, this processing method requires raw materials in metallic state. Also, chemically inert containers and controlled atmosphere due to reactive nature of scandium are required.

2.2.2. Metallothermic Reduction

This method is a high temperature metal production method in which a metal compound is reduced with an active metal reductant and a liquid metal/slag mixture is obtained at the end of the process. Having obtained the metal/slag mixture, the slag is removed from the metallic part and the metal is subjected to a purification processes.

In literature, there are several studies focused on the Al-Sc production via metallothermic reduction. The studies are divided into two according to the type of Sc compound (either Sc_2O_3 or ScF_3). In both of them, the aim is to somehow introduce high melting point alloying constituent scandium into molten aluminum to enable formation of Al_3Sc intermetallics in a cost effective way.

Although the reduction of Sc_2O_3 with a well-known deoxidizing agents like calcium and aluminum is not thermodynamically favorable, the reduction process becomes favorable when a sufficiently excess amount of reductant is used.

One example to this phenomenon is a patent supported by ALCOA. In this patent, the main metal to be alloyed was used as the reducing agent to form Al-Sc alloy in a direct way. The procedure of this process was as such that a compacted pellet composed of Sc_2O_3 and pure aluminum powder in excess amount was immersed in a molten aluminum bath to give the following reaction;

$$Sc_2O_3\,(s) + 8Al\,(l) = 2Al_3Sc\,(s) + Al_2O_3\,(s) \qquad (2.1)$$

Addition of excess amount of aluminum facilitates the reduction of Sc_2O_3 by decreasing the activity of scandium as a result of the formation of Al_3Sc intermetallics. The decrease in the activity of scandium causes an increase in the slope of the Sc-Sc_2O_3 equilibrium line on the Ellingham diagram whose slope is the function of activity of metal and the metal oxide. Then, the equilibrium lines for Sc-Sc_2O_3 and Al-Al_2O_3 plotted in Figure 2.2 will intersect with each other and the reduction of the Sc_2O_3 becomes thermodynamically feasible.

Due to poor wetting between molten aluminum and the pellet, the dissolution and the chemical reaction were slow. Then, several fluxes or salts such as AlF_3 - KF, NaCl-KCl or AlF_3 – Na_3AlF_6 mixture were used to both improve wetting and percent reduction of Sc_2O_3. Although the kinetics of the process was improved upon addition of flux, it was reported that the reduction efficiency of Sc_2O_3 with flux-salt addition was about 3% while it could be reached 85% efficiency without flux-salt addition [80].

In the study of Harata et.al [81], several experimental studies were carried out to analyze the reduction behavior of Sc_2O_3 with or without the molten aluminum acting as the collector metal. It was found that reduction of Sc_2O_3 was not completed when only Ca was used and $CaSc_2O_4$ was formed. However, when Ca (reducing agent) and Al (collector metal) were used together with Sc_2O_3 as starting material, it was shown

that Al-Sc alloy could be produced with Al_3Sc and Al_4Ca phases. The same result was obtained when ScF_3 was used as the Sc raw material. After each reduction experiment, the metal and the slag phase could not be separated from each other. For this reason, $CaCl_2$ was added into the system to enable the separation and dissolve CaO that occurred as a by-product.

As indicated in the Ellingham diagram given above, it is obvious that direct reduction of ScF_3 with Ca is feasible and does not require addition of flux or salt to make it reducible compound as is the case for Sc_2O_3. Therefore, chemically stable Sc_2O_3 compound is subjected to a high temperature fluorination process with HF in order to obtain a relatively less stable ScF_3 compound. The current production method of metallic scandium is based on this fluorination process and the subsequent reduction with Ca (AMES Process) [36]. Although the fluorination process brings an extra cost to overall metal production process, Al-Sc alloy production by reduction of ScF_3 with Ca and alloying in-situ with molten aluminum is more advantageous.

In the light of findings mentioned above, the first and second methods are the high temperature processes which require high purity starting materials, chemically inert reaction containers and may result with chemical or mechanical losses and contamination due to reducing agents.

However, the electrochemical extraction method does not require a high purity Sc raw material and reducing agent. In this method, the scandium compound will be reduced electrochemically in a suitable molten salt in which electrons act as the reducing agent while molten salt acts as a medium for transportation of the ions present. As a consequence, electrochemical reduction offers more advantages in comparison to other production methods.

2.3. Electrochemical Extraction

This method is basically the conversion of metal compounds into the metals or alloys by electrochemical processing. The energy required to drive the chemical reaction is

supplied by electricity. There are two electrochemical processes depending on the type of the used electrolyte: aqueous and molten salt electrolysis.

Aqueous electrolysis is not usually a feasible process for the metal extraction as most of the metals have electrode potentials more negative than that of hydrogen since it will evolve before extraction of metals and inhibit the extraction process. Therefore, a need for an alternative electrolyte arises for metal production. Molten salts fulfill this need as electrolyte material which have high ionic and electrical conductivity, thermal stability, low viscosity and high diffusivity. In addition to these features, another important property of molten salts is its ability to dissolve the metal compounds (e.g. oxides, sulfides). When molten salts are used as the electrolyte, the decomposition voltage of the salts must be greater than that of metal compound. Molten salts such as alkali or alkaline earth halide salts have considerably high decomposition potentials as shown in Figure 2.3 [82].

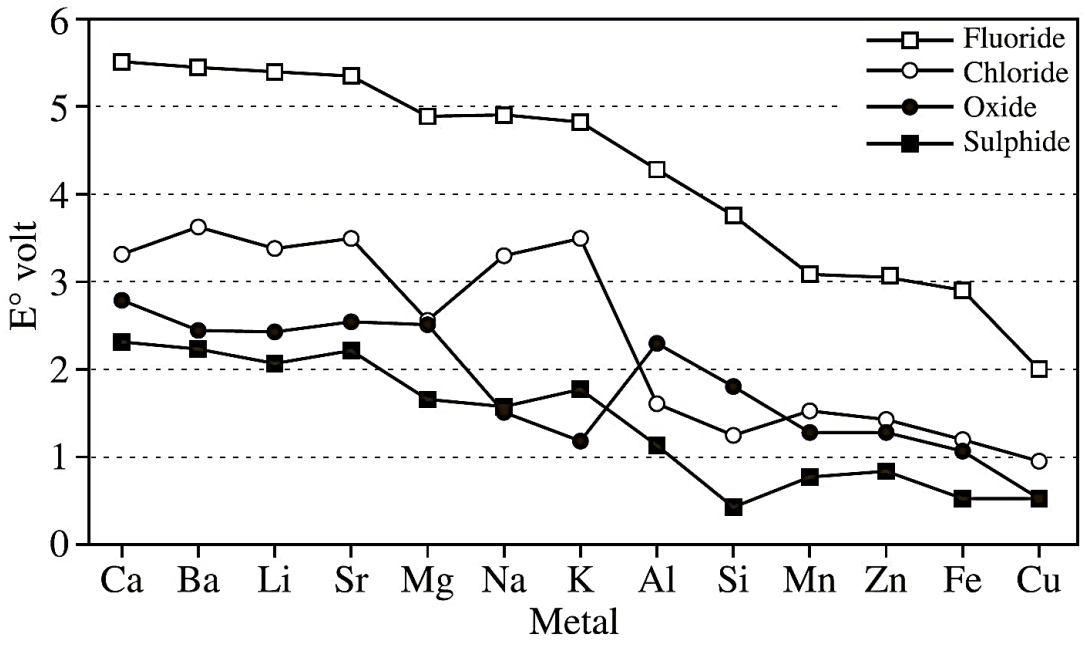

Figure 2.3. Decomposition voltages of metal compounds at 1000K [82]

With regard to the metal extraction from naturally occurring source (ore minerals) in a direct way, the thermodynamically nonspontaneous reaction given below would take place. In order for this reaction to proceed in the written direction, energy should be supplied and to supply the required energy, electrolytic cell should be used. (i.e. From the case of $\Delta G>0$, to the case of $\Delta G<0$) [83].

$$M_cX_d\,(s) = c\,M(s \text{ or } l) + d/2\,X_2\,(g) \quad \Delta G>0 \qquad \text{where X : O, F, Cl} \qquad (2.2)$$

As understood from the above case, the metal extraction process can be conducted with electrolytic cell. Most of the industrial applications in metallurgy like electrodeposition, electrorefining, electrowinning and molten salt electrolysis are the processes carried out by electrolytic cells.

For the electrochemical extraction of metal compounds via utilization of an electrolytic cell, an electrolyte containing ionic species, a pair of electrodes which are electronically conducting materials as anode and cathode, reaction container to hold electrolyte and a power source are necessary. Upon applying the voltage, the electrons flow externally through the cell while the ions present in the electrolyte carry the electrical current in the electrolyte. The negative ions move towards the positive electrode (anode) which donates electron whereas the negatively polarized electrode (cathode) being electron acceptor attracts the positively charged ions as shown in Figure 2.4.

Since the aim is to remove the impurity elements present in the metal compound and obtain pure metal at the end, these elements from the compound should somehow electrochemically be removed. There are two main electrochemical extraction methods. If the melting point of the metal to be extracted electrochemically is less than that of its compound like aluminum and aluminum oxide, then molten salt electrolysis will become a suitable choice as a first method. In this method, the metal compound is dissolved in a suitable molten salt or mixture and forms an ion pair of positive metal ion (cation) and negative impurity element's ion (anion) in the electrolyte. The metal

ions move toward to the cathode and form the pure molten metal while the anions are discharged at the surface of the anode and leave the system in the gaseous state. The second electrochemical extraction method, on the other hand, is the FFC Cambridge or electrodeoxidation process. This method is especially useful for the extraction of high melting temperature metals (W, Si, Ti, Cr, Zr) in a direct way in molten alkali and alkaline earth chloride salts which means that the ore mineral could be directly converted to its metal with or without any subsequent process.

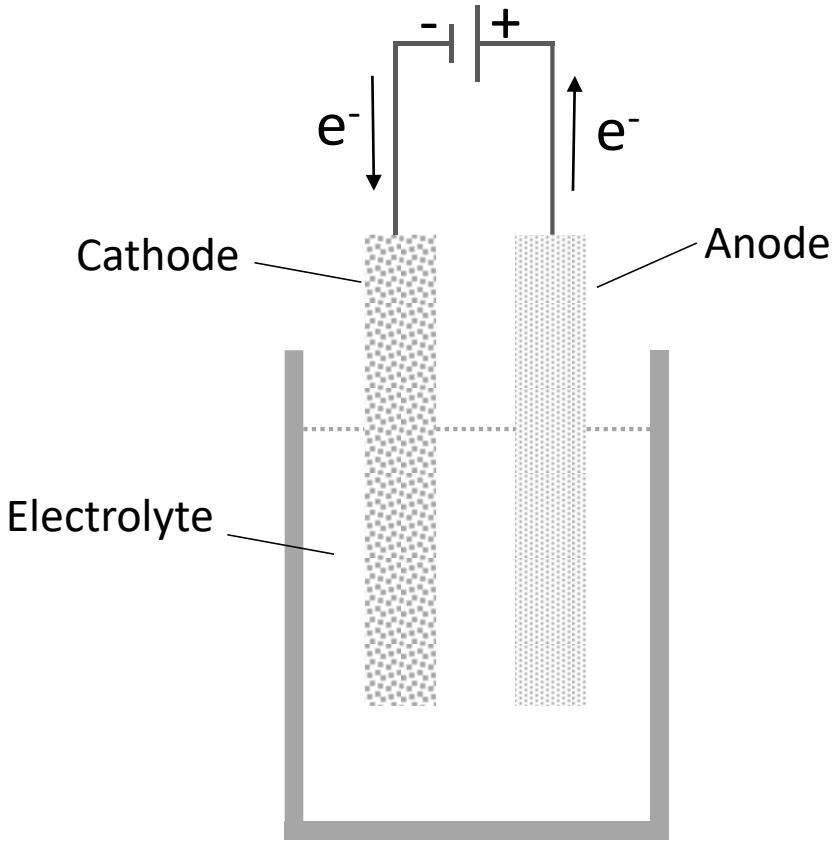

Figure 2.4. Schematic representation of an electrolytic cell

The mechanism of this method is to make the insoluble metal oxide or the metal/alloy containing oxygen as an impurity as cathode to remove oxygen by ionization which will be released at the anode surface in the form, most of the time, as CO or CO_2 due

to using graphite anode, which has several advantages in molten salt electrolysis, or in the form of O_2 if a non-consumable (inert) anode is used. Since the oxygen is removed electrolytically, this process is also called as electrodeoxidation [84,85]. It should be noticed that although this process is originally developed for the metal oxides, the metal sulphides, carbides, nitrides are also in the scope of this method.

Therefore, these two methods make direct metal production from the respective mineral in a high purity in the form of powder and bulk by using electricity and molten salts possible. In both of these mechanisms, molten salt solution acts as the medium for the transportation of metal ions from one electrode to the other. As aluminum electrolysis is considered an exception due to using fluoride type molten salt which is toxic, corrosive and requires high operating temperature. In general, chloride type molten salts such as $CaCl_2$, NaCl, KCl, LiCl are preferred due to nontoxicity, formation of a mixture with low eutectic point which enables to study at lower temperatures. To sum up, the electrochemical metal production route has more advantages over the other metal production processes in terms of metal purity, energy efficiency, environmental effects and the processing cost.

2.4. Electrochemical Production of Al-Sc Alloy in Molten Salt

As mentioned in the previous sections, electrochemical production route offers more advantages in production of Al-Sc alloy in terms of starting material, product yield, ease of processing and cost. Therefore, the following text is focused on the studies existing in the literature on electrochemical production of Al-Sc alloy.

The first detailed electrochemical study intended to produce metallic scandium was conducted by Fischer et.al in 1937 [30]. In the choice of the process for the preparation of the scandium metal, two aspects in particular were decisive. First, the process must be carried out with a few grams of material with the lowest possible scandium losses. Second, when working at elevated temperatures, only a few materials are suitable for

the construction of the equipment, since both Sc metal and many of its salts are extremely reactive.

In the light of considerations above, molten salt electrolysis was chosen for the purpose of production of metallic scandium. If oxide compound of scandium was used then fluoride type electrolytes, which are the well-known solvents for oxide compounds as is the case for aluminum electrolysis (dissolution of Al_2O_3 in molten Na_3AlF_6), should be used. Due to oxide-fluoride interaction, oxide type crucibles cannot show sufficient resistant to fluoride melts. The only possible solution, then, is to use graphite crucible although there is a possibility of formation of scandium carbide compounds [30,79].

Due to difficulties of processing with the oxide-fluoride system for scandium, Fischer and his coworkers decided to use relatively low melting point Sc compound/s which can be the halides such as chlorides, bromides and iodides. $ScCl_3$ was chosen as the scandium raw material among other halides. However, this compound has great volatility. The electrolyte to be chosen should have melting point as low as possible. Eutectic KCl-LiCl salt, which is the lowest melting point (i.e. $T_e = 353^oC$) alkali halide mixture, was chosen as electrolyte to decrease evaporation losses of $ScCl_3$.

Another important consideration in this electrolysis process is the operating temperature. If the operating temperature is below the melting point of scandium, the elecrochemically recovered scandium will be in dendritic form and have impurities from the melt which cannot be removed without oxidation. Therefore, scandium was collected in a liquid metal that should have a melting point close to that of electrolyte, vapor pressure much higher than scandium and sufficient solubility for scandium [86]. For this purpose, zinc was chosen as the auxiliary metal which acted as a liquid cathode by the polarization with tungsten wire which does not have any interaction with liquid Zn-Sc alloy. On the other hand, graphite crucible was chosen as anode which contained a calcined magnesium oxide crucible to hold Zn-Sc alloy to avoid interaction with the graphite as shown in Figure 2.5 [30].

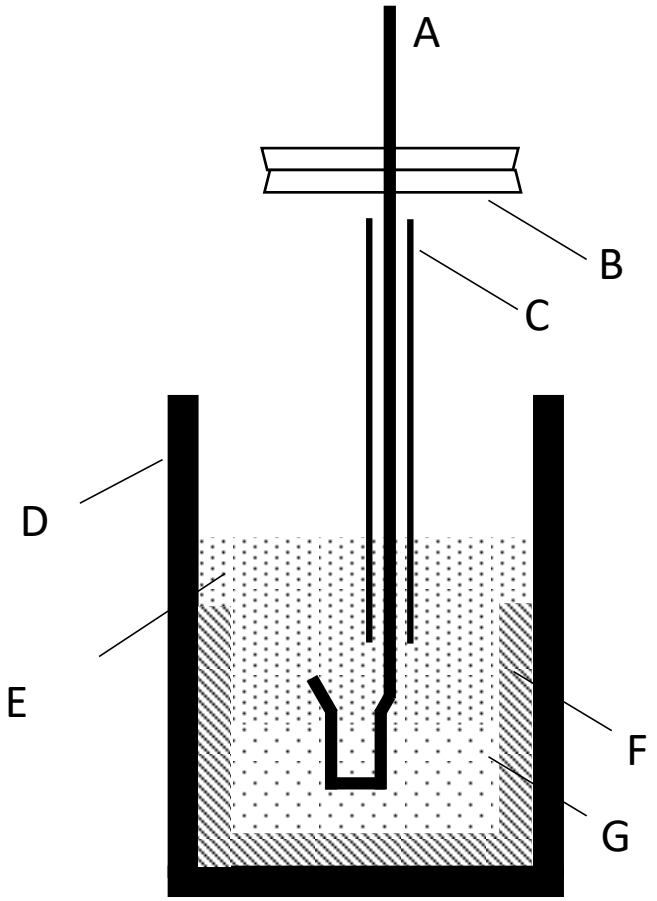

Figure 2.5. Electrolysis Cell for Scandium Production. (A: Tungsten wire (cathode), B: Quartz bell, C: MgO sheath, D: graphite crucible (anode), E: KCl-LiCl-$ScCl_3$ melt, F: MgO crucible, G: Zn-Sc alloy [30])

The electrolysis process was conducted at the starting temperature of 700^{o}C and the temperature was gradually increased to 800^{o}C while the applied voltage maintained at 3 to 3.5V for one hour to achieve approximately 90% efficiency.

During the electrolysis, Zn-Sc melt at the bottom of the magnesium oxide crucible was stirred with the tungsten wire to inhibit unwanted growths and sedimentation that might occur due to volatile nature of zinc. Also, the quartz bell assembled on top of the stirrer was for collection of $ScCl_3$ that is the another volatile component of the system. At the end of the electrolysis experiment, the solidified salt-alloy mixture was

mechanically crashed and separeted from each other by water leaching. After vacuum distillation to remove zinc, about 95% pure metallic scandium was obtained [30].

Although the aforementioned electrochemical process is for the extraction of reactive pure metals which entails several subsequent refining and purification processes due to intermediate alloying, this process formed the basis of using liquid metal cathode and subsequent formation of alloy especially when the metal to be recovered electrochemically is used as the alloying element with the cathode material. Utilization of liquid metal cathode gives chance to formation of intended alloy (i.e. intermetallic compounds) in a direct way with a fast diffusion rate. However, there are several requirements for the metal to be used as liquid cathode such as having sufficiently low melting point that does not require special equipment, having sufficiently low vapor pressure at operating temperature, sufficient solubility for the alloying constituent, being chemically inert with the reactants and reactor materials.

Recently, Al-Sc alloy was produced by electrochemical reduction of scandium bearing compounds and in-situ alloying with liquid aluminum that behaves both as cathode of the cell and the collector for electrochemically reduced scandium. The studies present in the literature for electrochemical production of Al-Sc alloy were mainly based on Sc_2O_3 raw material and two different types of electrolyte such as sodium (Na_3AlF_6) and potassium (K_3AlF_6) cryolite melts. The underlying reason for choosing the couple of oxide compound – fluoride type electrolyte comes from the well-known Hall-Héroult process. Researchers have investigated the possibility of production of Al-Sc alloy by applying the same method with a small difference that is addition of Sc_2O_3 as the Sc raw material with cryolite melt.

The main process paramaters in those studies [87,88] were cryolite ratio, current density and electrolysis temperature. Cryolite ratio (CR) is the most important parameter in aluminum electrolysis cell. It is basically defined as the molar ratio of NaF or KF to AlF_3 in the electrolyte. When the KF-NaF-AlF_3 mixture is used, then cryolite ratio becomes the ratio of total moles KF and NaF to AlF_3. The conventional

cryolite baths have CR in the range of 2-3. According to amount of KF and NaF, the liquidus temperature, which will affect the operation temperature, changes. In terms of the industrial experince and the experimental studies, it is known that addition of NaF increases the liquidus temperature whereas the opposite effect is seen upon addition of KF.

Guan et.al [89] and Wang et.al [90] conducted an experimental study using sodium cryolite-2wt%Sc_2O_3-3wt%Al_2O_3 melt with a cryolite ratio of 2.2 at 950^oC and current densities of 0.5 and 1 A/cm^2. LiF as 5wt% was added into the melts to increase electrical conductivity and enhance the charge transfer kinetics of the electrolyte. Both alumina and scandium oxide were added as raw materials. The reaction vessel was composed of graphite crucible (acting as cathode) with inner alumina lining to inhibit anode-cathode interaction during electrolysis. Both researchers reported that as the current density was increased, the scandium content of the alloy increased too. Also, as the duration of electrolysis procedures got longer at the same current density, the Sc content in the alloy increased. According to XRD and SEM-EDX analysis, Al_3Sc intermetallics were successfully formed in aluminum matrix. Wang et.al [90] also reported that $Al_{0.968}Sc_{0.032}$ phase became the dominant intermetallic phase when Sc content of the alloy was below 0.2 wt%. The crystal structure of this phase is similar to the aluminum with a small lattice parameter difference of 4.0495 angstrom for Al and 4.065 angstrom for $Al_{0.968}Sc_{0.032}$.

Potassium cryolite based melts, on the other hand, attracted particular attention for Al-Sc alloy production wit their low operating temperature (i.e. 750^oC) and low energy consumption in terms of Al-Sc alloy production. In the study of Liu et.al [91], the electrolysis process was carried out in potassium cryolite - 2wt%Sc_2O_3 melt having CR of 1.22 at 750^oC and the current density values of 0.5 and 1 A/cm^2. Graphite with alumina liner was used as the reaction crucible. As a result of the electrolysis, it was reported that Al-Sc alloy was successfully produced according to XRD, SEM and ICP results. Lineer sweep voltammetry and cylic voltammetry studies were also carried out to determine the mechanism of Al-Sc alloy formation on liquid aluminum working

electrode with respect to a tungsten wire. A unique cathodic peak was seen and this was ascribed to the reduction of Sc^{3+} ion on the liquid aluminum surface. The extreme limits of the process was also studied by increasing the temperature and current density separately. When current density was increased from 1 to 2A/cm^2, the Sc content of the alloy decreased. The authors suggested two scenearios for the decrease in Sc. The first one was that the reduction rate of Sc in the vicinity of cathode increased with increasing current density. However, the slow diffusion of Sc into liquid Al caused dissolution of Sc in the molten salt. Another scenario could have been that the increase in the current density increased the rate of gas liberated during the electrolysis and the resultant convective flow in the melt improved the solubility of Sc in the melt. On the other hand, it was observed that Sc content of the alloy increased as temperature was increased from 750^{o}C to 800^{o}C and 850^{o}C due to the increased solubility of Sc in Al as seen in the binary Al-Sc phase diagram [92]. The structural analysis of Al-Sc alloy demonstrated that faceted Al_3Sc intermetallic formed due to preferred orientation in <111> directions [93].

The studies given above report the preliminary results on the Al-Sc alloy formation in both sodium and potassium cryolite melts and do not mention about the solubility of Sc_2O_3 in these baths. However, relationship between Sc_2O_3 content and the cryolite ratio and $Sc_2O_3 – Al_2O_3$ interaction are essentials of the Al-Sc electrolysis procedure in cryolite melts. Rudenko and his co-workers [88] recently conducted a comprehensive study on the physicochemical interactions between Sc_2O_3 and cryolite melts. They performed successive thermal analysis to measure liquidus temperature in KF-NaF-AlF_3-Sc_2O_3 melt with respect to changing cryolite ratio, amount of NaF added and the concentration of Sc_2O_3. Quasi-binary diagrams with simple eutectics were obtained. In these diagrams, the increase in the liquidus temperature and the stability field of liquid phase upon increase in the cryolite ratio and amount of NaF added were observed. However, as the cryolite ratio decreased and the amount of NaF increased, the stability field of liquid phase became narrower which was undesired for these kinds of melt especially for industrial applications. The effect of Sc_2O_3 content

on the liquidus temperature of $KF\text{-}AlF_3$ system (low cryolite ratio melt) was also studied and it was found that the liquidus temperature increased upon the increase in the Sc_2O_3 content. The solubility values of Sc_2O_3 and Al_2O_3 were derived at 650°C, 730°C and 800°C again for low melting $KF\text{-}AlF_3$ melt. For this melt, both the solubility of Sc_2O_3 and Al_2O_3 increased as the temperature and the cryolite ratio increased. The solubility of Al_2O_3 was 1.5-2 times higher than that of Sc_2O_3 for the $KF\text{-}AlF_3$ melt, whereas the solubility values of both scandium and aluminum oxides in the $KF\text{-}NaF\text{-}AlF_3$ mixture were closer to each other at 800°C although the cryolite ratio was increased. The solubility difference of Sc_2O_3 in $KF\text{-}AlF_3$ and $KF\text{-}NaF\text{-}AlF_3$ mixture was ascribed to the formation of complex scandium compound, K_3AlF_6, resulting from chemical reaction between Sc_2O_3 and $KF\text{-}AlF_3$ melt. This compound was found to dissolve slightly in that melt.

A similar study carried out by the same research group [94] investigated the simultaneous solubility behavior of Al_2O_3 and Sc_2O_3 in sodium cryolite melt. It was found that solubility of Sc_2O_3 was affected by the solubility of Al_2O_3 in a given electrolyte and the temperature. Also, an interesting phenomena was observed during co-solubility of Sc_2O_3 and Al_2O_3. The solubility value upon co-solubility of these two oxides was found to be greater than the individual solubility values. It was attributed to the different solubility mechanism of Sc_2O_3 and Al_2O_3 in the sodium cryolite melts. Due to its industrial importance, the dissolution mechanism of aluminum oxide in sodium cryolite was studied and analyzed extensively with several investigators [95,96]. According to these studies, alumina was found to dissolve in sodium cryolite melt by formation of stable oxyfluoride aluminate anion complexes ($Al_2OF_6^{2-}$ and $Al_2O_2F_4^{2-}$) as a result of the chemical reaction taking place with alumina and the dissociated ions of sodium cryolite. On the contary, according to the raman spectroscopy analysis, different from Al_2O_3, the dissolution process of Sc_2O_3 took place in two steps with the help of the formation of fluoride and oxyfluoride ions such as ScF_6^{3-}, $Al_2OF_6^{2-}$ and $Sc_2OF_6^{2-}$. However, when Al_2O_3 and Sc_2O_3 coexisted and the concentration of dissolved Al_2O_3 increased in the cryolite melt, the oxyfluoride anion

complexes of aluminum and scandium alone were seen in the corresponding raman spectra [94]. It should be noted that although the formation of ion complexes enhance the solubility of oxides in fluoride melts, due to their thermodynamic stabilities, the activity of the metal ion to be electrowon decreases and reduction of oxides becomes more difficult which in turn decreases the process efficiency.

As understood from the studies on the electrochemical synthesis of Al-Sc alloy in cryolite based melts summarized above, the source of scandium was Sc_2O_3 due to availability, low price and its solubility in molten fluoride melts. However, it is well known from the aluminum electrolysis process that utilization of fluoride type melts poses several environmental drawbacks such as CO_2 evolution and perflurocarbon (CF_4 and C_2F_6) [97,98]. The alkali or alkaline earth halide salts like $CaCl_2$, NaCl are more promising electrolyte materials since they are low melting point salts, nontoxic, soluble in each other, non-reactive with electrodes and reactors and form low melting temperature eutectics.

Harata et.al. [76] developed a new method to produce Al-Sc alloy electrochemically in $CaCl_2$ melt by using Sc_2O_3 as scandium raw material in different weight percentages. Liquid aluminum was used as the collector similar to the studies given above [87–90, 94] at 1173K and the current density values in the range of 0.25-1 A/cm^2. The content of scandium oxide was in the range of 1.37-8 mol% during the process. The experimental studies conducted in a graphite crucible acting as the cathode. A graphite rod was used as the anode. Due to the lack of thermodynamic data on $CaCl_2$ – Sc_2O_3 system, the reaction mechanism for this process is not known. Therefore, the researchers suggested four possible reaction mechanisms from their experimental setup which was given in Figure 2.6 [76].

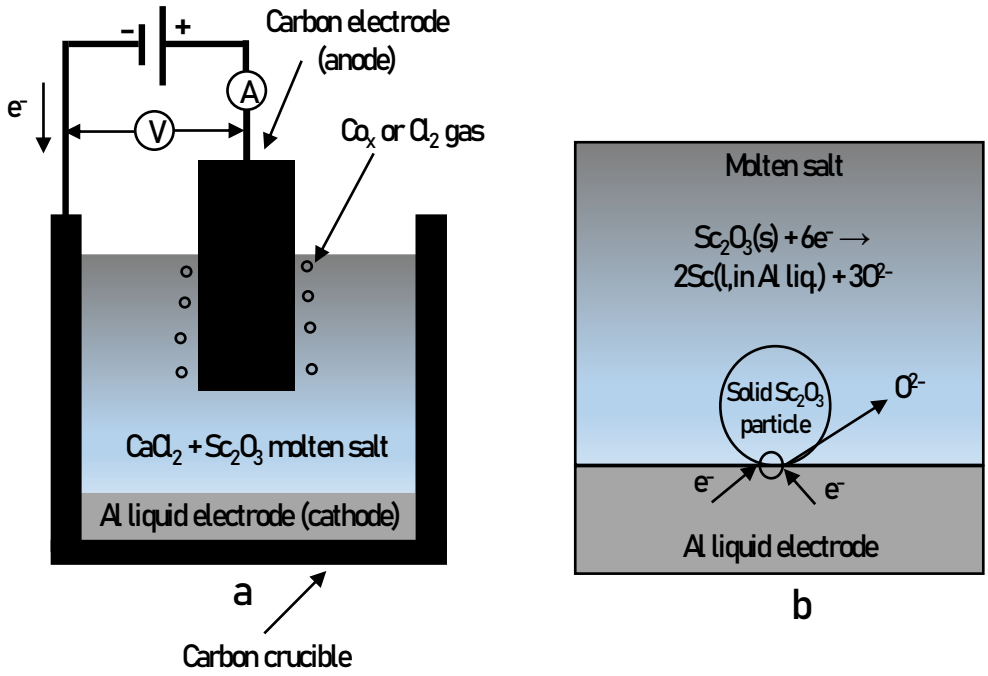

Figure 2.6. (a)The basic setup of electrolysis cell, (b) An example of possible reduction mechanism of Sc_2O_3 [76]

These mechanisms were listed as following;

i) Molten Salt Electrolysis: if the Sc_2O_3 compound is soluble in $CaCl_2$ melt, then Al-Sc alloy forms by reduction of Sc^{3+} ions in the melt.

Cathode: $Sc^{3+} + 3e^- \rightarrow Sc$ (in Al(l)) (2.3)

Anode: $C(s) + xO^{2-}$ (in salt) $\rightarrow CO_x$ (g) $+ 2xe^-$ (2.4)

ii) FFC Cambridge Process: If the Sc_2O_3 does not dissolve in $CaCl_2$ melt, it will go down and come into contact with the surface of liquid aluminum. Then, it will be reduced cathodically by ionization of the oxygen in Sc_2O_3 compound and Al-Sc alloy occurs in-situ on the surface of liquid aluminum.

Cathode: Sc_2O_3 (s) $+ 6e^- \rightarrow$ Sc (in Al(l)) $+ 3O^{2-}$ (2.5)

Anode: $C(s) + xO^{2-}$ (in salt) $\rightarrow CO_x$ (g) $+ 2xe^-$ (2.6)

iii) Calciothermic reduction: This process can also take place when Sc_2O_3 is not soluble. Calcium metal is produced cathodically by making the potential of cathode adequately negative. Electrolytically produced calcium metal is soluble in molten $CaCl_2$ [99] and it will act as a reducing agent for Sc_2O_3 in the melt. In the presence of the liquid aluminum, scandium will react with liquid aluminum to form Al-Sc alloy.

Cathode: $Ca^{2+} + 2e^- \rightarrow Ca\ (l)$ (2.7)

Anode: $C(s) + xO^{2-}\ (\text{in salt}) \rightarrow CO_x\ (g) + 2xe^-$ (2.8)
$2Cl^- \rightarrow Cl_2\ (g) + 2e^-$

$Sc_2O_3\ (s) + Al\ (l) + 3Ca\ (l) \rightarrow Al\text{-}Sc\ (l) + 3\ CaO\ (l)$ (2.9)

As a result of the electrolysis process, formation of Al-Sc alloy was confirmed by the formation Al_3Sc intermetallics via XRD analysis. The Sc content of the alloy samples was in the range of 0.81-32.3 wt%. From ICP analysis, 0.65wt% of Ca was detected in the alloy which was considerably lower as compared to metallothermic reduction experiments (11.1 – 22.5 wt%) performed by the same research group. It should be noted that the current efficiency, solubility of S_2O_3 and the dissolution mechanism of Sc_2O_3 are still under investigation.

It is expected that electrochemical reduction of scandium compounds in molten alkali and alkaline earth halide melts will offer a simple and efficient processing route to produce Al-Sc alloy in comparison to the cryolite melt. Furthermore, using a different scandium raw material which is relatively less stable than Sc_2O_3 and resistant to moisture as compared to $ScCl_3$ such as ScF_3 may decrease the difficulty during the reduction process.

CHAPTER 3

EXPERIMENTAL

In this study, two grades of aluminum (1050 and 6060) were used as the aluminum source. 1050 alloy in the form of tube was used in the first two experiments. For the remaining experiments, 6060 alloy in the form of rod was used. The reason of changing the aluminum source in the experiments will be explained in the following chapter.

3.1. Experimental Study

3.1.1. Cell Assembly

Electrochemical cells employing three types of cathode designs were used in this study. The main difference among them was the design of cathode. The first set of experiments were conducted with the cell schematically shown in Figure 3.1. In all these three cells, a closed end quartz tube having 600 mm height and 50 mm diameter was used as the reactor or container for the other cell components. Other cell components were placed into the cell from the open end at the top of the tube. A polyamide lid was used to close the tube. There were four holes on the lid. Two of them (ϕ:7mm) were for argon gas inlet and outlet. The one located at the center (ϕ:3.5 mm) was for the anode. The final one (ϕ:3.5mm) was for the cathode. Hollow stainless steel bolts employing rubber O-rings were used to extend electrodes and gas connection tubes out of the reactor. These bolts were screwed to the lid firmly before each experiment to avoid gas leakage from the atmosphere.

The quartz cell vessel which was resistant to high temperature and chemicals, was put into the vertical tube furnace. The top section of the cell remained outside the furnace. Vertical electrode movements could be performed easily by the extensions of electrodes from the top section of the cell which was necessary for both putting the electrodes into cell before experiment and immersing at the beginning of experiment for easy operation.

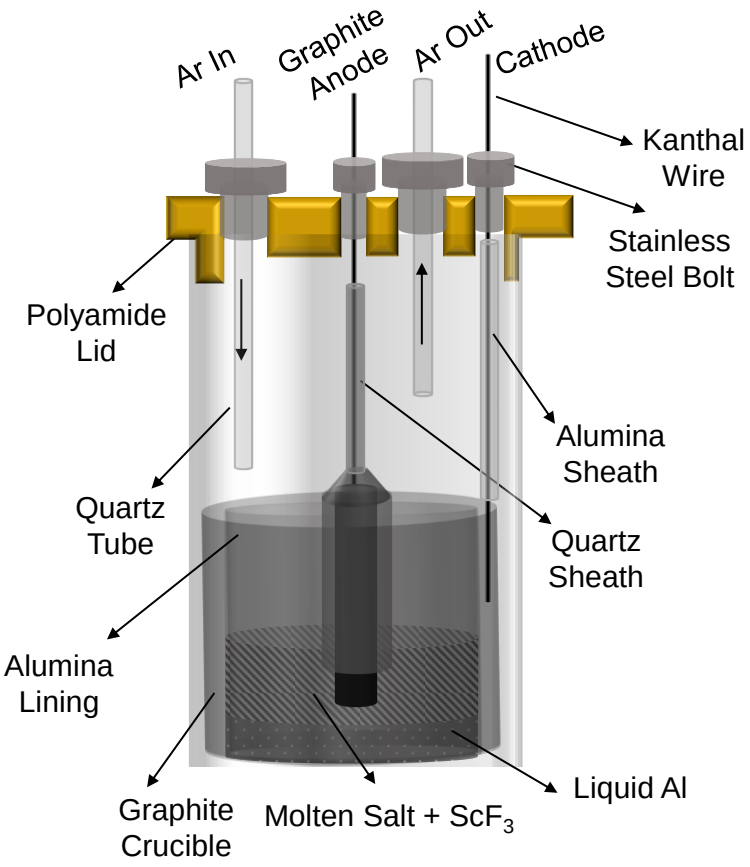

Figure 3.1. Schematic drawing of the first electrochemical cell assembly

In addition to the electrode movements, external electrical connections and gas supply could also be done in a practical way while the bottom of the cell was operating at a high temperature.

In the first cell shown in Figure 3.1, the graphite crucible at the bottom of the cell served as a container for the raw materials and also acted as the cathode. Graphite rod located at the center of the cell served as the anode. An alumina tube was used to avoid short circuit and limit the volume to control raw material consumption during electrochemical reduction experiments. The second set of experiments were conducted adopting the cell design shown in Figure 3.2.

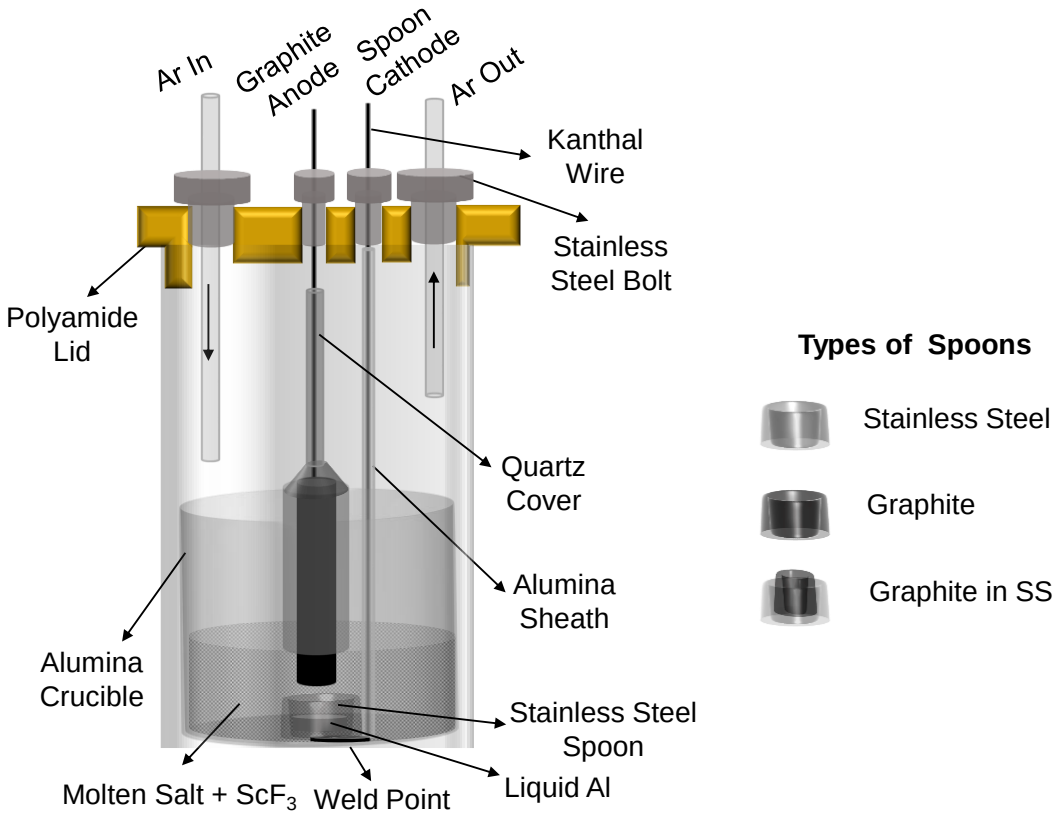

Figure 3.2. Schematic drawing of the cell design with spoon cathode

In this cell, alumina was used as the crucible material, to inhibit the reaction between redox active impurities and the crucible. In addition, the poor current efficiency caused by graphite dust formation was aimed to be eliminated by using alumina crucible. On the other hand, the cathode design was changed. A spoon shaped cathode, which is like a mini crucible, was used. As spoon cathode materials, stainless steel and graphite were selected. At first, stainless steel and graphite were used as the individual cathodes. For some of the experiments, a two-layer spoon that had a mini graphite crucible placed inside a stainless steel spoon as shown in Figure 3.2 was used. For both anode and cathode, high temperature resistant and non-magnetic Cr-Ni alloy (Kanthal) wire with a diameter of 3.5 mm was used for extending them through the cell. The extensions of the electrodes were prepared differently. For graphite rod anode and graphite crucible cathode, Kanthal wires were threaded and then screwed firmly. For spoon cathodes, the Kanthal wire was bended and welded to the bottom of the spoon by spot welding. Since the experiments were conducted at a considerably high temperature (i.e. 800^{o}C), ceramic sheaths made of quartz and alumina were used to protect the electrodes and their extensions from oxidation.

The third cell was the modified form of the first one. The alumina lining was removed and the porous mullite and alumina prepared by gel casting method were used as the membrane. Both have approximately 40% porosity for infiltration of the electrolyte and ion transportation. The cast porous ceramic samples in the spherical or cube form were drilled in green state as such that one end was kept closed as shown in Figure 3.3. After that they were sintered partially at 1200^{o}C. Finally, they were stuck to the tip of the graphite anode with a special adhesive resistant to high temperatures. When mullite membranes were used, the upper portion of graphite anode was protected only with quartz sheath. On the other hand, when the alumina membranes were used, graphite anode was protected with a cylindrical fused alumina sheath by putting the graphite electrode in the sheath.

Figure 3.3. Drilled ceramic membranes to be sintered

3.1.2. Auxiliary Apparatus

For a complete electrochemical reduction experiment, auxiliary apparatus supporting the cell assembly was necessary. The schematic view of experiment medium with auxiliary apparatus is given in Figure 3.4. A Lindberg LHTF322C vertical split furnace having maximum temperature limit of 1100^{o}C was used to heat the cell assembly to the desired temperature by programming the heating cycle properly with a controller. An Agilent N6700 B DC power supply, having 400 W capacity, was used to supply the required electrical power to run the experiments. The power supply was connected to a computer to both monitor and collect the current – time history for each experiment with a self-made program written in Visual Basic. During the experiments, the reaction chamber was protected with the continuous Argon flow of about 200cc/min. The gas coming out of the furnace was vented out by the aspiration system.

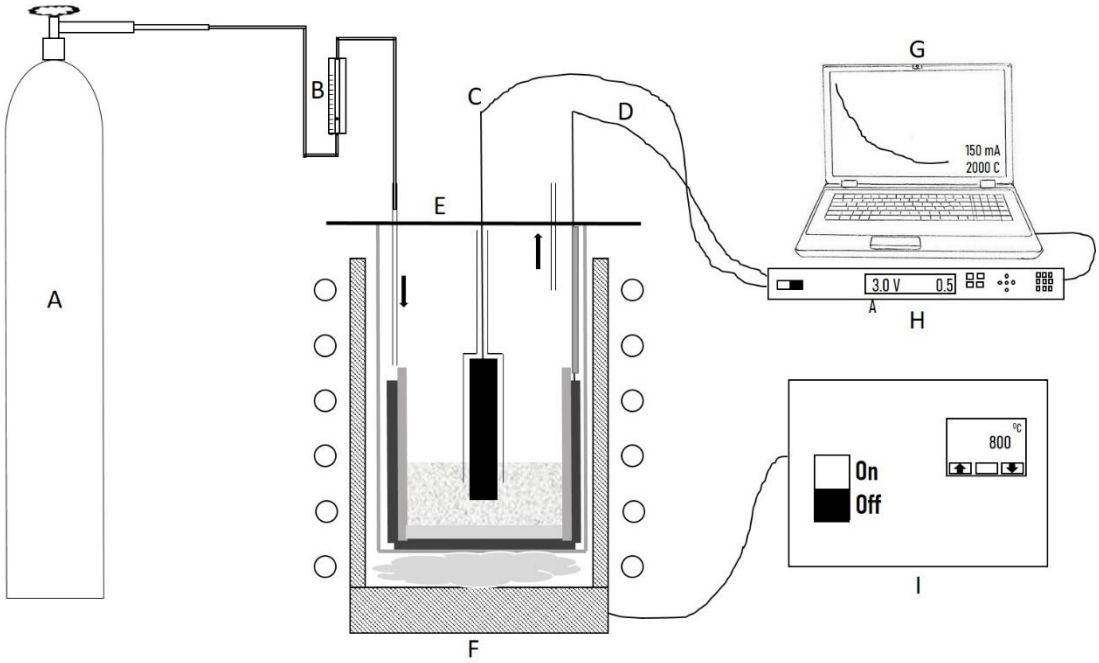

Figure 3.4. Schematic representation of the experimental setup (A: Argon Gas Cylinder, B: Flowmeter, C: Anode connection, D: Cathode Connection, E: Cell Assembly, F: Vertical Tube Furnace, G: Computer for data collection, H: DC Power Source, I: Furnace Controller Unit)

3.2. Experimental Procedure

3.2.1. Cell Feed Preparation

3.2.1.1. Sc Raw Material

In this study, two different Sc bearing compounds were used as Sc source. The source of these compounds was the lateritic nickel ore in Çaldağ site near Manisa. A domestic mining company, META Nickel Cobalt Company, conducted the extraction and recovery processes of Sc bearing compound from the leach residue. Since the extracted compound was an ammonium based by-product, it contained several impurity elements like Na, Fe, Si. Therefore, it was subjected to several processes such as calcination and acid leaching to purify. Ammonium was removed by calcination while the impurity elements were removed by acid leaching process.

The first Sc raw material used in the first set of experiments had only been subjected to calcination and it was supplied in the form of powder. This powder was characterized by X-Ray Diffractometer (XRD) (Cu K_α radiation with wavelength of 1.5418 Å, tube voltage: 40kV and scan speed: 2°/min) for phase identification by DIFFRAC. SUITE EVA software developed by BRUKER. The XRD pattern of this powder is given in Figure 3.5.

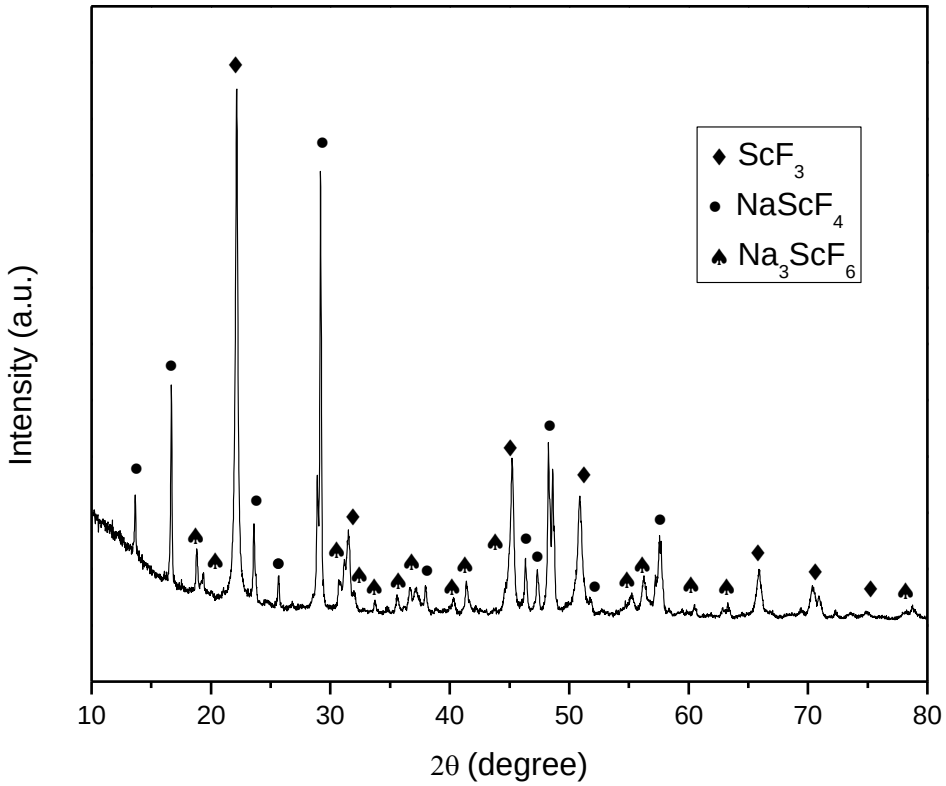

Figure 3.5. XRD result of the calcined Sc compound used in the first set of experiments

According to the result of XRD analysis, the major phase in this mixture was ScF_3. $NaScF_4$ and $NaSc_3F_6$ were the minor phases.

The second Sc raw material used in the subsequent experiments was subjected only to the acid leaching to increase the phase fraction of ScF_3 and remove the impurity

elements as much as possible. In the same manner, this material was also analyzed by XRD for phase identification. The resultant XRD pattern is shown in Figure 3.6.

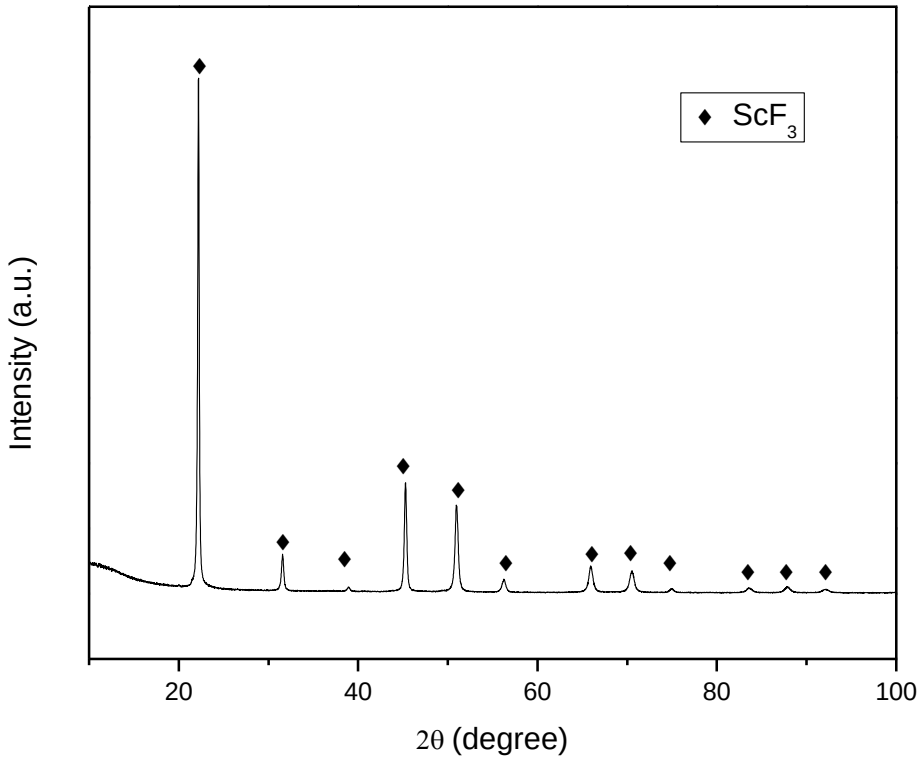

Figure 3.6. XRD result of ScF_3 compound obtained after acid leaching process

It was obvious from the XRD result that the only Sc bearing phase in the second powder was ScF_3 as expected.

3.2.1.2. Al Raw Material

In the first two experiments, AA 1050 grade aluminum was used. For the rest of the experiments, AA 6060 aluminum alloy, which is produced in the form of an extruded bar, was used as the matrix material for Al-Sc alloy. AA 1050 contains minimum 99.5% Al while AA 6060 contains up to 99% Al. The common impurity elements in both alloys are iron and silicon, coming mainly from aluminum ore since removal of these two elements is difficult with the existing aluminum production technology. For

AA 6060, magnesium is the other important alloying element. A sectioned cylindrical sample of AA 6060 used in the experiments was analyzed with Optical Emission Spectroscopy (OES) to determine the chemical composition of the sample and its result is given in Table 3.1.

Table 3.1. *Chemical composition of AA6060 sample determined by OES*

Material	*Fe*	*Si*	*Mg*	*Cu*	*Ti*	*V*
AA6060	0.189	0.396	0.29	0.008	0.025	0.01

Another sectioned sample was examined under SEM to determine the structure of AA 6060 as shown in Figure 3.7.

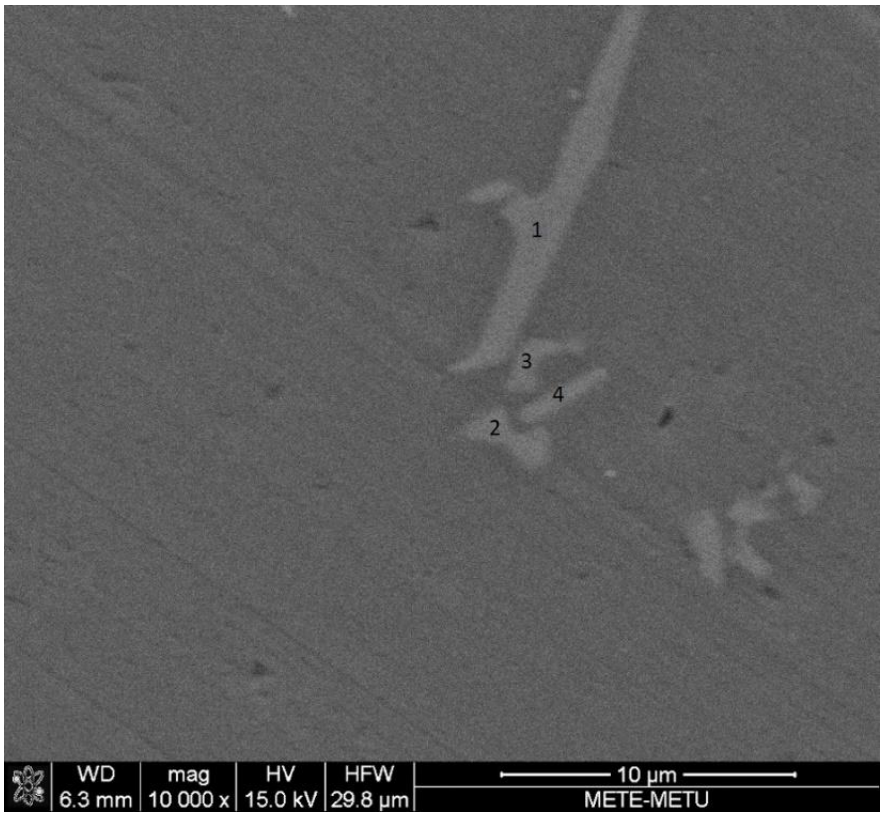

Figure 3.7. SEM micrograph of AA 6060 Sample. The numbers indicated the positions from which EDS analyses were performed.

Depending on the Fe content of the alloy, different intermetallic compounds form in the aluminum matrix. EDS analysis was carried out from the numbered intermetallic compounds and the results of the analyses are given in Table 3.2.

Table 3.2. *EDS analysis taken from the intermetallic particles*

Analysis Number	*Fe (at%)*	*Si (at%)*	*Al (at%)*
1	14.59	9.95	75.46
2	11.26	7.87	80.87
3	12.06	8.78	79.16
4	11.37	6.84	81.79

The results obtained by EDS was compared with literature results of the samples having similar chemical composition which was analyzed by EBSD, EDX, TEM and confirmed by THERMOCALC software [100]. As a result, it was concluded that the AA 6060 containing 0.2wt% Fe contained a mixture of β-Al_5FeSi (major) and α_c-AlFeSi (minor).

3.2.1.3. Electrolyte

In electrochemical reduction experiments, $CaCl_2.2H_2O$ (Merck, 102382), anhydrous $CaCl_2$ (Merck, 102378) and NaCl (Sigma Aldrich, 13423) salts were used as the electrolyte. It is well known that alkali and alkaline earth chlorides are highly susceptible to moisture. Thus, these salts were subjected to a dehydration procedure under vacuum before experiments to obtain anhydrous forms. A thermal drying procedure was followed. The heating program for thermal drying process included four steps: 1) heating the salt or salt mixture from room temperature (20°C) to 110°C at a rate of 2°C/min, 2) waiting for an hour at 110°C, 3) increasing the temperature from 110 to 300°C at 4°C/min, 4) waiting for at least for 4 hours at 300°C. While holding the temperature at 110°C, removing physically absorbed water which would

be absorbed during preparation of experimental setup was aimed. In the final two steps, the aim was to remove crystal water which had been chemically bonded.

As can be seen in Figure 3.8, there is an intermediate monohydrate phase in between anhydrous and dehydrated forms of calcium chloride. Anhydrous calcium chloride can be obtained at high temperatures and low H_2O equilibrium partial pressure.

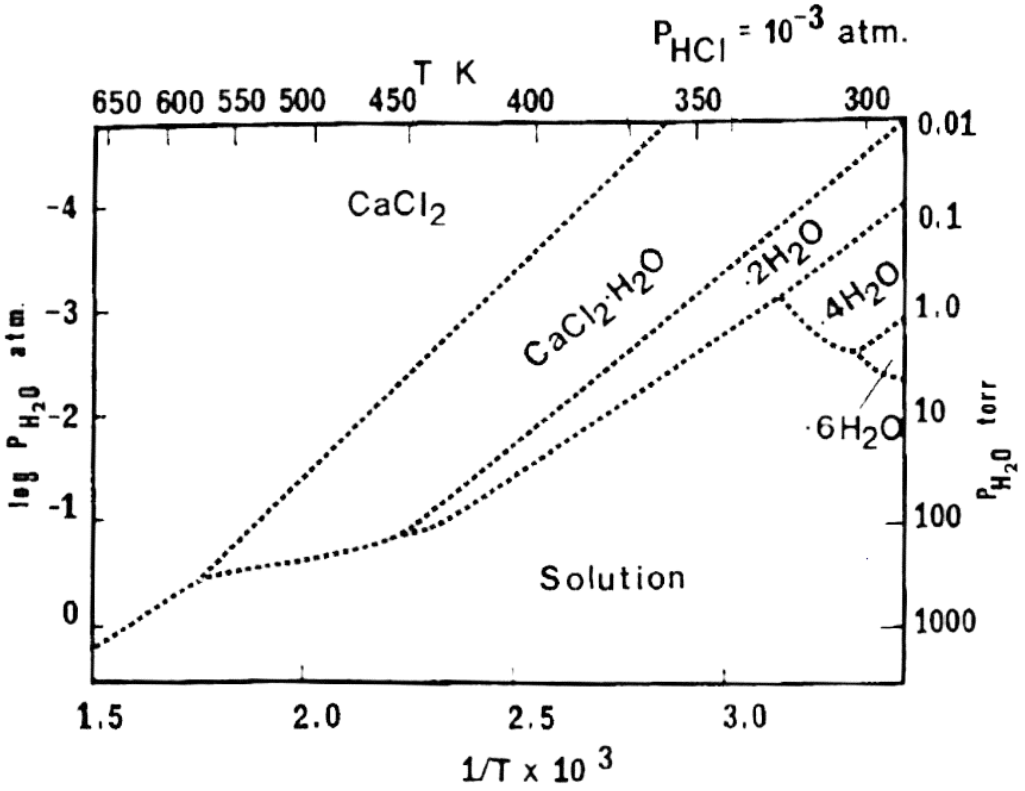

Figure 3.8. Phase equilibria among $CaCl_2$,$CaCl_2.xH_2O$ and solution phases at pHCl=10^{-3} atm separated by dashed lines [101]

The equilibrium reactions which may take place during dehydration can be written for calcium chloride salt as [101];

$$CaCl_2.2H_2O\ (s) = CaCl_2.H_2O\ (s) + H_2O\ (g) \quad (3.1)$$

$$CaCl_2.H_2O\ (s) = CaCl_2\ (s) + H_2O\ (g) \quad (3.2)$$

These reactions proceed in the written direction as the temperature increases. However, due to kinetics of the reactions, the reaction mechanisms become complicated and the following reactions may take place when H_2O vapor pressure exceeds the equilibrium value [101].

$$CaCl_2\,(s) + H_2O\,(g) = CaOHCl\,(s) + HCl\,(g) \quad (3.3)$$

$$CaCl_2.H_2O\,(s) = CaOHCl\,(s) + HCl\,(g) \quad (3.4)$$

$$CaCl_2.2H_2O\,(s) = CaOHCl\,(s) + H_2O\,(g) + HCl\,(g) \quad (3.5)$$

At higher temperatures below melting point of $CaCl_2$, oxide formation is possible as shown in the following reactions;

$$CaCl_2\,(s) + H_2O\,(g) = CaO(s) + 2HCl\,(g) \quad (3.6)$$

$$CaOHCl\,(s) = CaO\,(s) + HCl\,(g) \quad (3.7)$$

When both these undesired reactions and the equilibrium diagram given in Figure 3.8 are taken into account, the dehydration process must be carried out carefully in order not to produce oxide, oxychloride, hydroxychloride or hydroxide. Since the equilibrium partial pressure of H_2O required to form calcium oxide and calcium hydroxide are higher for calcium chloride, the phases are not seen in the equilibrium diagram in Figure 3.8.

Although dehydration process for $CaCl_2$ is complicated, this is not the case for NaCl. According to the equilibrium diagram of NaCl-H_2O given in Figure 3.9, the required partial pressure to form NaOH is very high as compared to $CaCl_2$. Therefore, formation of NaOH is not possible at atmospheric pressure and it is sufficient to dry under atmospheric conditions before mixing with the other salts.

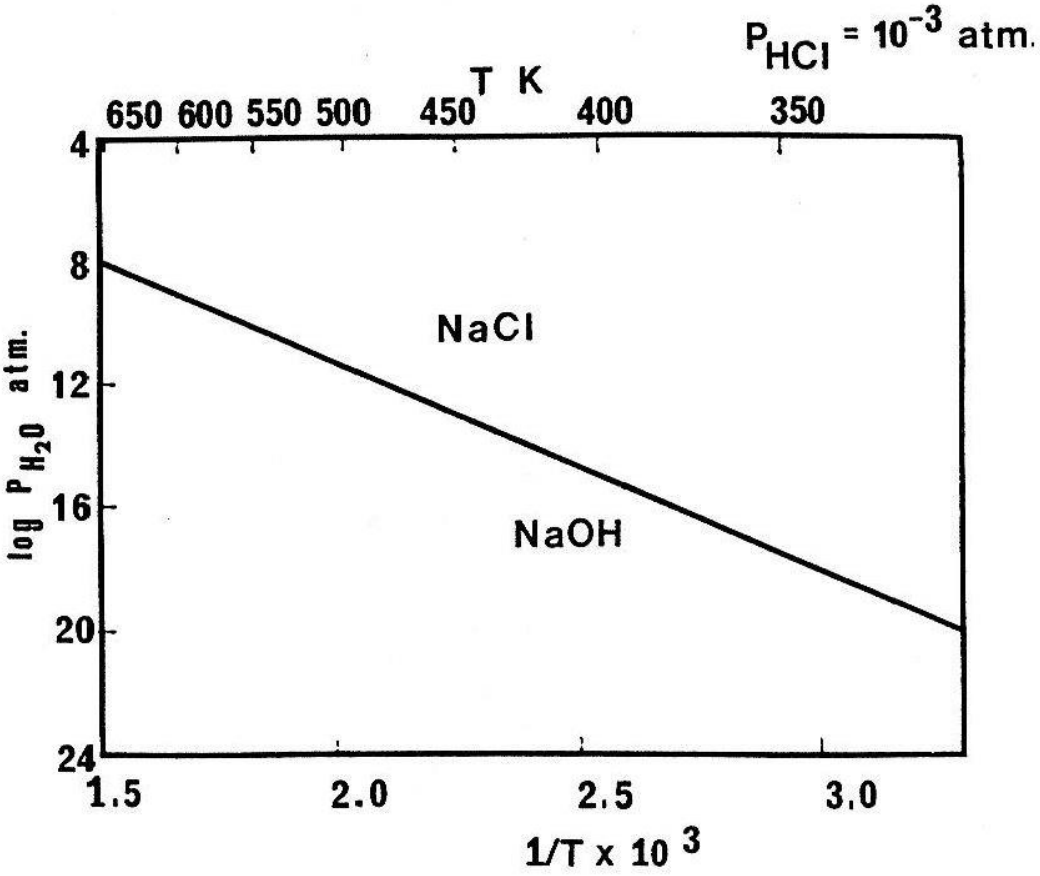

Figure 3.9. Equilibrium diagram of NaCl-H_2O system at pHCl=10^{-3} atm [101]

3.2.2. Cell Operation

The preparation process for electrochemical reduction experiments started with charging the raw materials into graphite crucible. A small piece of aluminum weighing between 2.5-3 grams was placed at the bottom of the crucible. After that pure $CaCl_2$ or $CaCl_2$-20 wt% NaCl, $CaCl_2$-50 wt% NaCl salt mixture, which had been subjected to dehydration process, was placed together with 2 or 4 wt% of ScF_3 powder into graphite crucible over the aluminum sample. Having filled the graphite crucible, Kanthal wire was screwed to the crucible for electrical connection and was covered with alumina sheath for protection against oxidation. Then, the crucible was placed into quartz reaction vessel. Next, the graphite anode sheathed with quartz tube

extended with a Kanthal wire was placed to the polyamid lid and the quartz vessel was closed as shown in Figure 3.1. When the alumina crucible was used as the container for raw materials, the experimental setup shown in Figure 3.2. was used. Three different types of spoon were used as cathode while the graphite rod was used as the anode. In this setup, the salt or salt mixture together with ScF_3 powder was charged in the same manner. The only difference was the way of introducing aluminum into the alumina crucible. The aluminum sample was placed into the cathode spoon with the Kanthal wire extension. Both electrodes were protected by alumina and quartz sheaths against high temperature oxidation. After placing the crucible into the quartz vessel, the cathode spoon and the graphite anode were placed on top of salt together with the polyamide lid. The quartz cell closed and sealed firmly. Finally, the cell vessel was placed into the vertical furnace. After the argon gas connection to the quartz vessel was completed, the heating process was started. In all experiments, the heating program was as such that ramping the temperature firstly to 200^oC at a rate of 3^oC/min and argon rate of about 250 ml/min to remove any residual moisture from the salt. If any moisture condensation was seen in the upper part of quartz vessel, the argon rate was increased to 500 ml/min and the heating process was paused until the moisture was totally removed. Then, the temperature was increased to 800^oC with a heating rate of 6^oC/min. After achieving the operation temperature, a sufficient dwell time was given for stabilization of temperature and homogenization of the salt or salt mixture. Then, electrodes were immersed slowly into the electrolyte to the level which was determined prior to the experiment. It should be noticed that when graphite crucible acting as cathode was used, only the graphite anode was immersed. However, both cathode spoon and the graphite anode were immersed when alumina crucible was used. Having immersed the electrodes into the electrolyte, the electrical connections were made to DC power source as shown in Figure 3.4. Finally, the electrochemical reduction process was started by applying 3.2 V. This value is very close to the theoretical decomposition potentials of $CaCl_2$ (E^o =3.27) and NaCl (E^o = 3.24). However, when overpotentials and the potential drops due to electrolyte resistance

and the electrical connections are taken into account, the operating potential becomes smaller than 3.2 V.

Current versus time diagrams together with calculated electrical charge for each experiment were recorded with utilization of self-made Visual Basic program. The durations of the experiments were determined according to the electrical charge required to reduce added ScF_3. Having reached the theoretical electrical charge requirement, the electrochemical reduction process was terminated by turning off the power supply and the furnace. After that the graphite anode and the cathode (for alumina crucible) were taken out of the crucible and the cell was left to cool down under flow of argon. After the cooling process, solid Al-Sc alloy samples were recovered from the crucible by washing and dissolving solidified salt around the sample. Then, the samples were weighed by a precise balance to determine the weight difference and amount of scandium introduced by electrochemical reduction of ScF_3 and in-situ alloying with liquid aluminum. Finally, the produced alloy samples were analyzed by utilization of different characterization tools for identifying physical and chemical nature of the alloys.

3.3. Electroanalytical Tests

Linear Sweep Voltammetry (LSV) and Cyclic Voltammetry (CV) analyses were done to determine reaction mechanisms and the possible reactions taking place during the experiments by using GAMRY Reference 3000 Potentiostat/Galvanostat/ZRA. The resultant voltammograms were analyzed by Echem Analyst software developed by GAMRY. The experimental setup used for these analyses is shown in Figure 3.10.

Two and three terminal cell setups were used in both tests. The graphite crucible and graphite rod electrode were working electrode and counter electrode, respectively in three-terminal cell setup. Tungsten wire, which is inert in molten salt electrolyte, welded to a Kanthal wire acted as reference electrode. In this setup, half-cell potentials were measured with respect to the reference electrode by changing the potential between working and counter electrodes. On the other hand, the potential difference

between working and counter electrodes with respect to the working electrode was measured in two-terminal electrode setup.

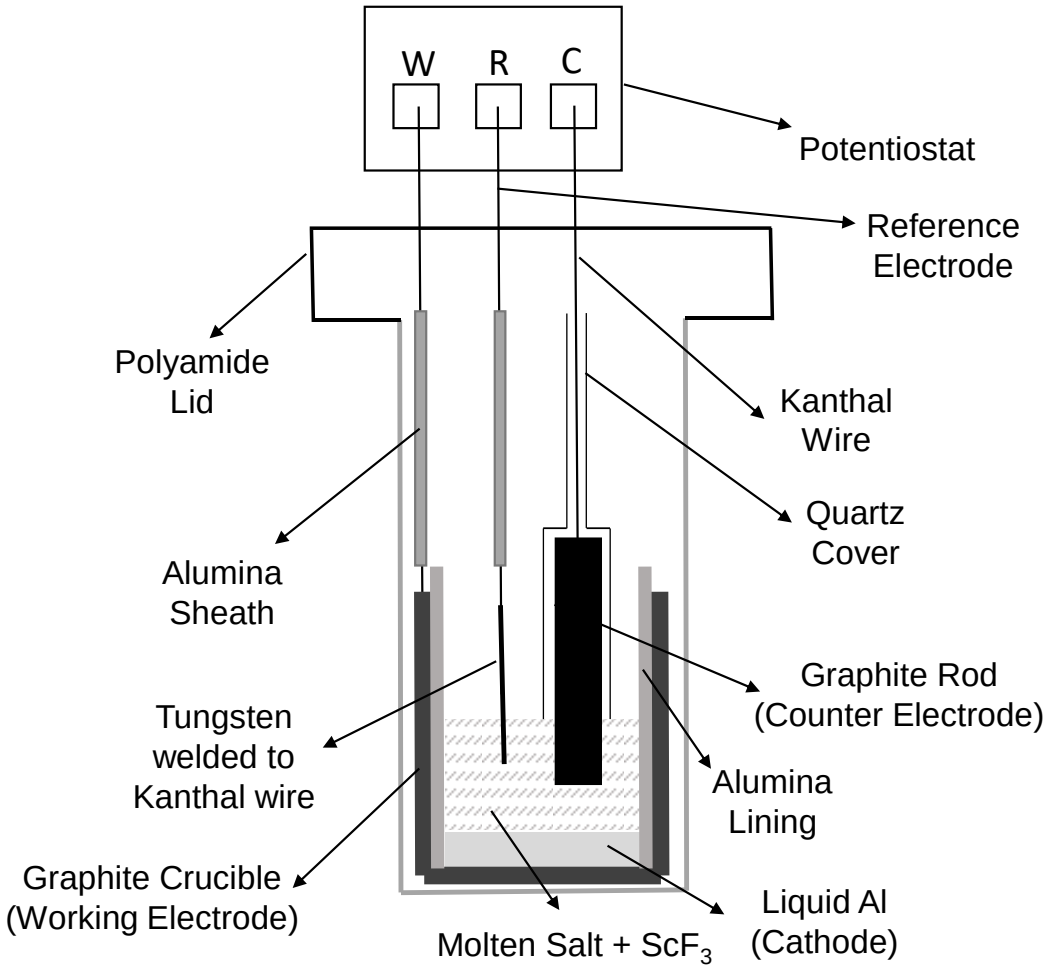

Figure 3.10. Schematic representation of experimental setup used for CV analyses

The procedure of these electroanalytical measurements was similar to the electrochemical reduction experiments. As electrolyte, only $CaCl_2$ salt was used. At the end of the measurements, I-V diagrams were obtained.

3.4. Characterization

Raw materials, electrolysis products and the solidified salt samples were characterized by the characterization tools classified according to type of analysis given in Figure 3.11.

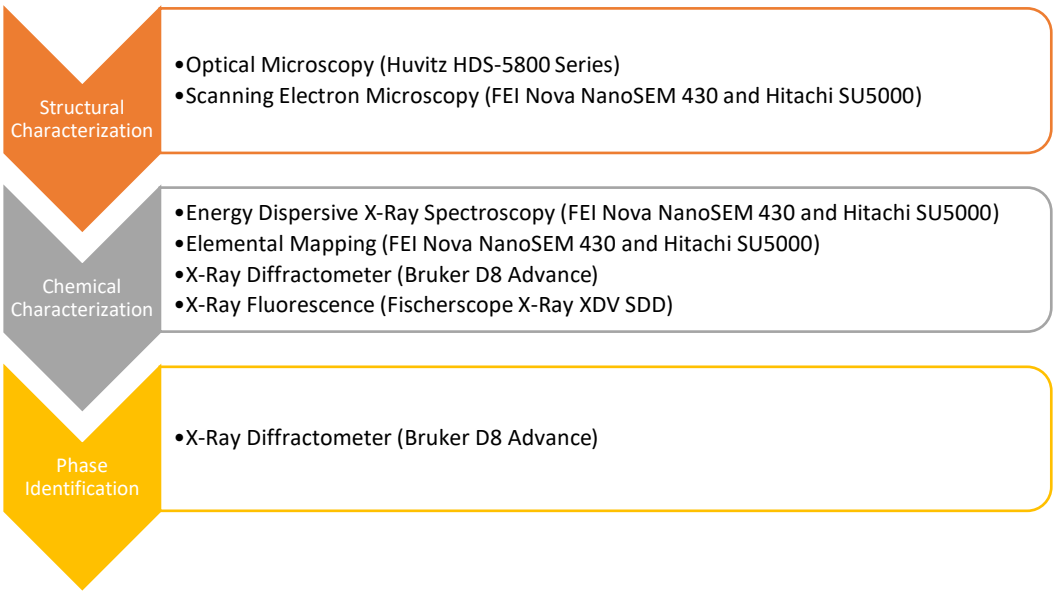

Figure 3.11. Characterization tools used for examination of raw materials and electrolysis products

After electrolysis, the salt layer was removed from Al-Sc alloy samples. The weights of samples were measured with a precision balance to find the amount of Sc accumulated in aluminum matrix from the weight difference before and after the electrochemical reduction.

After weight measurement, the alloy samples were prepared according to the procedure given in Figure 3.12 a-d) for structural examination. Firstly, a thin slice shown by blue color was taken from the middle of the sample for XRD analysis as shown in b. Then, one of the remaining half of the sample (c) was cut perpendicular to the surface showing by blue color as shown in c to obtain the sample in d. Finally,

the samples in c and d were mounted in either into bakalite or epoxy resin. This sample preparation procedure enables to examine Sc distribution through the alloy.

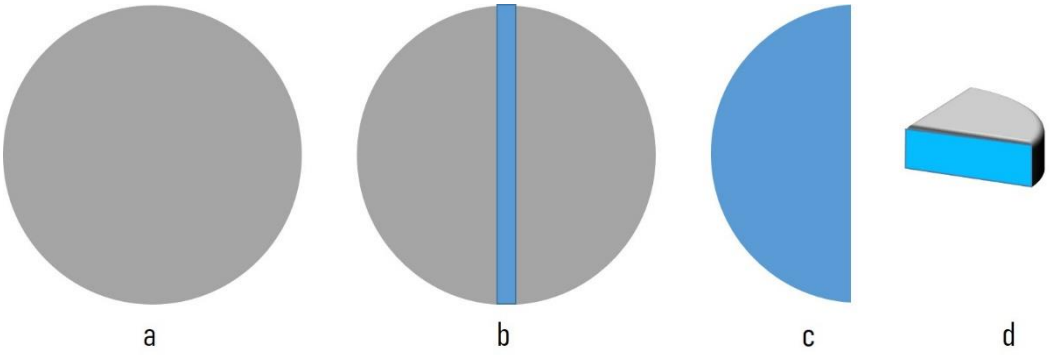

Figure 3.12. Sample preparation procedure for structural examination of an Al-Sc alloy sample

CHAPTER 4

RESULTS AND DISCUSSION

The experimental results are given in two separate parts according to the type of the electrolyte used in this study. The details of all of the experiments are given in Table 4.1. All electrochemical reduction experiments were conducted at 800^{o}C except for Exp.9 which was conducted at 850^{o}C.

Table 4.1. *The details of the experiments conducted in $CaCl_2$ and $CaCl_2$-NaCl mixtures*

Experiment Run	*Applied Voltage (V)*	*Amount of Al charged (g)*	*Amount of ScF_3 (g)*	*Charge passed (C)*	*Theoretical Charge (C)*	*Amount of Al-Sc alloy recovered (g)*	*Theoretical amount of Al-Sc alloy (g)*	*Duration of Experiment (mins)*
Experiments with pure $CaCl_2$ (Weight of Electrolyte : 25 grams)								
1	*	3 (1050)	1.5	18256	4257	3.49	3.661	708
2	2.3	3 (1050)	1.5	2074	4257	3.17	3.661	240
3	3.2	2.66 (6060)	1	3347	2840	3.03	3.10	180
4	3.0	2.64 (6060)	1	3523	2840	2.71	3.08	240
5	3.2	2.53 (6060)	1	3953	2840	2.87	2.97	101
6	3.2	2.79 (6060)	1	6007	2840	2.90	3.23	95
Experiments with $CaCl_2$-NaCl mixtures (Weight of Electrolyte : 25 grams)								
7	3.2	2.44 (6060)	1	3790	2840	2.54	2.88	68
8	3.2	2.32 (6060)	1	4627	2840	2.41	2.76	112
9	3.2	2.73 (6060)	1	5277	2840	2.83	3.17	112
10	3.0	2.78 (6060)	0.5	3939	1420	2.9	3.0	137

*The applied voltage was varied during the experiment to analyze the electrochemical reduction behavior of ScF_3

4.1. Electrochemical Production of Al-Sc Alloys in Molten $CaCl_2$

In the first part of the experimental studies, pure $CaCl_2$ was used as the electrolyte. The experiments were conducted in the electrochemical cell as shown in Figure 3.1 at 800^oC according to the experimental procedure given in the previous chapter. In these experiments, Al-$CaCl_2$ interaction, effect of voltage and duration of the electrolysis on Sc recovery rate and the effect of CaO left from the dehydration process on the purity of Al-Sc alloy were investigated.

The electrochemical reduction process was monitored by a self-made computer program that collecting data every two seconds and giving the corresponding current-time diagram and electrical charge passed through the cell as shown in Figure 4.1.

Figure 4.1. A screenshot from the computer program recording current-time diagram of electrolysis experiments

The progress and duration of the electrochemical reduction of ScF_3 in molten $CaCl_2$ or $CaCl_2$-NaCl mixture were determined according to the Faraday's Law of Electrolysis related to the amount of a substance produced or dissolved electrochemically with the electrical charge passing through the cell as given in the equation 4.1 [62]

$$Q = \int I\, dt = \frac{W_{th} nF}{M_w * CE} \tag{4.1}$$

In this equation, Q represents the total theoretical charge required for electrochemical reduction of ScF_3 in coulombs, I is the current passing through the cell in amperes, t is the duration of electrochemical reduction in seconds, W_{th} is the theoretical weight of the ScF_3 to be reduced in grams, n is the valence number of Sc, F is the Faraday's constant corresponding to 96,485 coulombs/mole and M_w is the molecular weight of the ScF_3 in grams/mole [1]. In the experimental studies, the total theoretical charge required for reduction of 1 gram of ScF_3 was calculated as 2839 coulombs when M_w was taken as 101.95 and n as 3. If all the current passing through the cell was used for the redox reactions meaning that current efficiency is 100%, then the current value achieved at the end of the electrochemical reduction should be close to zero theoretically. However, most of electrochemical processes especially those taking place at high temperatures deviate from the Faraday's Law due to thermodynamic and/or kinetic factors such as back reactions of primary products, side reactions, dissolution of reduced metal in the electrolyte and electronic conduction. The extent of deviation from the Faraday's Law can be expressed numerically by calculating the ratio of actual amount of substance produced or dissolved to theoretical amount. This ratio is also named as current efficiency.

Current versus time diagrams for the selected electrochemical reduction experiments of ScF_3 taking place at a constant voltage at 800°C in molten $CaCl_2$ electrolyte are given in Figure 4.2. These diagrams are plotted in the modified form due to the difficulty of the analysis of the electrochemical behavior of the experiments which will be discussed in the proceeding sections.

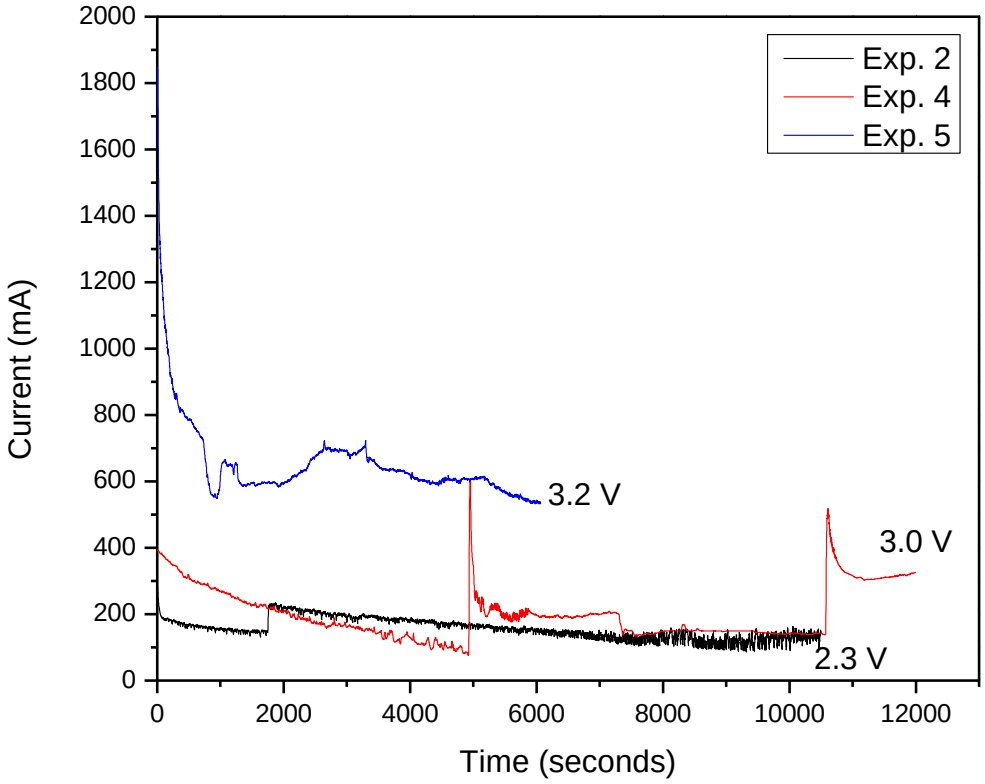

Figure 4.2. Current vs. Time diagrams recorded during electrochemical reduction of ScF_3 in molten $CaCl_2$ at 800ºC with three different applied voltages

Each curve given above is the result of an experiment performed at different applied voltage. The blue curve is for the experiment carried out under 3.2 V. The red curve represents the experiment conducted at 3.0 V. For the black curve, experiment was started at 2.3 V and then the voltage was increased to 2.4 V. As can be seen from each plot, current falls with time. This is due to the fact that current is dependent on time and concentration of electroactive species as stated by Cottrell [102]. The rapid decline of the current in a short time can be attributed to the increase in solution resistance (IR drop) due to beginning of mass transport in the electrolyte. After rapid decline, the current became reasonably constant and achieved steady state condition indicating a homogeneous distribution of applied voltage, concentration and temperature through electrode/electrolyte interface.

Different from the typical current-time response, increases in current at specific instants were seen for Exp.4 and Exp.5. This increase was intentional for both of the experiments to see the effect of voltage and anode-cathode distance (ACD) on the progress of electrochemical reduction experiments. In Exp.2, the increase in the current was due to the increase in the applied voltage from 2.3 to 2.4. On the other hand, the current increased with decreasing ACD from 2 to 1 cm by 0.5 cm steps in different time intervals. Since all experiments were conducted under constant voltage and the applied voltage was the sum of standard potential, anodic and cathodic overpotentials, IR drop due to solution resistance and resistance of electrical connections, any change in the applied voltage and ACD result could be directly seen in the current – time diagram.

After finishing electrochemical reduction experiments, the electrical power was cut, the graphite anode was lifted up and finally, the furnace was turned off. Then, the cell was left to solidify under continuous argon flow. As the temperature of the reaction vessel became closer to room temperature, the argon gas flow was stopped and the vessel was taken out of the furnace. The polyamide lid was opened and the graphite anode and the graphite crucible (cathode) were taken out of the quartz vessel. In Figure 4.3a and b, the photographs of the graphite crucible with alumina lining at the end of an experiment as well as the surface of the solidified salt can be seen. The black layer on the surface of the solidified salt was due to graphite dust accumulation occurring after disintegration of graphite anode in the molten salt during the electrochemical experiments. Below this salt layer, Al-Sc alloy sample, which was produced upon electrochemical reduction of ScF_3 and in-situ alloyed with liquid aluminum, was present. Therefore, after each experiment the salt layer was removed by dissolving it in the water to recover the alloy sample for characterization. Figure 4.3c and d, show the typical appearance of Al-Sc alloy samples obtained after the experiment. As seen in the figures, the solidified alloy samples had a spherical shape due to surface energy minimization and interfacial tension between graphite and liquid aluminum. Sometimes small Al drops together with a big spherical sample as shown in Figure

4.3d was recovered due to the entrapment of the salt into the liquid aluminum and the coalescence behavior of the aluminum sample.

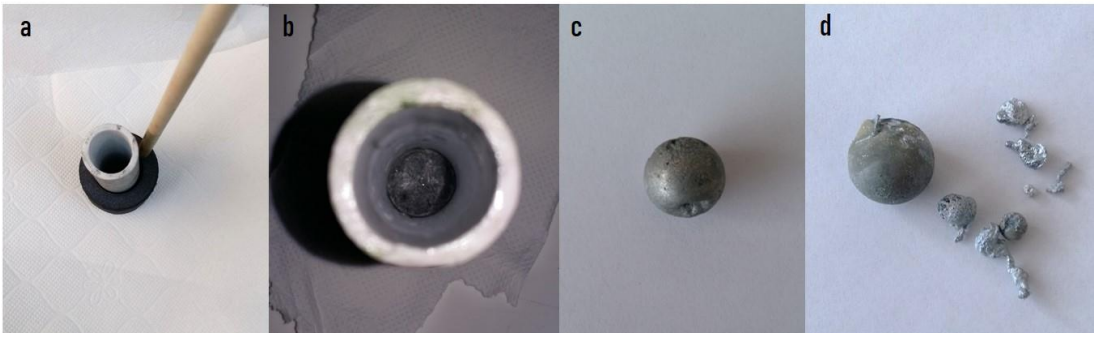

Figure 4.3. The photographs of a) top view of graphite crucible (cathode), b) inner part of graphite crucible with solidified salt, c) solidified Al-Sc alloy sample, d) another Al-Sc alloy sample with small spheres

4.1.1. Graphite-Liquid Aluminum-Molten $CaCl_2$ Interaction

In the electrochemical studies (e.g. electrowinning, electrorefining) involving molten salts as electrolyte, the operating temperature should be slightly greater than the melting point of the salt or salt mixture to ensure completely liquid phase. In this study, $CaCl_2$, which melts at 771°C, was used as the electrolyte and the operating temperature was chosen accordingly as 800°C. During the heating of the solid mixture of aluminum, ScF_3 and $CaCl_2$ before starting the experiment, aluminum was the first constituent transforming into liquid phase due to having the lowest melting temperature as given in Table 4.2. Upon melting of aluminum, $CaCl_2$ will start to melt near 771°C. When the temperature of the system reaches 800°C, the appearance of the system in graphite crucible will be one of the scenarios given in Figure 4.4 depending on the solubility of ScF_3 in molten $CaCl_2$ salt which will be discussed in the proceeding sections.

Table 4.2. *Melting points, Densities at Room Temperature and near Melting Temperatures of Raw Materials used in Experiments* [1]

Raw Material	*Melting Point* (^oC)	*Density at* T_{room} (g/cm^3)	*Density near* $T_{melting}$ (g/cm^3)
Aluminum	660	2.71	2.38
Calcium Chloride ($CaCl_2$)	771	2.15	2.09
Scandium Fluoride (ScF_3)	1541	2.53	-

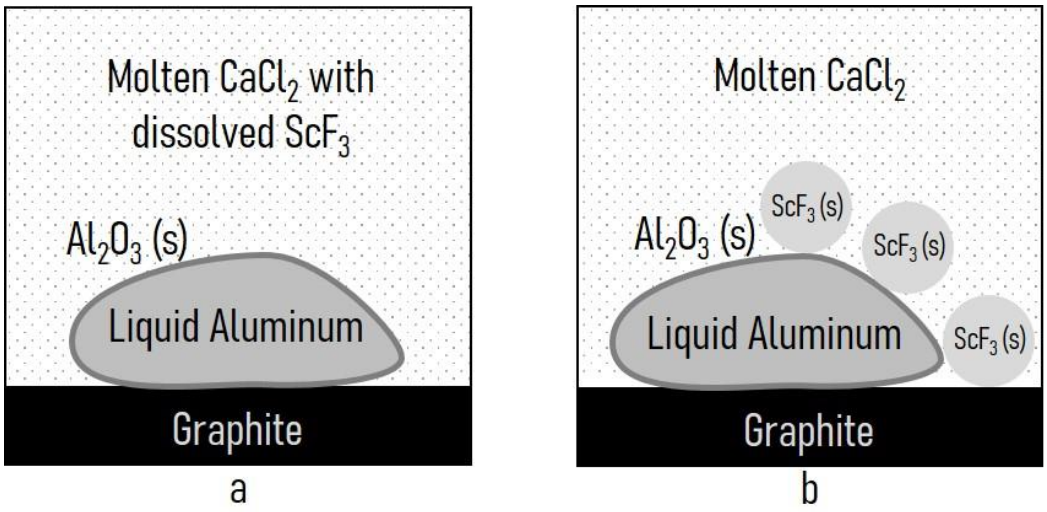

Figure 4.4. The schematic representation of appearance of the system at 800^{o}C when ScF_3 is a) soluble and b) inslouble

According to physical properties given in Table 4.2, liquid aluminum should be at the bottom of the graphite crucible while molten calcium chloride would be on top of liquid aluminum at 800^{o}C due to density difference. A common solid phase appearing in both of the scenarios is aluminum oxide layer covering the liquid aluminum. Due to existence of a very thin layer of the oxide phase, there is a poor wetting between graphite and liquid aluminum with a contact angle greater than 90^o when the temperature of the melt is below 1000^{o}C. Above this temperature, it was argued that wetting started by penetration of liquid aluminum from the defects occurred due to

thermal expansion on the surface of aluminum oxide layer. In addition to these, it is the interfacial tension that gives the equilibrium shape of liquid aluminum given in Figure 4.4. [103,104].

Since the aim is to make the Al-Sc alloy in molten salt medium, the oxide layer covering the liquid aluminum should be removed for diffusion of electrochemically reduced Sc into liquid aluminum. It is well known that molten salts (i.e. alkali or alkaline earth chlorides, fluorides and their mixture) are used as flux materials in secondary aluminum production especially in the recycling of scraps of beverage cans, to strip the oxide layer and facilitate the coalescence of aluminum [105–107]. For this study, molten salt was used as an ionic medium for electrochemical reduction of ScF_3. The effect of the salt on the recovery and coalescence behavior of Al-Sc alloy will be discussed in the next section.

4.1.2. Recovery and Coalescence Behavior of Al-Sc Alloy

Coalescence of metal droplets in molten salt is dependent on the ability of the salt or salt mixture to strip the oxide layer. For the case of aluminum, there is always a thin layer of protective oxide film covering the metal and it becomes more stable as the aluminum gets purer. Therefore, the choice of the aluminum grade for alloying with Sc is critical to obtain a one-piece sample in terms of process efficiency and qualitative analysis.

In Figure 4.5a and b, the photographs of the alloy samples prepared for microstructural examination are seen. For both of the samples, the same amount of aluminum (1050 grade aluminum chips obtained by cutting the tube) was used. The difference between these alloys was the contact time between the molten aluminum and the molten salt. It can be deduced from these figures that the exposure time of direct contact of molten aluminum and molten salt affects the coalescence behavior drastically.

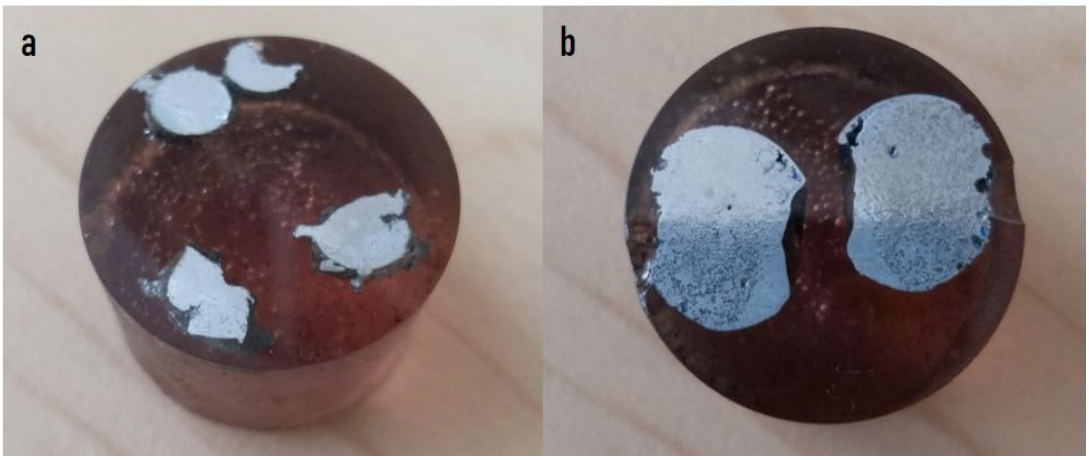

Figure 4.5. The photographs of the Al-Sc alloys recovered after a) 4 hours and b) 11 hours 48 minutes (Matrix material: 1050 grade aluminum)

As stated in the study of Roy et.al [106], the coalescence ability of chloride melts is poor and it is necessary to wait for hours to have i) penetration of the salt from the cracks on the outer surface of oxide due to the thermal stress, chemical attack of the salt ii) weakening of the oxide layer and iii) stripping of the oxide layer. Addition of several fluoride salts (e.g. NaF, CaF_2, LiF, KF, Na_3AlF_6) with a considerably low amount as flux into the chloride melts was found to decrease the time required for coalescence from hours to a few minutes due to the ability of the fluorides to dissolve the oxides. When chloride and fluoride melts were compared in terms of the metal loss after coalescence tests, the metal loss in the chloride melt was found to be considerably low [106].

Since the salt mixture used in the experimental studies were chloride based and the initial aluminum contained low amount of alloying element for scandium to be effective as an alloying element, 6060 grade aluminum alloy available in extruded bar form was used as the aluminum raw material instead of the 1050 grade aluminum. It has been experienced that charging one piece of cylindrical sample cut from 6060 grade extruded bar instead of several pieces of chips cut from 1050 grade tube decreased the total surface are of aluminum oxide layer being in contact with the

molten salt. Furthermore, it is believed that the presence of Mg and Si in aluminum matrix decreased the activity of aluminum oxide due to presence of oxides of Mg and Si and had a positive effect on the coalescence behavior of the aluminum and hence the metal recovery from the salt.

4.1.3. Characterization of Al-Sc Alloys produced in Molten $CaCl_2$

Al-Sc alloy samples recovered at the end of the experiments always had a salt film covering the outer surface or the salt entrapment in the aluminum matrix since aluminum solidifies before the salt and the chloride salts are not soluble in the aluminum matrix [105–107]. This makes sample preparation process challenging. Thus, the salt in the form of entrapped inclusion or film covering the aluminum was removed by dissolving it in a suitable solvent like water, alcohol or acetic acid before structural examination.

After removing the salt from the recovered Al-Sc alloy samples, the weight of the samples were measured with a precision balance to find the amount of Sc accumulated in aluminum matrix from the weight difference before and after the electrochemical reduction. The weight measurements and the duration of the selected experiments are presented in Table 4.3.

Table 4.3. *The details of the selected experiments conducted in molten $CaCl_2$*

Experiment Run	*Amount of Al charged (g)*	*Amount of ScF_3 (g)*	*Charge passed (C)*	*Theoretical Charge (C)*	*Amount of Al-Sc alloy recovered (g)*	*Theoretical amount of Al-Sc alloy (g)*	*Duration of Experiment (mins)*
2	3 (1050)	1.5	2074	4257	3.17	3.67	240
4	2.64 (6060)	1	3523	2840	2.71	3.08	240
5	2.53 (6060)	1	3953	2840	2.87	2.97	101

In Figure 4.6 a-f), the optical microscopy images of Al-Sc alloy samples produced at different applied voltages in molten $CaCl_2$ are shown. They were etched with Keller's reagent, which is a typical etchant for aluminum alloys, for revealing the contrast

between aluminum matrix and the intermetallic phases. As can be seen from a-c), the phase fraction of Sc in Al matrix increased with increasing applied voltage. At the same anode-cathode distance, an increase in the applied voltage will cause increase in the current passing through the cell and the amount of Sc reduced electrochemically will increase in accordance with the Faraday's law.

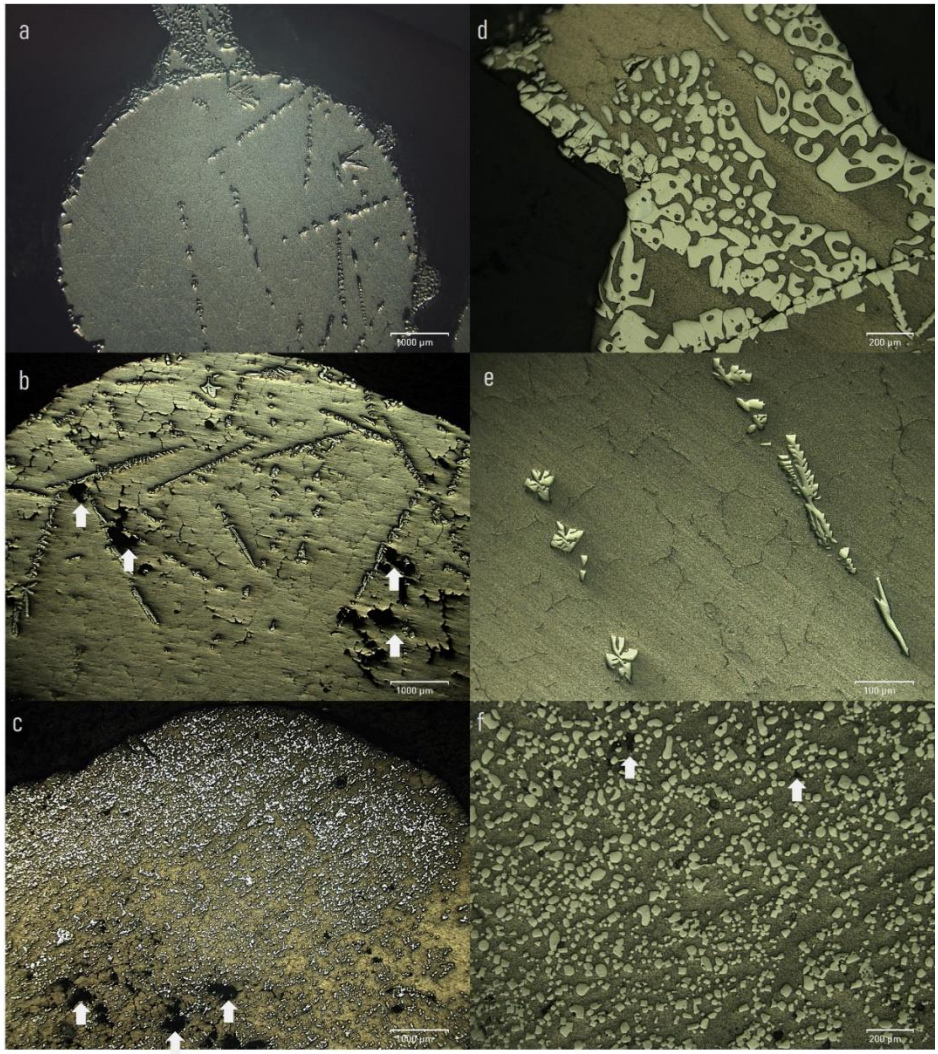

Figure 4.6. Optical microscopy images of etched Al-Sc alloy samples produced in molten $CaCl_2$ salt at 800°C under a) and d) 2.3 V, b) and e) 3.0 V, c) and f) 3.2 V

Other remarkable details in the optical microscopy images are the Al-Fe-Si intermetallics (Figure 4.6e) and surface cavities (Figure 4.6b,c and e) spread over the aluminum shown by white arrows due to salt entrapment in aluminum matrix. In the same figures (a-c), surface segregation of white Al-Sc intermetallic particles can be seen clearly due to the enrichment of scandium rich intermetallic at the surface with respect to the bulk concentration.

According to the ratio of weight of recovered Al-Sc alloy to weight of Al raw material, which can be calculated from the values given in Table 4.3, it is expected to produce Al-Sc alloys with scandium weight percent ranging between 5-12. When Al-Sc binary phase diagram [92] given in Figure 4.7 is analyzed, it is obvious that the equilibrium microstructure should include alpha aluminum as matrix and Al_3Sc as the intermetallic phase.

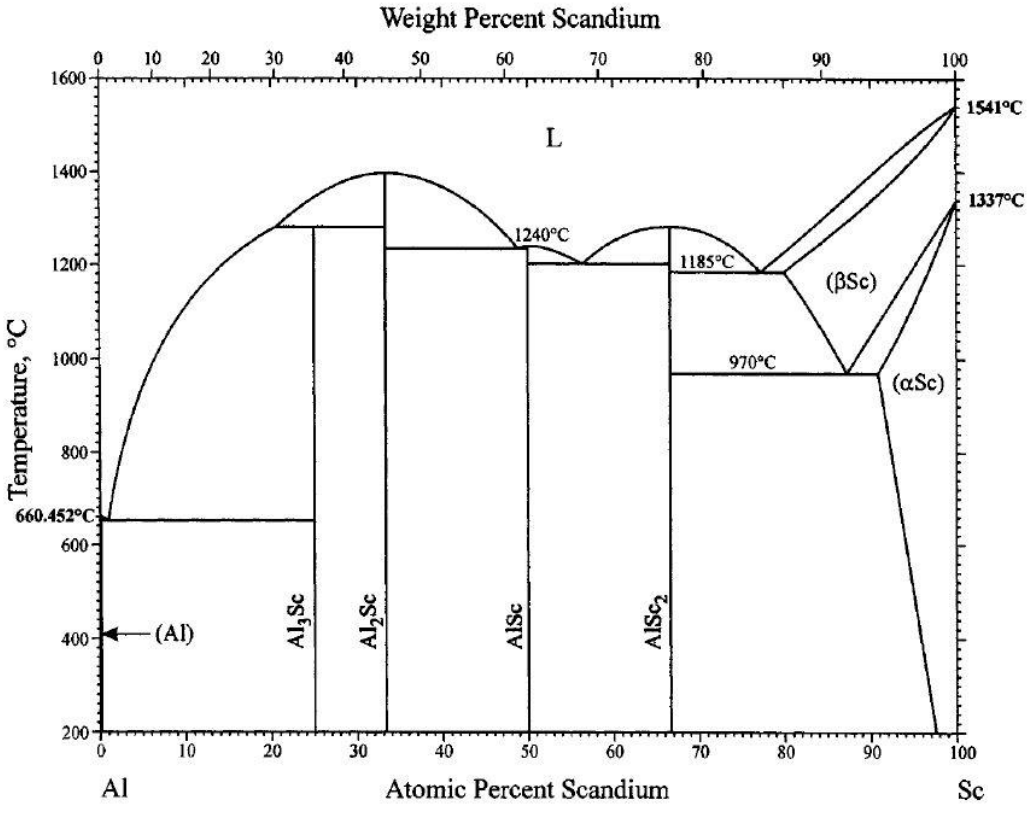

Figure 4.7. Al-Sc Binary Phase Diagram [92]

To verify the microstructure with the Al-Sc phase diagram, SEM-EDS analysis was performed from a few of the white intermetallic particles shown in optical micrographs in Figure 4.6. The result of one of EDS analyses is given in Figure 4.8.

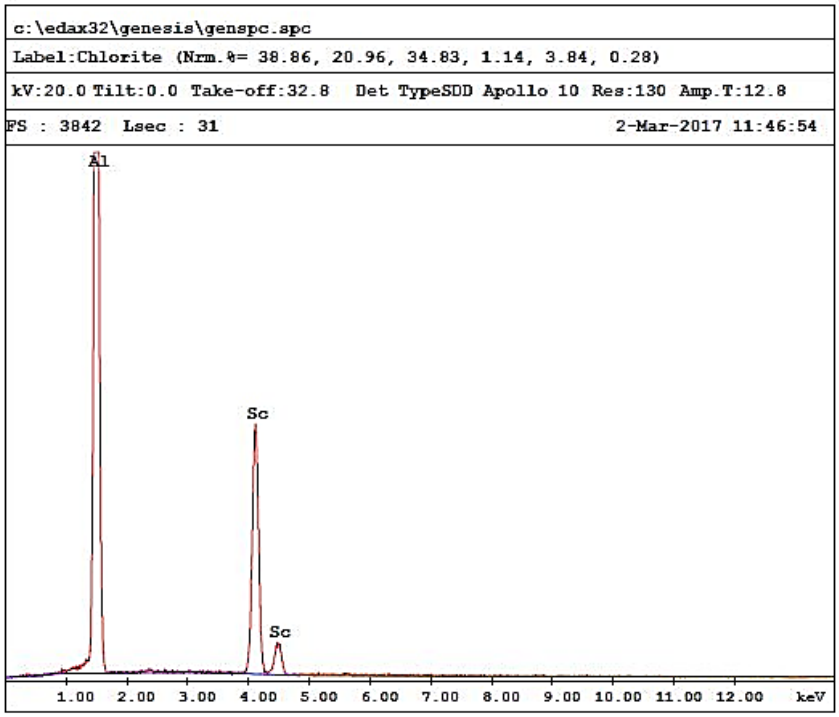

Element	Wt %	At %	K-Ratio	Z	A	F
AlK	63.89	74.67	0.4882	1.0222	0.7462	1.0017
ScK	36.11	25.33	0.3197	0.9553	0.9266	1.0000
Total	100.00	100.00				

Element	Net Inte.	Bkgd Inte.	Inte. Error	P/B
AlK	1612.98	7.67	0.45	210.35
ScK	542.02	9.46	0.78	57.31

Figure 4.8. A representative SEM-EDS analysis result of a white intermetallic particle of Al-Sc alloy

As seen from the EDS result, there is a 3:1 ratio between the atomic percentages of Al and Sc which indicates that the stoichiometric Al-Sc intermetallic compound is Al_3Sc. In addition to the SEM-EDS analysis, two thin slices taken from the Al-Sc alloys produced at different applied voltages were analyzed under X-Ray Diffractometer. The resultant XRD patterns of two Al-Sc alloy samples are given in Figure 4.9 and

Figure 4.10. As seen in these figures, the number of Al_3Sc peaks increases with the increase in the applied voltage values which is an indication of the increase in the amount of Sc in the aluminum. Sc distribution throughout the Al matrix and the segregation of Sc near the surface along with voltage change, affect the intensity and the number of Al_3Sc peaks in the resultant XRD pattern. This can be verified from the optical micrographs in Figure 4.6. For instance, the XRD pattern given in Figure 4.9 corresponds to the optical microscopy image in Figure 4.6b where Sc in the form of Al_3Sc segregated near the surface and there was a decreasing trend of Sc concentration from surface to the center of the sample. On the other hand, Sc distribution was relatively homogeneous in Figure 4.6c although the segregation behavior of Sc existed in this sample. Therefore, the resultant XRD pattern of this sample involved more apparent Al_3Sc peaks with higher intensities.

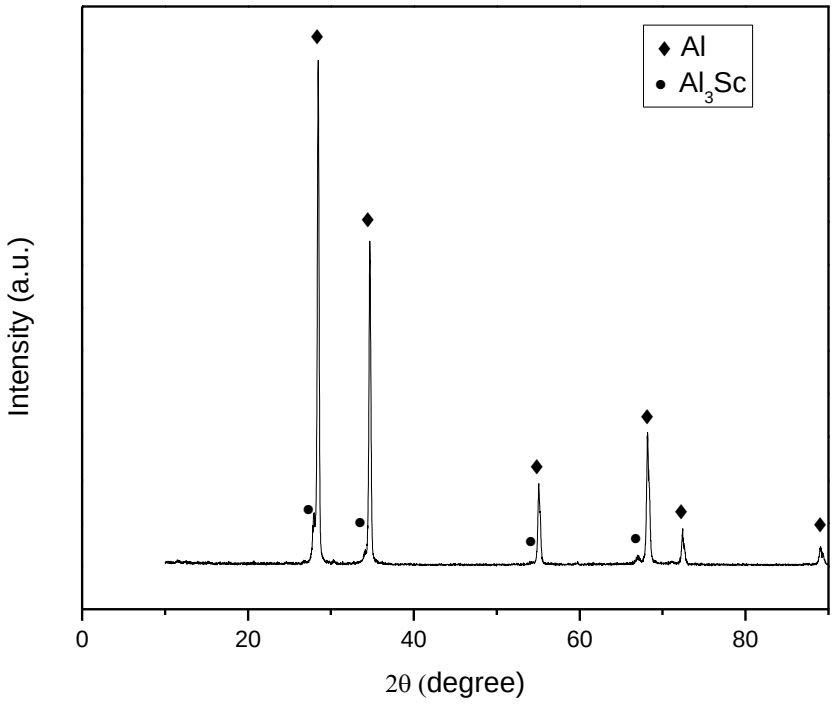

Figure 4.9. XRD Pattern of an Al-Sc alloy sample produced in molten $CaCl_2$ at 3.0 V

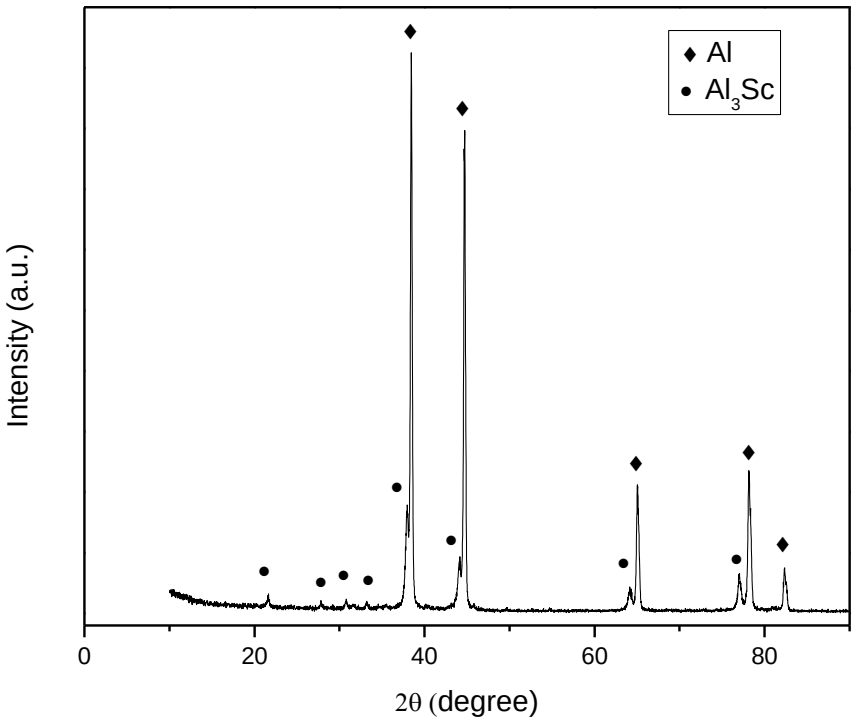

Figure 4.10. XRD Pattern of an Al-Sc alloy sample produced in molten $CaCl_2$ at 3.2 V

4.1.3.1. Calcium Contamination in Al-Sc Alloy produced in Molten $CaCl_2$

In the electrochemical studies using pure $CaCl_2$ as the electrolyte, it is inevitable that $CaCl_2$ is going to contain certain amount of CaO left from thermal drying process which is a commonly applied process for $CaCl_2$ due to its strong affinity to moisture [101]. Fray et.al. [108] reported that CaO content in thermally dried $CaCl_2$ could be decreased to 0.1wt% with a controlled drying process. The presence of CaO in $CaCl_2$ may affect adversely the electrochemical processing by taking part in the electrode reactions and cause calcium contamination in the product.

In the production of Al-Sc alloy in molten $CaCl_2$, calcium contamination was observed in the form of Al-Ca intermetallics. In order to visualize and compare the extent of calcium contamination in Al-Sc alloys produced in molten $CaCl_2$, two of the alloy

samples were chosen and analyzed with EDS Mapping and XRD. The experimental details for both of the samples are tabulated and presented in Table 4.4.

The salt used as the electrolyte was different for the samples, while Al raw material, the heating rate in the preheating step and the applied voltage were the same. Another important detail was the exposure time of salt to air. It was known that the salt preparation procedure for the 6th run was longer. Thus, the expectation was that the extent of calcium contamination in the alloy of the 6th run would be larger.

Table 4.4. *The details of preheating process and experimental variables for selected experiments conducted in molten $CaCl_2$*

Experiment Run	*Al Raw Material*	*Type of Salt*	*Heating Rate* ($^oC\ min^{-1}$)	*Applied Voltage (V)*
3	AA 6060	$CaCl_2.2H_2O$	3	3.2
6	AA 6060	Anhydrous $CaCl_2$	3	3.2

In Figure 4.11 and Figure 4.12, the elemental mapping analysis results are shown for both of the alloys. The common elements appearing in both of maps are Al, Sc, Ca and Fe. The presence of Si in the second map (Figure 4.12) can be attributed to the segregation or change in the distribution of elements in the representative section of the alloy sample. As can be seen, Si atoms were clustered in a specific region where Ca atoms were present. On the other hand, eutectic Al-Ca intermetallic particles were precipitated along grain boundaries and faceted Al_3Sc intermetallic particles precipitated randomly in the aluminum matrix.

According to EDS analysis taken from Al-Ca eutectic particles, the ratio of atomic percentages of Al and Ca was 4:1. Thus, the chemical formula of eutectic Al-Ca phase was Al_4Ca as shown in Figure 4.13. In addition to EDS analysis, a sample taken from alloy obtained after the 6th experiment was examined under XRD. According to XRD pattern given in Figure 4.14, the presence of Al_4Ca can be also verified.

The presence of Al_4Ca in aluminum matrix affects both purity of Al-Sc alloy product and interferes the electrochemical processing. However, formation of Al_4Ca can be inhibited by decreasing the amount of CaO in $CaCl_2$ with a controlled dehydration and preheating process conducted at a heating rate as slow as possible. An alternative way is the use of a suitable $CaCl_2$ based salt mixture such as $CaCl_2$ – NaCl and $CaCl_2$ – LiCl to decrease activity of CaO.

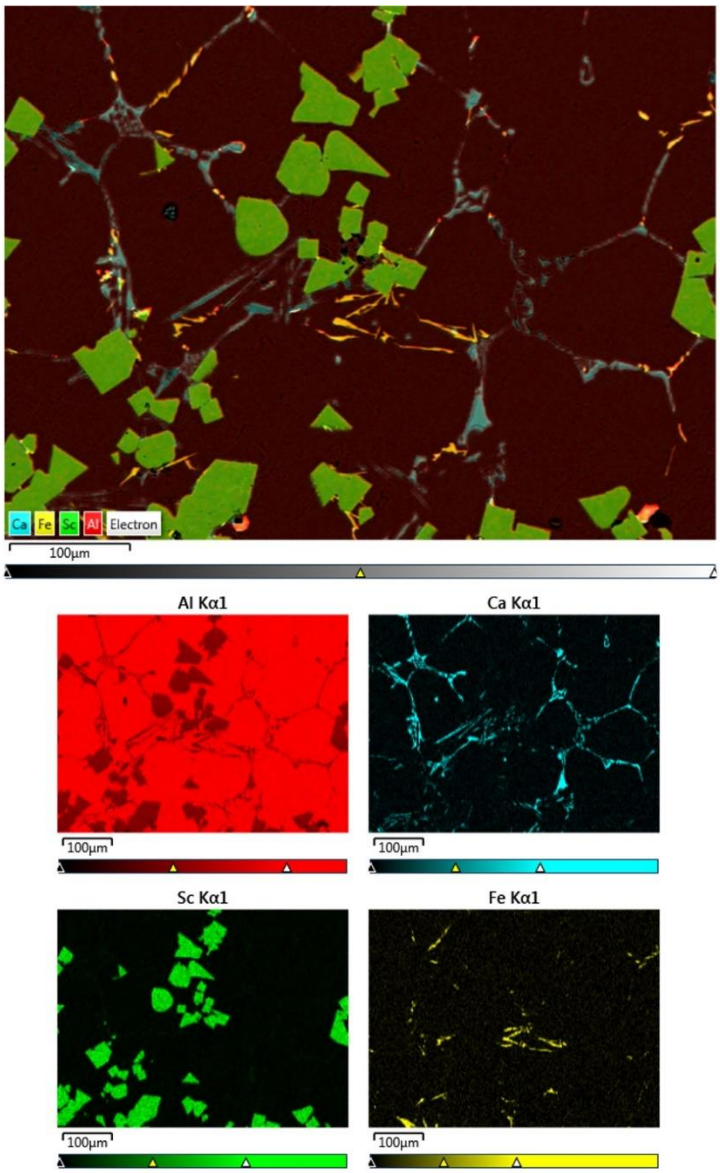

Figure 4.11. Elemental Mapping of the Al-Sc alloy recovered after the 3rd experiment

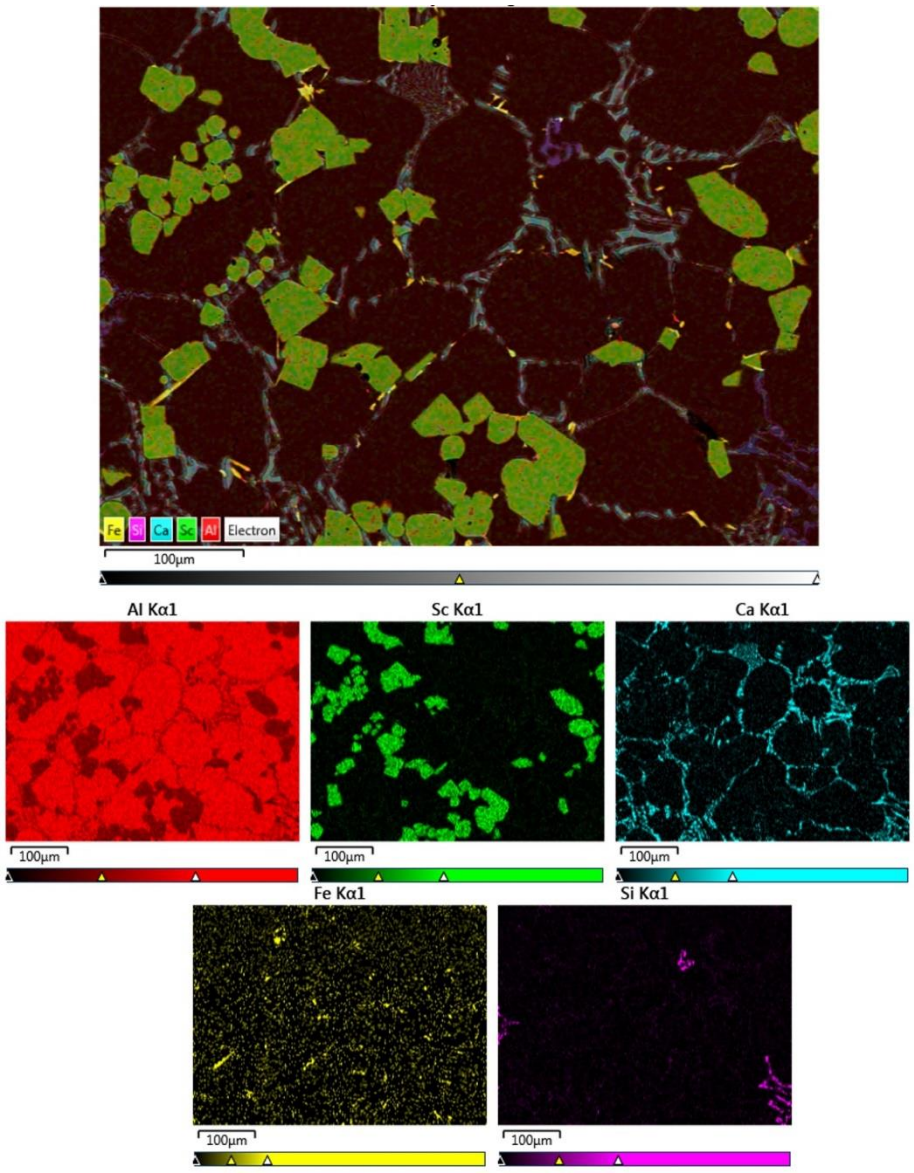

Figure 4.12. Elemental Mapping of the Al-Sc alloy recovered after the 6th experiment

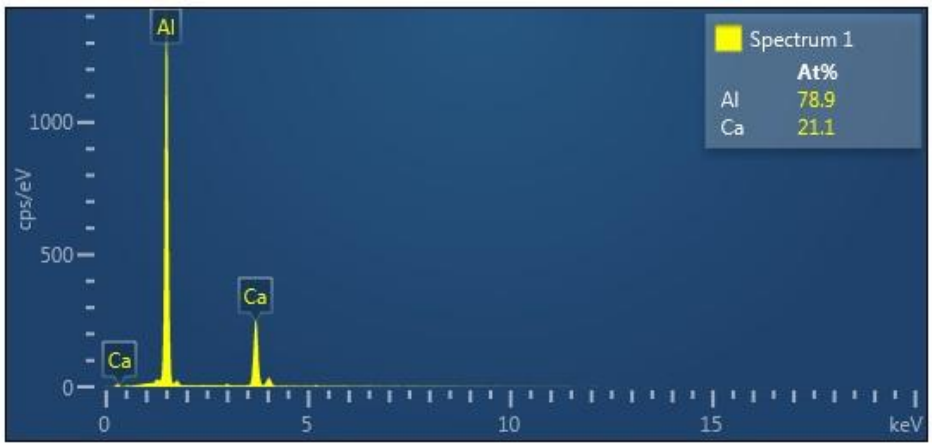

Figure 4.13. SEM-EDS analysis of eutectic Al-Ca intermetallics

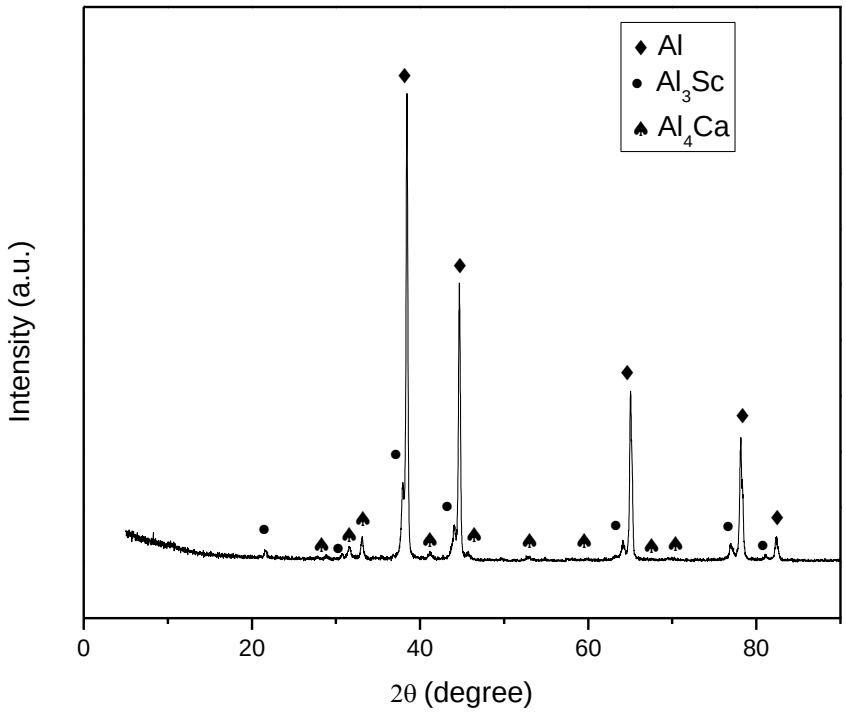

Figure 4.14. XRD pattern of the Al-Sc alloy sample recovered from the 6th experiment

4.2. Electrochemical Production of Al-Sc Alloys in Molten $CaCl_2$-NaCl Mixture

In the previous section, electrochemical production of Al-Sc alloys in molten $CaCl_2$ was discussed and it was concluded that Sc recovery rate increased with increasing applied voltage and CaO in the salt should be controlled in order not to have an impure Al-Sc alloy product and poor process efficiency. In the light of these findings, it was decided that the electrolyte composition should be changed by adding other salts into the calcium chloride. It is well known that the mixtures of alkali and alkaline earth chlorides have several advantages such as low temperature eutectic points, high electrical conductivity, stability in high operation temperatures. Among the mixtures of chlorides with $CaCl_2$, $CaCl_2$-NaCl binary mixture was chosen due to availability of both salts and the features of water solubility, nontoxicity and high electrical conductivity [109]. In addition to these, this mixture has a unique stable liquid phase over a large composition region at 800°C which is the operating temperature of experiments as shown in Figure 4.15 [110].

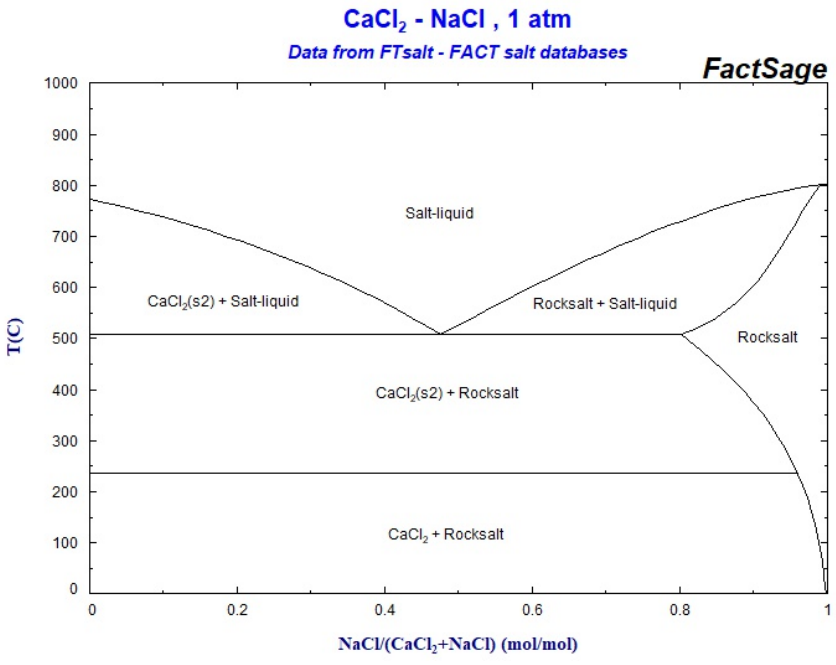

Figure 4.15. $CaCl_2$-NaCl binary phase diagram [110]

The present section will therefore focus on the experimental studies carried out in $CaCl_2$-NaCl mixture where the same electrochemical cell setup given in Figure 3.1 was used at 800^oC in accordance with the experimental procedure given in the previous chapter. In the experiments, the applied voltage and operating temperature were determined as 3.2 V and 800^oC, respectively, for higher Sc recovery rate and faster reactions kinetics in liquid aluminum-liquid salt system. It should be noted that when pure $CaCl_2$ was used as the electrolyte, the operating temperature should be greater than the melting point of this salt. However, when a salt mixture is used instead of a pure salt as electrolyte, the new criterion for operating temperature becomes the eutectic point of the interested salt mixture. Although $CaCl_2$-NaCl mixture makes it possible to work at as low as 504^oC which is below the melting point of aluminum acting as cathode and collector metal of Sc, the operating temperature was kept constant as 800^oC to avoid slow mass transportation and dendritic growth in solid state. During the experiments, two different electrolyte compositions were used such as $CaCl_2$-20wt%NaCl (X_{NaCl}:0.32) and $CaCl_2$-50wt%NaCl (X_{NaCl}:0.65).

In Figure 4.16, current versus time diagrams for three of the experiments taking place in molten $CaCl_2$-NaCl salt mixtures with different electrolyte composition and temperature are given. The sudden current increases in first 15 minutes, 45 minutes and 60 minutes can be clearly seen. As the content of NaCl in the electrolyte increased along with temperature, the sudden current increases were gradually postponed which might have been due to increase in electrical conductivity of the molten salt.

The sudden current increases can be attributed to several cases such as gas evolution and escape from the surface of graphite anode and the direct contact between freshly formed solid Al_3Sc intermetallics on liquid aluminum-molten salt interface with graphite anode causing short circuit or current spikes. However, the gas evolution in the present experimental condition was not an expected case. The most probable cause of sudden current increases was the accumulation and movement of freshly formed solid Al_3Sc particles towards the surface of graphite anode.

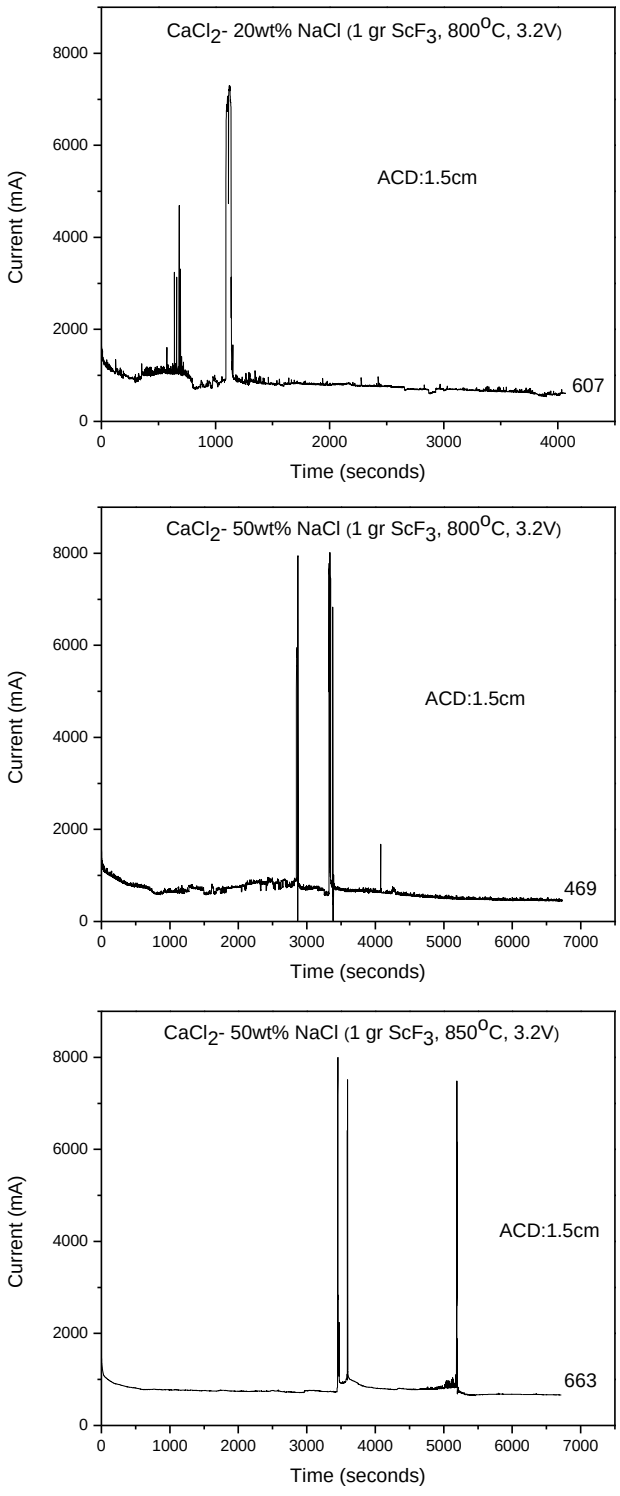

Figure 4.16. Current vs. Time diagrams recorded during electrochemical reduction of ScF_3 in molten $CaCl_2$-NaCl mixtures

The sudden increases in current were avoided by moving the graphite anode up and down whose effect can be seen as the secondary increases from the current-time diagrams.

The presence of large current fluctuations in the current-time diagrams inhibits the accurate discussion of the electrochemical behavior of the experiments. Therefore, the sudden current increases taking place in a short time period (i.e. a few minutes) were omitted from the recorded data to obtain a typical current-time response of an electrochemical cell for a better understanding.

The modified current-time diagrams for the experiments carried out in molten $CaCl_2$ – NaCl mixture are given in Figure 4.17a and b. In both figures, the effect of changing electrolyte composition on the electrochemical behavior of the system for the reduction of 1 gram of ScF_3 at 800^oC and under 3.2 V is shown. In Figure 4.17a, the gradual increase in the current after the initial decay and high background current were remarkable for molten $CaCl_2$ – NaCl mixtures as compared to pure molten $CaCl_2$. This was probably due to the electronic conduction caused by the carbon dust spread over the molten salt. After each experiment, a black layer was seen on the surface of the solidified salt which originated from the carbon dust due to disintegration from graphite electrode as shown in Figure 4.3b. There are several reasons for disintegration of carbon particles from the surface of graphite: i) air leakage into the reactor and subsequent oxidation of carbon, ii) absorption of molten salt into the micro pores on the surface of the graphite, iii) the reaction between CaO and C when CaO present in the electrolyte and subsequent formation of CO or CO_2 and CO_3^{2-} ion by dissolution of one of the oxides of the carbon in the molten salt and transformation of CO_3^{2-} ion to solid carbon via electrochemical reduction. The first two statements were more probable for the current cell while the last one was not and it is generally observed in the electrodeoxidation of metal oxides [111].

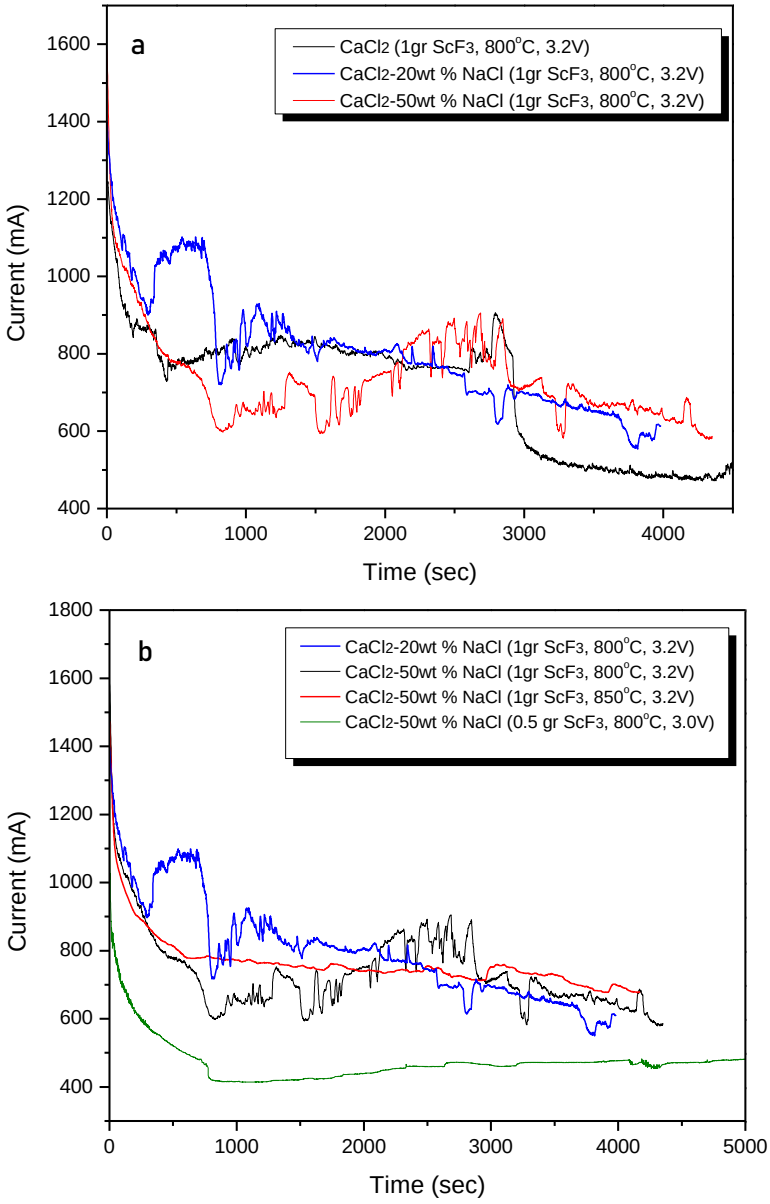

Figure 4.17. Comparison of Current vs. Time diagrams of the experiments conducted in a) molten $CaCl_2$ and $CaCl_2$-NaCl mixtures at 800ºC and b) molten $CaCl_2$-NaCl mixtures at different temperatures

On the other hand, when the current-time diagrams of the experiments in $CaCl_2$-NaCl mixtures in Figure 4.17b are compared, it was seen that the time of achieving steady-state got shortened with increasing electrical conductivity of salt upon increasing the content of NaCl and the temperature. This effect is more pronounced for the diagram plotted with red color. Another important detail in the same figure is the current-time behavior of the curve plotted with green color. The current-time diagrams plotted with blue, red and black color were in modified form due to the sudden current increase. However, the one indicated by green color was in its original form. This behavior could be attributed to relatively slower electrochemical reduction rate due to voltage decrease and the increase in energy required to reduce ScF_3 with decreasing the activity of ScF_3 in the molten $CaCl_2$-50wt%NaCl mixture as compared to the activity of 1 gr ScF_3 in the same molten salt mixture.

4.2.1. Characterization of Al-Sc Alloys produced in Molten $CaCl_2$-NaCl Mixture

The Al-Sc alloys recovered from molten $CaCl_2$-NaCl mixtures exhibited similar behavior with the ones recovered from pure molten $CaCl_2$ in terms of the graphite-aluminum-salt interaction and coalescence. Therefore, the final shapes of the Al-Sc alloy samples were closer to spherical form as shown in Figure 4.3c and d, except for one alloy sample in Figure 4.18a, which climbed upwards to the surface of alumina tube acting as a protective layer to inhibit interaction between graphite crucible and graphite electrode.

As in the previous case, the solidified salt layer on the surface of the samples was removed using suitable solvents. Then, the weights of the alloy samples were measured and tabulated together with other experimental details in Table 4.5.

Table 4.5. *The details of the selected experiments conducted in molten $CaCl_2$ – 50 wt% NaCl mixture*

Experiment Run	*Amount of Al charged (g)*	*Amount of ScF_3 (g)*	*Charge passed (C)*	*Theoretical Charge (C)*	*Amount of Al-Sc alloy recovered (g)*	*Theoretical amount of Al-Sc alloy (g)*	*Duration of Experiment (mins)*
8	2.32 (6060)	1	4627	2840	2.41	2.76	112
9	2.73 (6060)	1	5277	2840	2.83	3.17	112
10	2.78 (6060)	0.5	3939	1420	2.82	3.0	137

In Figure 4.19a, the alloy solidified upwards on the surface of alumina with its tiny particles is shown. The solidification direction of the alloy is indicated by a blue arrow. The reason of such a behavior can be explained by the decrease in surface tension and wetting angle between aluminum-alumina interface upon increase in temperature [112]. In addition, the movement of Al_3Sc intermetallic particles, which become more mobile with increasing temperature, in a less viscous liquid aluminum may have a role in such behavior.

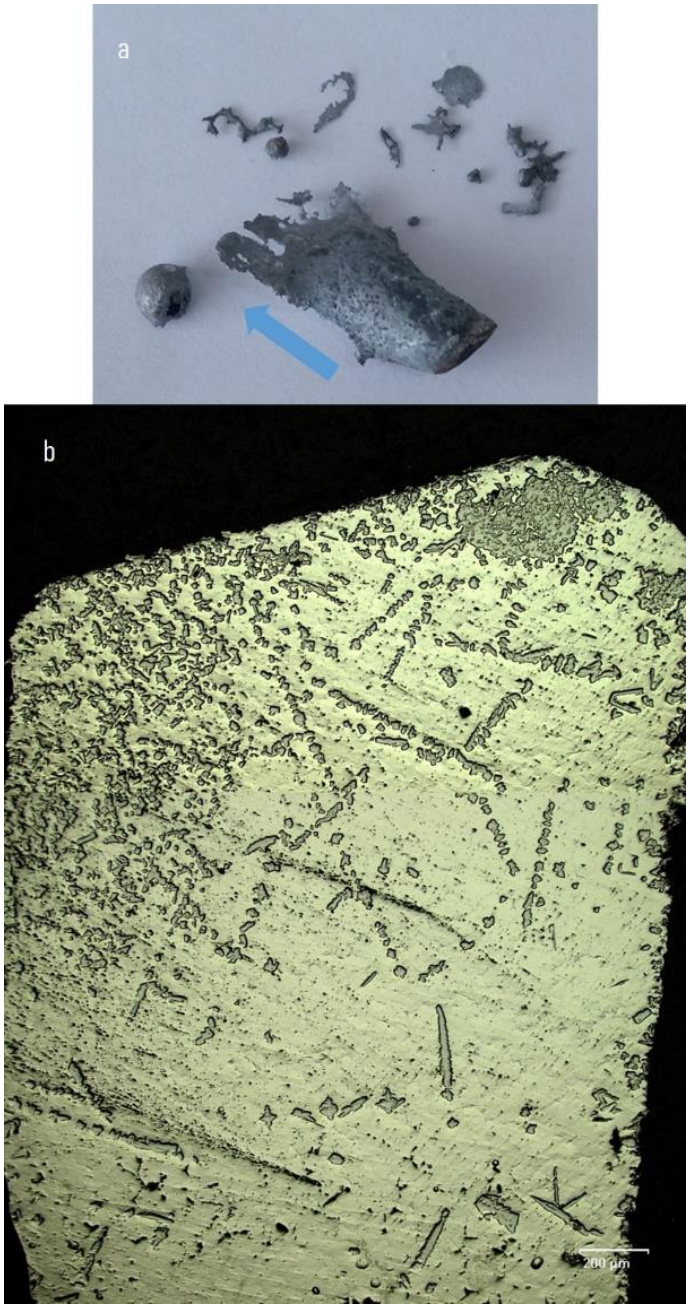

Figure 4.18. a) Al-Sc alloy produced in molten $CaCl_2$-50wt%NaCl at 850ºC and 3.2 V and b) the corresponding as polished microstructure of the same alloy

In Figure 4.19 a-d), the optical microscopy images of Al-Sc alloy samples produced at different applied voltages in molten $CaCl_2$-50wt%NaCl at 800ºC are shown. The images were taken in polished condition. As can be seen, the surface segregation of Al_3Sc intermetallics seemed to be a common problem in Al-Sc alloys which is independent from the electrolyte composition. In Figure 4.19b and d, the effect of faster cooling rate on microstructure of the Al-Sc alloy cooled in air is shown. Since the time for diffusion of Sc from surface to middle part is very short (see Figure 4.19b) as compared to the furnace cooled alloy sample shown in Figure 4.19a, the Al3Sc intermetallics were clustered in limited region and could not grow as much as the ones cooled in a furnace environment.

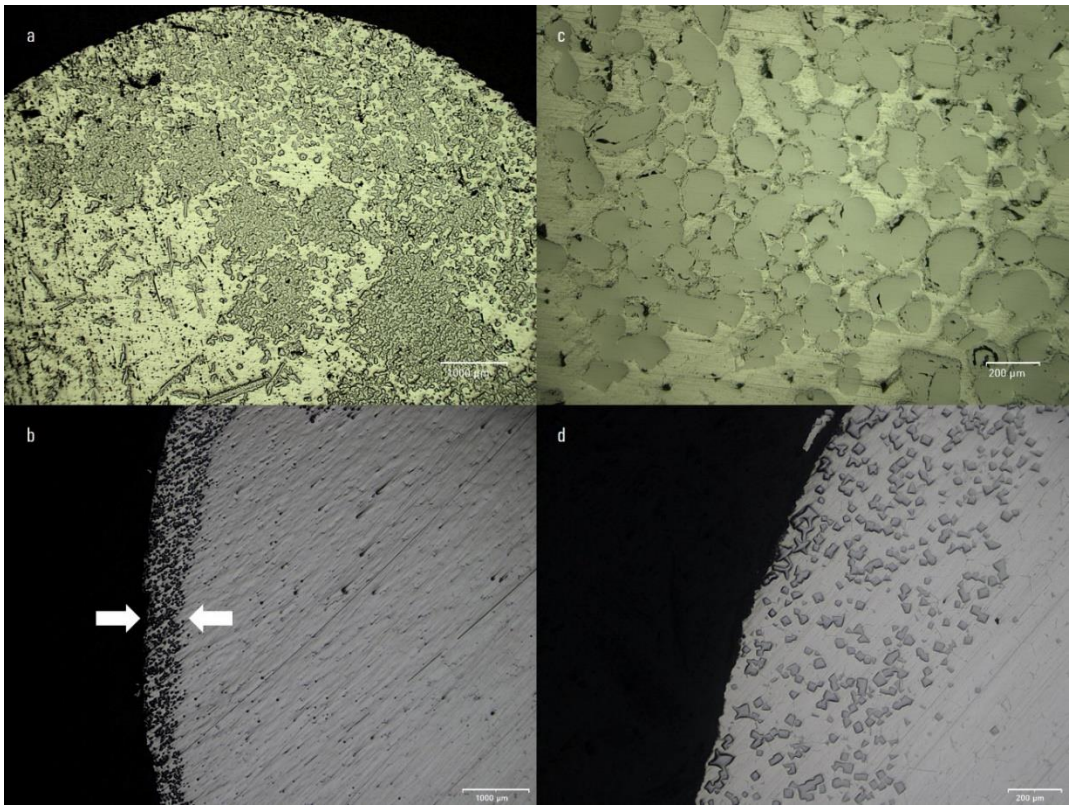

Figure 4.19. Optical microscopy images of as polished Al-Sc alloy samples produced in molten $CaCl_2$-50wt%NaCl salt at 800ºC under different applied voltages: a) and c) 3.2 V, b) and d) 3.0 V

At the very beginning of this section, it was stated that the primary aim of using $CaCl_2$-NaCl salt mixture as the electrolyte was to find a remedy for the calcium contamination problem by decreasing the activity of CaO. In the optical microscopy images given above, such a problem was not observed. For a better understanding, same alloys examined under optical microscopy, were also examined by elemental mapping technique under SEM. The results of this examination are given in Figure 4.20. The elemental mapping images are correspondent to the optical microscopy images given in Figure 4.19c and d, respectively. Calcium element was not detected in this analysis as expected. In addition to elemental mapping analysis, two alloy samples produced at the same temperature and voltage in different molten salt mixtures were analyzed with XRD to see whether the composition of electrolyte affected the calcium contamination. According to the results of the XRD analysis given in Figure 4.21a and b, the indicator of calcium contamination, Al_4Ca, was not detected by XRD analysis, either.

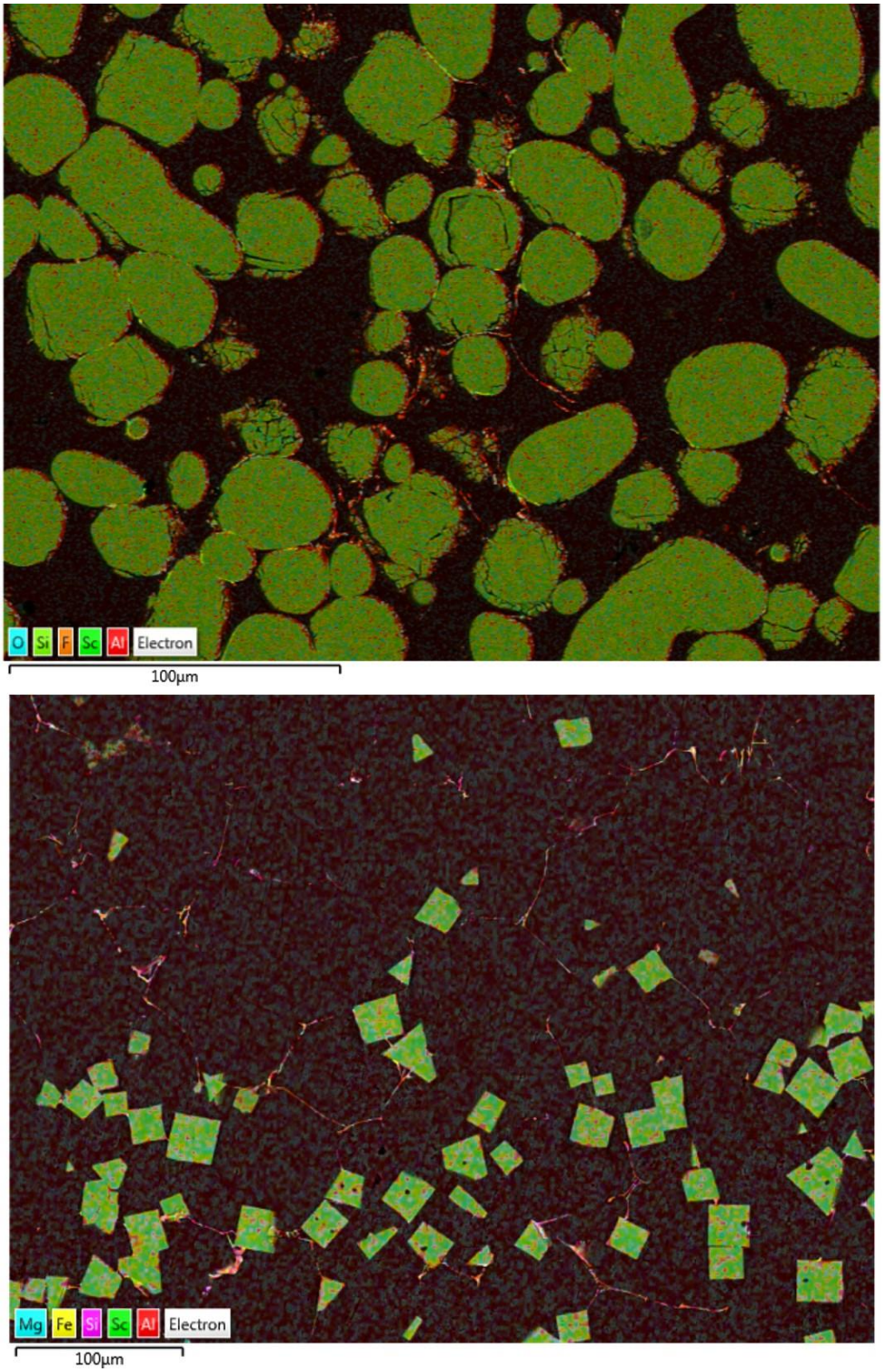

Figure 4.20. Elemental Mapping of the Al-Sc alloys recovered in molten $CaCl_2$-50w%NaCl

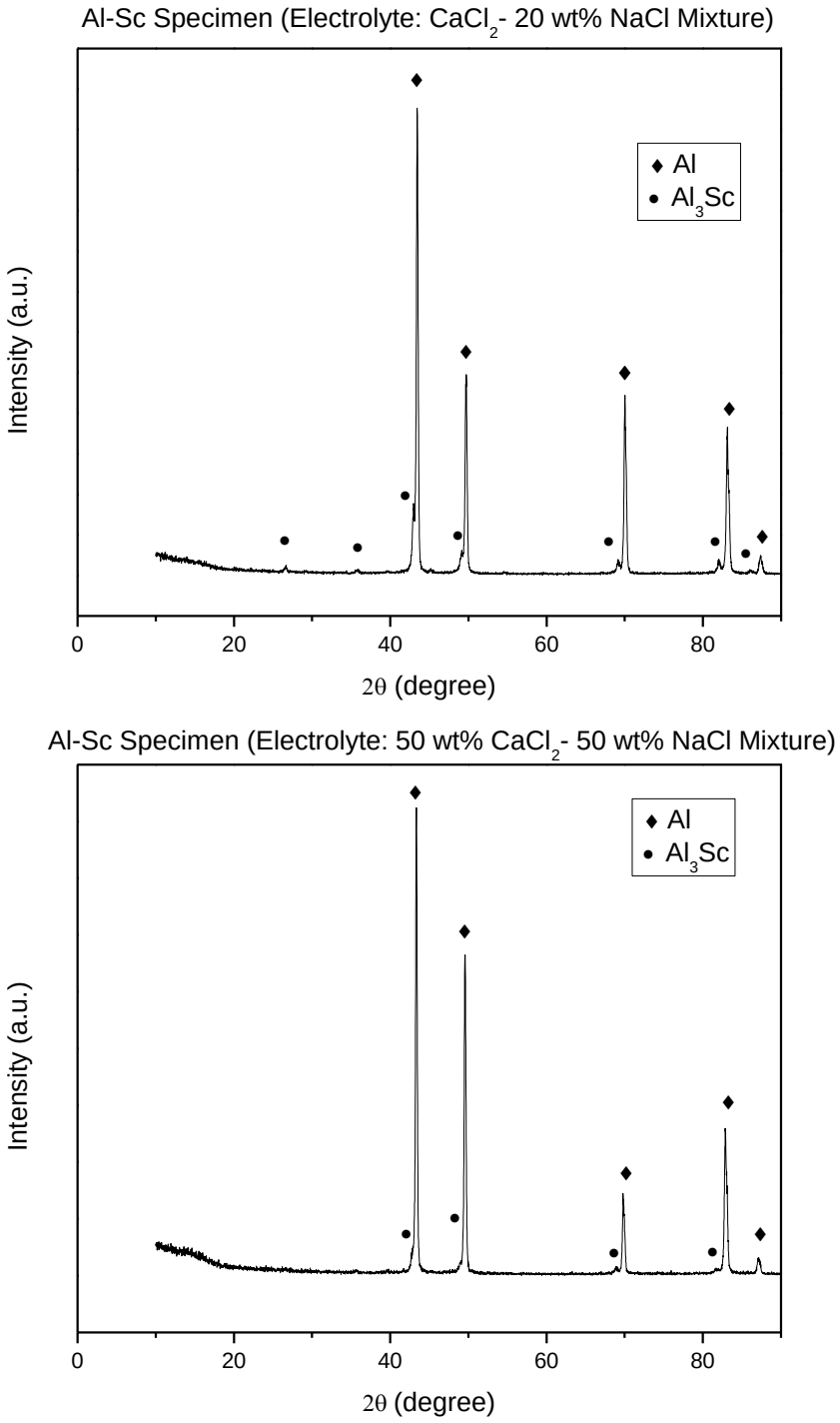

Figure 4.21. XRD patterns of the Al-Sc alloy samples produced at 800°C and 3.2 V in molten: a) $CaCl_2$-20wt%NaCl and b) $CaCl_2$-50wt%NaCl mixture

4.3. Solubility of ScF_3 in Molten $CaCl_2$ and $CaCl_2$-NaCl Salts

In electrochemical production of Al-Sc alloy in molten $CaCl_2$ and $CaCl_2$-NaCl mixtures, the solubility of ScF_3 in these salts is a critical issue. Depending on the solubility of that compound, it may be determined whether the Al-Sc alloy is produced by molten salt electrolysis or FFC Cambridge method.

Fischer and his coworkers proved for the first time that scandium could be produced electrochemically by molten salt electrolysis of $ScCl_3$ in eutectic LiCl-KCl mixture [30]. Castrillejo et.al [113] verified the findings of that study by carrying out successive electroanalytical tests such as square wave voltammetry, cyclic voltammetry and chronopotentiometry. They concluded that the electrochemical reduction of scandium ion occurred in a one-step electron exchange from Sc(III) to Sc (0). The same group [114] investigated the solubility of several rare earth chlorides including YCl_3 in eutectic LiCl-KCl mixture and equimolar $CaCl_2$-NaCl mixture at different temperatures by calculation of activity coefficients of each rare earth chlorides in both of the chloride melts. They argued that rare earth chlorides of Y, Nd, Ce, Pr and La were less solvated by chlorine ions present in $CaCl_2$-NaCl mixture in comparison with the solvation capacity of eutectic LiCl-KCl mixture. Since when a divalent metal chloride (i.e. $CaCl_2$) and an alkali metal chloride (i.e. NaCl) makes a solution and the mole fraction of MX_2 in that solution is greater than or equal to 0.33, it has been verified both experimentally and theoretically that a tetrahedrally coordinated complex ions in the form of MCl_4^{2-} are formed [115–117]. Due to formation of such a complex ion in the equimolar $CaCl_2$-NaCl mixture, the concentration of free chloride ions present in the melt is less than that of eutectic LiCl-KCl. For such a solubility behavior, the following reaction schemes were proposed [113]. Reaction 4.1 was proposed for the formation of rare earth chloro complex ion in eutectic LiCl-KCl melt while the reaction 4.2 was proposed for the equimolar $CaCl_2$-NaCl melt.

$$RE(III) + 6Cl^- = RECl_6^{3-} \quad (4.1)$$

$$RE(III) + 2CaCl_4^{2-} = RECl_6^{3-} + 2Ca(II) + 2Cl^- \quad (4.2)$$

In addition to the activity coefficient, ionic radius of the rare earth cations and the operation temperature affect the solubility significantly. As the ionic radius gets smaller, the solvation of those ions become more feasible. The rare earth cation with smallest ionic radius will have a higher polarizability ,which is the ratio of charge to ionic radius, and be solvated more in the chloride melts [113].

When the significant chemical similarity between the scandium and yttrium together with the smallest ionic radius of scandium are considered, the solvation of scandium by the same chloride melts is more likely.

In addition to the study of Castrillejo et.al [113], it is also known from the experimental studies that scandium halides have considerable solubility in respective alkali halide melts (AX, e.g. CsCl, CsI) and form several different chlorocomplexes [118,119]. Furthermore, Kononov et.al [120] investigated that the solubility of ScF_3 in KCl-NaCl melt at 730^{o}C and yielded Sc^{3+} cations and they were electrochemically reduced in NaCl-KCl melt by a one-step electron exchange from Sc(III) to Sc(0) as in the case of $ScCl_3$ in eutectic LiCl-KCl melt.

In this study, the solubility behavior of ScF_3 in molten $CaCl_2$ and $CaCl_2$-NaCl salts was investigated by analyzing the salt samples taken after the experiments under X-Ray Diffractometer. The results obtained by XRD analysis are given in Figure 4.22 and for pure $CaCl_2$, $CaCl_2$-20wt%NaCl and $CaCl_2$-50wt%NaCl. The intensity values present in these XRD patterns were normalized intentionally to carry out a more accurate phase analysis. In all three XRD patterns, CaClF, Sc_7Cl_{12} and $ScCl_3$ appear as the common phases with varying peak intensities within the same range of diffraction angle (i.e. 2Θ: 30^o - 40^o). The presence of these phases indicates that ScF_3 interacts with the pure $CaCl_2$ and $CaCl_2$-NaCl mixtures and is solved by the corresponding chlorine melts.

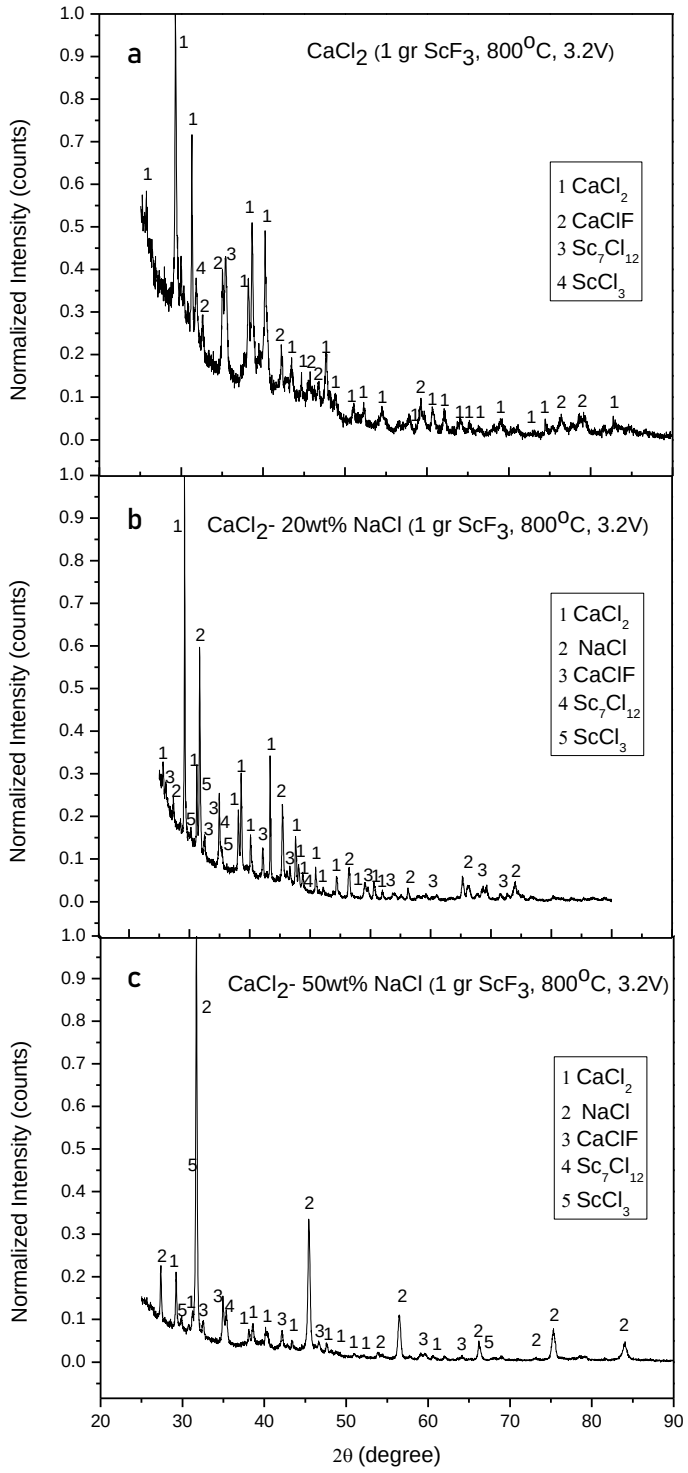

Figure 4.22. XRD patterns of the solidified salt samples taken after experiments: a) pure $CaCl_2$, b) $CaCl_2$-20wt%NaCl and c) $CaCl_2$-50wt%NaCl mixture

The compounds, CaClF, $ScCl_3$ and Sc_7Cl_{12} appearing in the XRD results, was thought to form by a reaction or reaction series including scandium chloro and/or chlorofluoro complexes.

As can be seen from the XRD patterns, as the concentration of NaCl increases, the peak intensities of the CaClF, Sc_7Cl_{12} and $ScCl_3$ phases decrease. This may be attributed to the content of free chloride ions present in the melt. According to the studies focused on the complex anions present in charge asymmetrical molten halides [115–117], the mole fraction of free chloride ion in $CaCl_2$-NaCl increases with the increase in the mole fraction of NaCl. As a result, the solvation capacity of $CaCl_2$-NaCl salt with the highest NaCl content increases and ScF_3 may be dissolved in a greater extent as compared to pure $CaCl_2$ and $CaCl_2$-20wt%NaCl.

This can be verified by the comparison of the area fraction of Al_3Sc intermetallic particles in the Al-Sc alloys produced in the respective chloride melts. For this purpose, three representative sections with closer areas were chosen and examined under optical microscopy. According to the optical micrographs given in Figure 4.23 a-c), the area fraction of Al_3Sc intermetallic particles increases with the increase in NaCl content of the electrolyte. In Figure 4.23a and b, Al_3Sc is the only phase appearing in the aluminum matrix, while Al_4Ca and Al_3Sc phases both exist in the alloy produced in pure $CaCl_2$ as shown in Figure 4.23c and d. The presence of Al_4Ca phase indicated by black arrows in Figure 4.23d decreases the area fraction of Al_3Sc intermetallics.

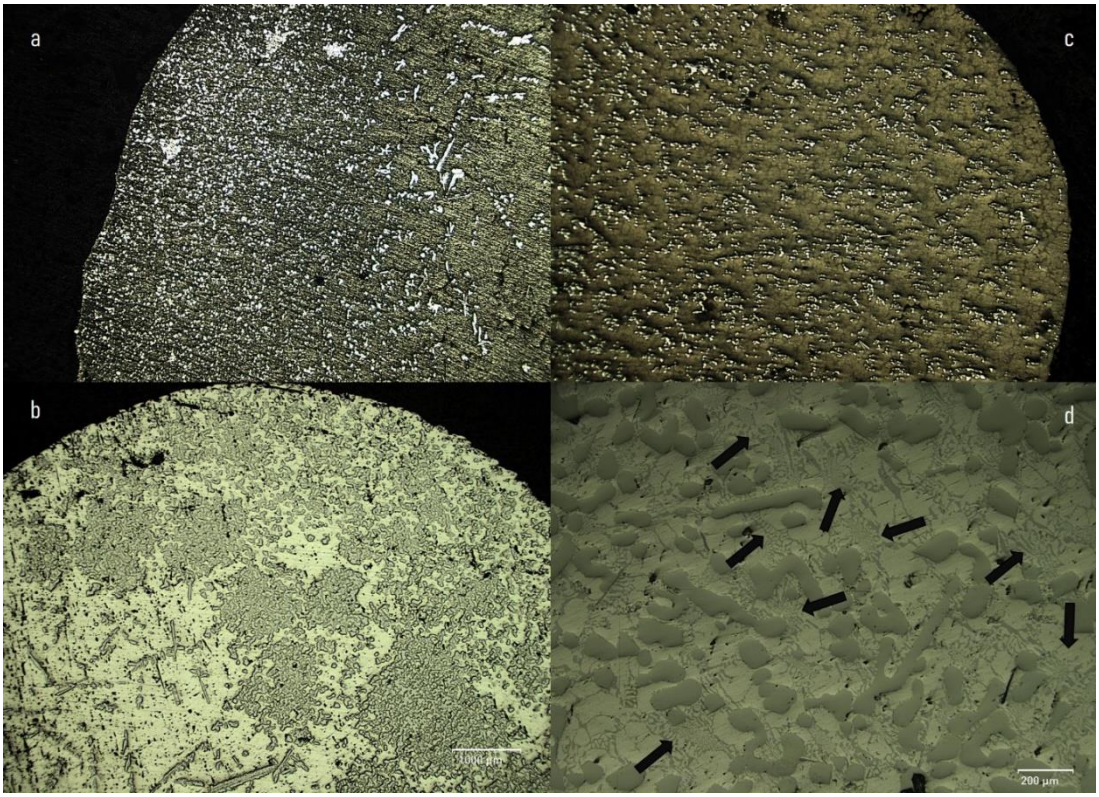

Figure 4.23. Optical Micrographs of as polished Al-Sc alloy samples produced at 800ºC and 3.2V in molten a) $CaCl_2$-20wt%NaCl, b) $CaCl_2$-50wt% NaCl, c and d) pure $CaCl_2$

The effect of the change in the concentration of the tetrahedral chlorocomplex and free chloride ions in the $CaCl_2$-NaCl mixture on the electrochemical behavior of the cell can be seen in Figure 4.16. The sudden increase in current expected to occur due to the formation of Al_3Sc intermetallics was gradually postponed as the molten salt mixture got richer in terms of NaCl due to the increase in the solvation power of chloride salt mixture and the scandium complexes in the melt.

All in all, it can be concluded that scandium fluoride compound is more likely soluble in molten $CaCl_2$-20wt%NaCl and $CaCl_2$-50wt%NaCl mixtures at 800ºC due to the concentration of free chloride ions present in the melt and having the smallest ionic radius among the other rare earth elements. Hence, it is reasonable to suppose that electrochemical production of Al-Sc alloy occurs via molten salt electrolysis.

4.4. Formation and Solidification Behavior of Al_3Sc Intermetallics in Molten $CaCl_2$ and Molten $CaCl_2$-NaCl Salts

4.4.1. Al_3Sc Phase

The graphite-liquid aluminum-molten chloride interaction at 800°C was discussed and a schematic drawing was presented to visualize the appearance of the system in a closed reactor. According to Figure 4.4, there is an oxide layer surrounding the liquid aluminum. This oxide layer should be removed for alloying the liquid aluminum with scandium. According to the experimental results given in the previous sections, it was obvious that Al-Sc alloy was produced successfully in both salts and Al_3Sc intermetallic particles were distributed throughout the aluminum matrix. In the light of these findings, it can be concluded that the oxide layer at the outer surface of the liquid aluminum was removed and electrochemically reduced Sc was in contact with the surface of liquid aluminum to form Al_3Sc.

According to the binary Al-Sc phase diagram in Figure 4.7, Al-Sc alloy should contain at least 0.55wt%Sc for proeutectic Al_3Sc intermetallic particles to be present in aluminum matrix. When such an alloy in liquid form starts to solidify, the first phase appearing in liquid aluminum matrix upon crossing the liquidus line is the primary Al_3Sc particles. As the solidification progresses and the temperature decreases below the eutectic point, it is expected that liquid aluminum remaining will solidify isothermally and continuous coupled growth of α-Al and Al_3Sc phases will occur. However, coupled growth was not observed in the real microstructure as can be seen in optical micrographs and elemental mapping of the Al-Sc alloys. The transformation of liquid aluminum into α-Al occurs by nucleation of alpha aluminum on Al_3Sc particles and growth outwards from these. This kind of behavior is a typical divorced eutectic which occurs due to limited Sc solubility of Al at eutectic point and slow growth kinetics of Al_3Sc as compared to α-Al. Divorced eutectic formation in Al-Sc alloy is the reason of Al_3Sc being as an efficient grain refiner [121]. When a hypereutectic Al-Sc alloy is examined under microscopy, it is mostly observed that

Al_3Sc intermetallic particles are found at the center of aluminum matrix. This is due to a structural similarity between Al and Al_3Sc phases. Al_3Sc phase has an ordered structure the atoms which are located on the face centers at Al FCC lattice. Both phases have FCC structures with a small mismatch of 1.57% as given in Table 4.6 [122].

Table 4.6. *Physical properties of Al and Al_3Sc phases* [122]

Phase	*Structural Prototype*	*Lattice Parameter, a, Å*	*Crystal Structure*	*Density, g/cm^3*
Al	Cu	4.0496	FCC	2.699
Al_3Sc	Cu_3Au	4.103	FCC	3.026

4.4.2. Electrochemical Formation and Segregation Behavior Al_3Sc Intermetallics in Molten Chloride Salts

In the previous section, according to the results of XRD analysis of the salt samples, it was stated that ScF_3 might be soluble in respective chloride melts. Therefore, Sc ions (i.e. Sc^{3+}) could be present in the molten salt and be discharged and electrochemically reduced to metallic scandium at the liquid aluminum-molten salt interface. The metallic scandium obtained after the electrochemical reduction diffused into the liquid aluminum and formed Al_3Sc intermetallic particles. However, due to the slow growth kinetics of Al_3Sc as discussed earlier, Sc might have accumulated on the surface of liquid aluminum and caused the formation of a Sc rich layer as schematically shown in Figure 4.24. This layer probably inhibited the further electrochemical reduction and excess Sc might have dissolved in the salt. Another reason for the surface segregation might be the electron transportation distance between the Sc^{3+} ions and the electrons coming from the contact surface of graphite and liquid aluminum. Electrons could be transported easily from the graphite crucible to the bottom part of the aluminum. However, as the electrons were transferred towards upper portion of the aluminum to meet with the Sc^{3+} for discharging, the distance became longer, making the rate of discharge slower. Thus, the concentration

of Al_3Sc intermetallics was higher in the bottom part of aluminum which was in contact with graphite crucible due to faster discharge rate [123].

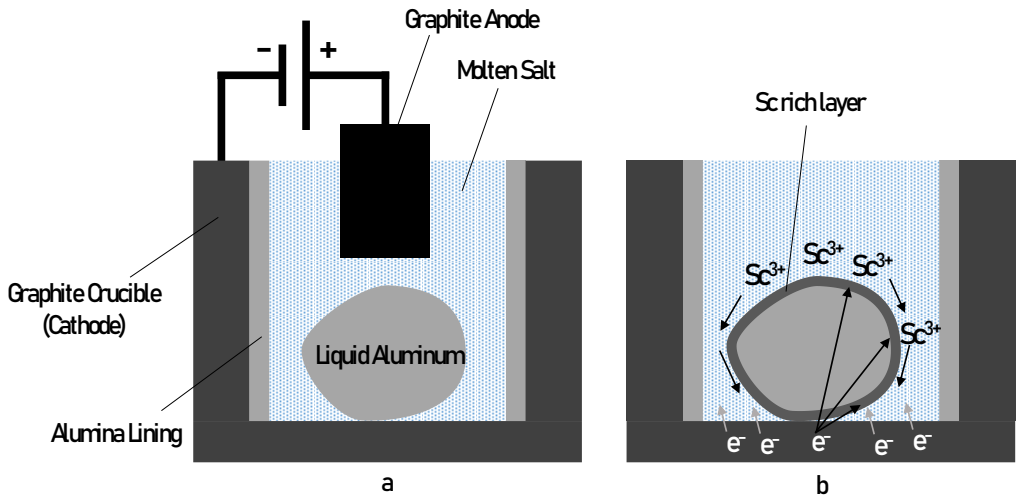

Figure 4.24. Schematic representation of a) molten salt electrolysis cell and b) electrochemical reduction of Sc^{3+} ions and formation of Sc rich layer [123]

According to microstructural investigation in the previous sections, the morphology of Al_3Sc intermetallics were mostly faceted, which could be attributed to high entropy of fusion causing anisotropic growth. However, these particles had other morphologies such as triangle, star, cuboid and dendrite. The cooling rate and mass transport of Sc through Al determined the equilibrium morphologies of the Al_3Sc intermetallics. Faceted morphology was a typical morphology observed in slowly cooled Al-Sc alloys where growth occurs along {100} planes. Cuboid, star and triangle shapes occurred under faster cooling rate where preferential growth occurred along <111> directions as can be seen in Figure 4.19b [93].

It could be inferred from these findings that formation of Sc-rich layer during electrochemical processing and the length of electron transport distance were probably the origins of the surface segregation in electrolytic Al-Sc alloys which were reported by the other researchers [76,89–91]. The cooling rate of the electrolytic Al-Sc alloy

had a very little effect on the surface segregation as can be seen in Figure 4.19 where the alloy in a) was cooled in furnace while the alloy in b) was cooled in air.

4.5. Determination of Electrochemical Reaction Mechanism of Al-Sc Alloy in Molten $CaCl_2$

In electrochemical production of Al-Sc alloys in molten chloride melts, the experiments were conducted under constant voltage due to the convenience of the Nernst equation ($\Delta G = -nFE$) which enables the calculation of decomposition potentials of the metal compounds to be reduced and the respective salt. According to the decomposition potential values, the applied potential is estimated such that the voltage value should be less than the decomposition potential of the salt while it should be greater than the decomposition potential of the metal compound. However, the presence of the kinetic factors in electrochemical processing brings additional terms which contribute to the applied voltage. The electrical resistance of electrode leads, the resistance of electrolyte and the overpotentials originating from activation energy barrier and concentration change of the ions in the melt are the reasons which cause deviation of the observed cell potential from the theoretical potential.

Therefore, the applied cell voltage can be expressed by considering the kinetic terms as following;

$$E_{applied} = E_{reaction} + E_{electrical\ connections} + E_{electrolyte} + \eta \quad (4.5)$$

In equation 4.5, the term $E_{reaction}$ is the theoretical potential required for cell reaction and is expressed as

$$E_{reaction} = -\frac{\Delta G_{reaction}}{nF} \quad (4.6)$$

where $\Delta G_{reaction}$ is Gibbs Free Energy change of the cell reaction, n is the number of electrons transferred through the cell and F is the Faraday's constant.

The terms $E_{electrical\ connections}$ and $E_{electrolyte}$ represent the voltage drop due to the resistance of electrode leads and the electrolyte, respectively. The numerical values of these terms are calculated by multiplication the current passing through the cell (I) and the electrical resistance of each term. The final term in equation 4.5 is the overpotential due to activation energy barrier and concentration change of the ions near the electrodes.

During the electrochemical reduction experiments, the electrochemical behavior of the cell for each experiment was monitored by current-time diagrams recorded with the help of a software. However, a current-time graph alone is not sufficient to understand the complete electrochemical behavior. For example, the reaction taking place at different voltage values and the reaction products could not be realized by this diagram. Therefore, potential sweep techniques scanning the potential with time while measuring the corresponding current response to give an I-V diagram, should be used. Among these techniques, cyclic voltammetry, which scans potential in both positive and negative directions and backs to the starting point after completion of the cycle, was preferred to investigate the electrode reactions in both directions [83].

In cyclic voltammetry experiments, two and three terminal cell setups were utilized as shown in Figure 3.10. A three-terminal cell setup involves a reference electrode, a counter electrode and the working electrode while a two-terminal cell setup is made up of counter and working electrodes. In both cell setups, the reaction or reactions taking place at the working electrode is of interest. Between these two techniques, three terminal cell setup gives more precise results since the potential is measured with respect to reference electrode while the current passes in between working and counter electrode. The voltage measured in this manner does not involve kinetic parameters such as voltage drop and overpotentials and is very close the value obtained by thermodynamic data according to Nernst Equation. On the other hand, the voltage in two-terminal cell is measured with respect to working electrode and kinetic factors will contribute the measured voltage values.

The cyclic voltammogram of the cathode with respect to tungsten reference electrode is given in Figure 4.25. The voltage was scanned between 0 and -2 V with a scan rate of 20 mV/s. This measurement was repeated three times at the same scan rate and different limiting voltages to see the reproducibility of the voltammetric responses. As can be seen in the voltammogram, diagrams start with a positive current which means a galvanic current (spontaneous reaction) from cathode to anode in a short time interval. This may be attributed to the formation Al_4C_3 phase due to direct contact between liquid aluminum and graphite since the aluminum is not protected cathodically when this positive current passes for a very short time interval. Another feature of this cyclic voltammogram is that there is a single cathodic wave starting at about -0.75 V indicating the beginning of a cathodic reaction, which is a typical case encountered when the working electrode is in the liquid form [124]. When the potential reaches to -1.4 V, a fluctuation occurs in the voltammogram which continues until the positive current passes through the cell. This can be attributed to the nucleation and growth of Al_3Sc intermetallic phase at the liquid aluminum/molten $CaCl_2$ interface, which has a slower kinetics as discussed earlier. In addition to this, the activity of scandium decreases due to the formation of Al_xSc_y intermetallic phases and the potential value which represents the formation of Al_xSc_y phase will increase according to the equation 4.7.

$$E_{Sc(III)/Al_xSc_y} = E_{Sc(III)/Sc(0)} - \frac{RT}{nF}\, ln\left[a_{Sc}\left(in\ Al_xSc_y\ \right)\right] \qquad (4.7)$$

The decrease in the activity of scandium causes the potential shift to a more positive value as compared to an inert working electrode where reduction potential of Sc has a more cathodic value.

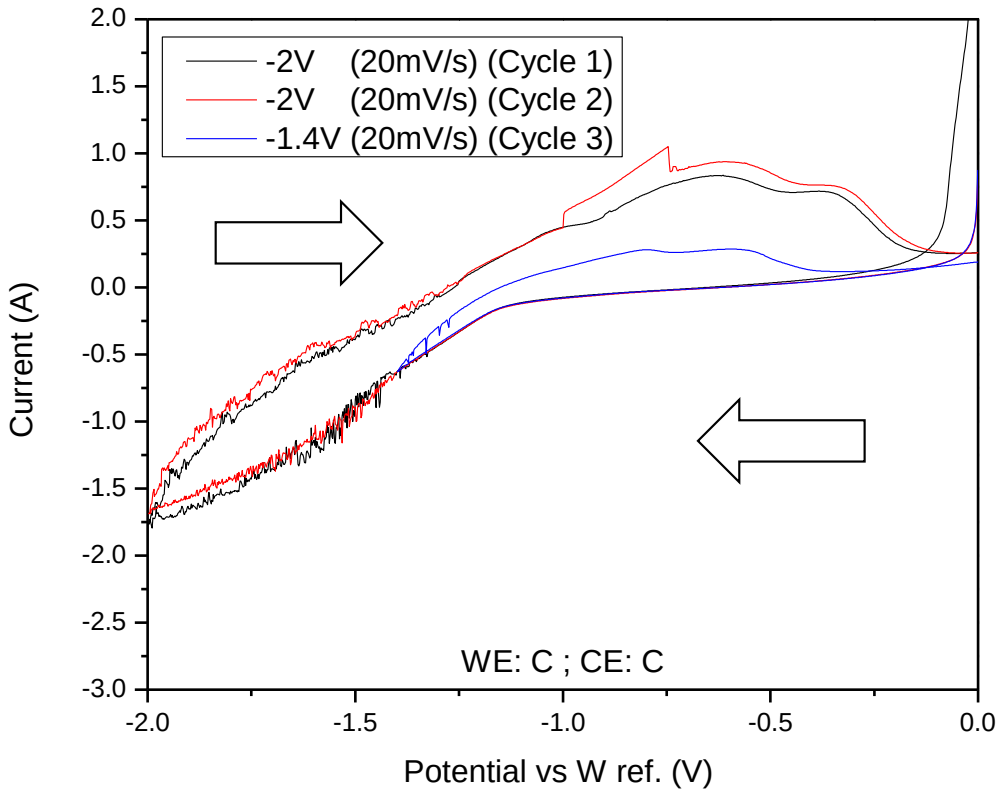

Figure 4.25. Cylic voltammograms of the reduction of ScF_3 in the pure molten $CaCl_2$ at liquid aluminum electrode with respect to tungsten reference electrode at 800°C

For three of the voltammograms of the cathode, the cathodic response is not clear due to slower rate of Al-Sc intermetallic phase formation. In contrast, anodic response at the cathode is quite distinct as can be shown in Figure 4.26 which represents the voltammogram indicated in blue in Figure 4.25. When the upper voltage limit is decreased, identification of the interested peaks becomes more clear as visualized in this figure. There are four peaks or shoulders appearing in the anodic part of the voltammogram indicated with roman numerals. These peaks or shoulders represent most probably the anodic dissolution of the four Al-Sc intermetallic compounds present in Al-Sc binary phase diagram in Figure 4.7.

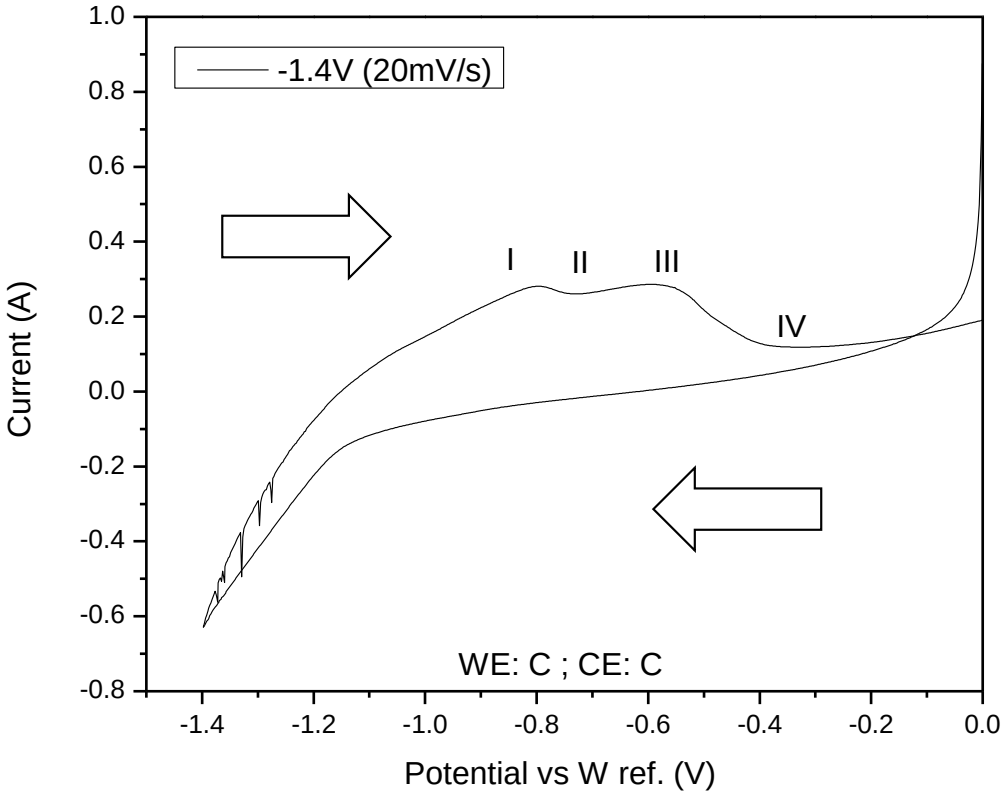

Figure 4.26. Cyclic voltammogram of the cathode recorded between 0 and -1.4 V at a scan rate of 20 mV/s

These peaks or shoulders could be associated with the following dissolution reactions as in the study of Castrillejo et.al.[125].

I	$AlSc_2 + 3e^- \rightarrow AlSc + Sc^{3+}$	(4.8)
II	$2AlSc + 3e^- \rightarrow Al_2Sc + Sc^{3+}$	(4.9)
III	$3Al_2Sc + 3e^- \rightarrow 2Al_3Sc + Sc^{3+}$	(4.10)
IV	$Al_3Sc + 3e^- \rightarrow 3Al + Sc^{3+}$	(4.11)

Although there are several indications on the formation of Al-Sc intermetallic phases inferred the voltammograms of the cathode, the cyclic voltammogram of the cathode alone is not sufficient to predict the existence of these intermetallic phases. Therefore, the same analysis should be performed for a two-terminal cell setup to identify the reactions taking place at the real electrochemical reduction experiments.

The cyclic voltammogram obtained using a two-terminal cell setup is given in Figure 4.27. This voltammetric study simulates the electrochemical reduction experiments carried out at a constant voltage and 800^{o}C where the applied voltage involves the voltage terms occurring due to thermodynamic and kinetic factors as in the equation 4.5. The voltage was scanned between 0 and -2.2 V with a scan rate of 20 mV/s. As being in the voltammogram of the cathode, this measurement was repeated two times at the same scan rate and different limiting voltages to see reproducibility of the voltammetric response. However, the one recorded at a lower voltage limit was presented due to the fact that the cathodic and anodic responses were more clear as compared to the other voltammogram.

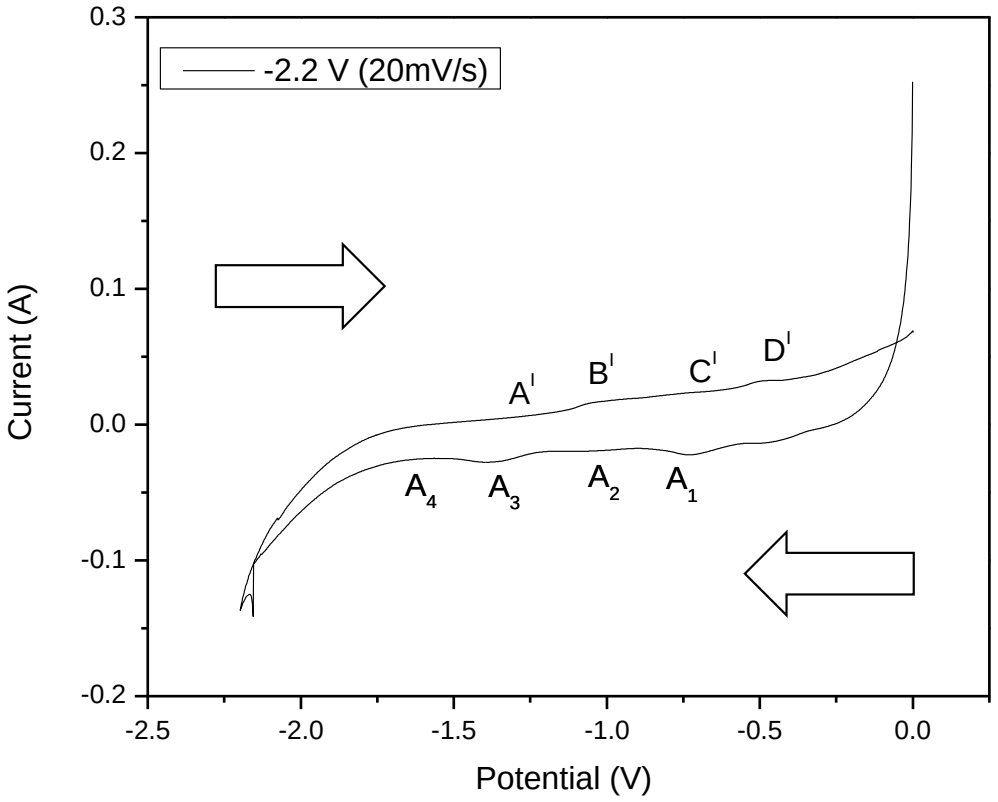

Figure 4.27. Cyclic voltammogram recorded using two-terminal cell setup

The four peaks or shoulders in the cathodic region and other corresponding four signals in the anodic region are assumed to be the formation and dissolution of the Al-Sc intermetallic phases, respectively.

The following reactions (i.e. 4.12 - 4.15) are predicted to be those taking place at A_1, A_2, A_3 and A_4 voltage values respectively, using the thermochemical data from FACTSAGE database [126,127]. The Gibbs Free Energy of formation for Al_xSc_y intermetallic compounds were taken from the study of Cacciamani et.al [92] who studied Al-Sc system by conducting calorimetric measurements.

$Al(l) + 2Sc(s) = AlSc_2(s)$	ΔG^o_{1073}=-97413 J/mole E^o= -0.168 V	(4.12)
$Al(l) + Sc(s) = AlSc(s)$	ΔG^o_{1073}= -75527 J/mole E^o= -0.26 V	(4.13)
$2Al(l) + Sc(s) = Al_2Sc(s)$	ΔG^o_{1073}= -116698 J/mole E^o= -0.40 V	(4.14)
$3Al(l) + Sc(s) = Al_3Sc(s)$	ΔG^o_{1073}= -132390 J/mole E^o= -0.46 V	(4.15)

Among four intermetallic phases, Al_3Sc is the primary Al-Sc phase occurring at the end of electrochemical reduction experiments. Other Al-Sc intermetallic phases appearing as the reaction products such as Al_2Sc, AlSc and $AlSc_2$ were not observed during structural and chemical characterization of the Al-Sc alloys. There is no conflict between the voltammetric and characterization results since the absence of abovementioned phases are expected due to overall composition of Al-Sc alloy produced with reference to Al-Sc phase diagram [92]. The appearance of these phases during CV analysis can be attributed to the fast voltage scan which makes formation of peaks or shoulders possible.

4.6. Utilization of Different Cathode Materials and Ceramic Membrane in Electrochemical Production of Al-Sc Alloy

In the electrochemical reduction of ScF_3 in molten $CaCl_2$ and $CaCl_2$-NaCl mixtures, high background current was observed as a common problem for both of the melts. This causes a decrease in current efficiency and makes monitoring the experiments challenging. This problem is attributed to the electronic conduction originating from the graphite-graphite interaction between graphite anode-electrolyte interface. The experimental setup was modified to overcome this problem. All the results presented until now were obtained from the cell setup given in the Figure 3.1. The results of the experiments carried out in the cell setup shown in Figure 3.2 will be discussed in this section. The main difference in this setup was the use of a separate cathode in the form of a spoon to hold aluminum sample.

A blank test without ScF_3 was conducted at 800^oC by applying 3.0 V between the graphite anode and the steel spoon cathode holding aluminum to gather information on background current. This experiment was an example of pre-electrolysis of the electrolyte which was conducted commonly to remove redox active impurities before the electrochemical reduction experiments. The corresponding current-time response of this experiment is shown in Figure 4.28. The beginning and background current in this experiment were considerably low since the electrolyte did not contain a compound to be reduced electrochemically and any oxide or hydroxide compound left from the dehydration process which was the indication of an efficient dehydration.

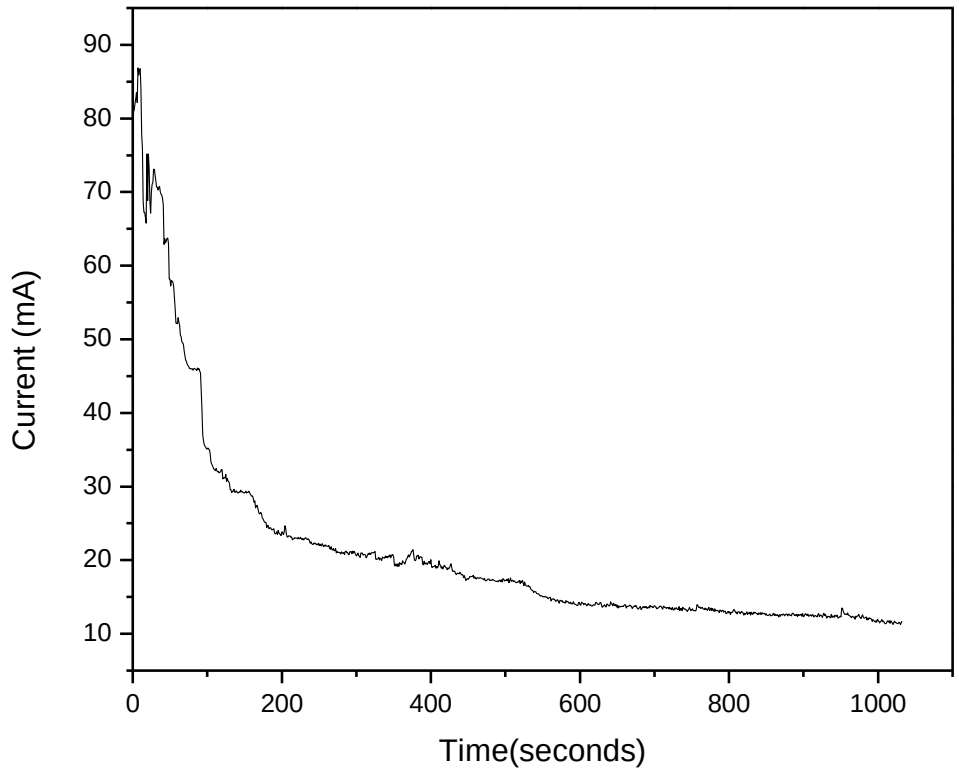

Figure 4.28. Current-Time response of the constant voltage experiment at 3.0 V without ScF_3 in molten $CaCl_2$ (Cathode: Stainless Steel Spoon)

After the experiment, aluminum could not be recovered from the steel spoon cathode due to strong adherence which could probably be due to the chemical interaction between aluminum and oxide compound/s of the steel (e.g. Cr_2O_3, Fe_2O_3). Therefore, an alternative cathode enabling aluminum recovery and increasing current efficiency, was used. In this setup, stainless steel spoon cathode containing a mini graphite crucible was used as the cathode. An interesting result was obtained this time as shown in Figure 4.29. The current started with a high value, decreased progressively and reached to a very low background level when the theoretical charge limit was attained.

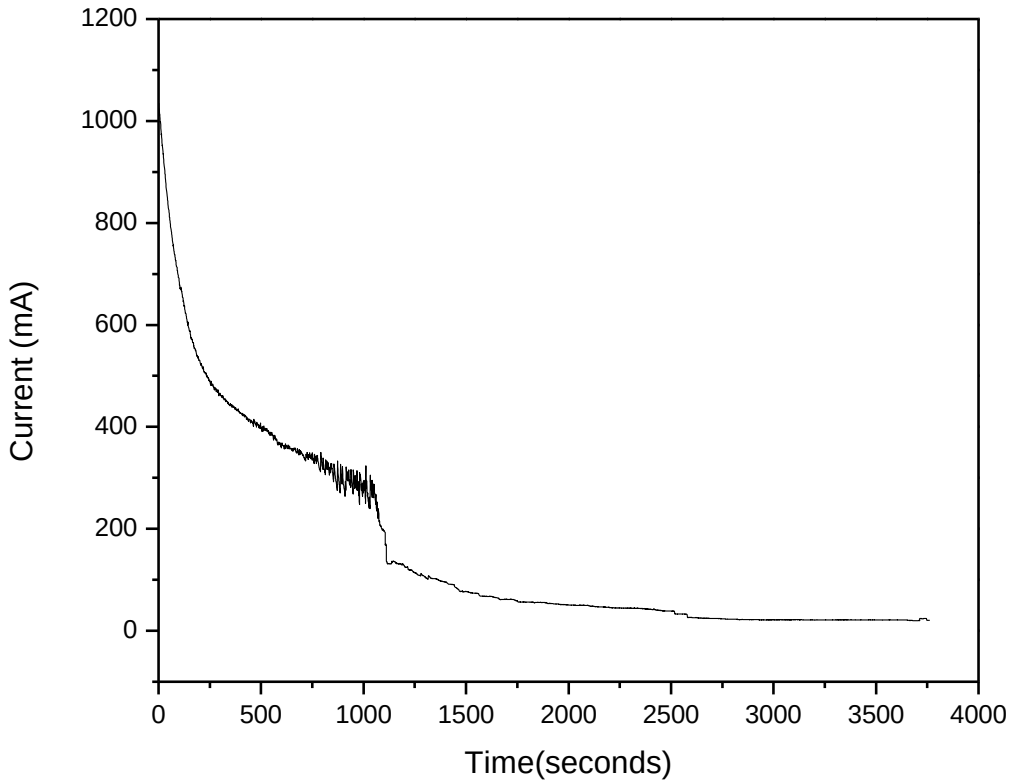

Figure 4.29. Current-Time response of the electrochemical reduction experiment at 800ºC and 3.2 V in molten $CaCl_2$ (Cathode: Stainless steel spoon involving a mini graphite crucible)

A similar experiment was repeated by increasing the scandium fluoride content of the electrolyte up to 1 wt%. According to the current-time diagram indicated in Figure 4.30, a similar electrochemical behavior with the experiments conducted in the cell setup given in Figure 3.1 was observed. The experiment started with a high current value and finished with a high back ground current which was ascribed to the disintegration of graphite anode causing electronic conduction as the duration of the experiments got longer.

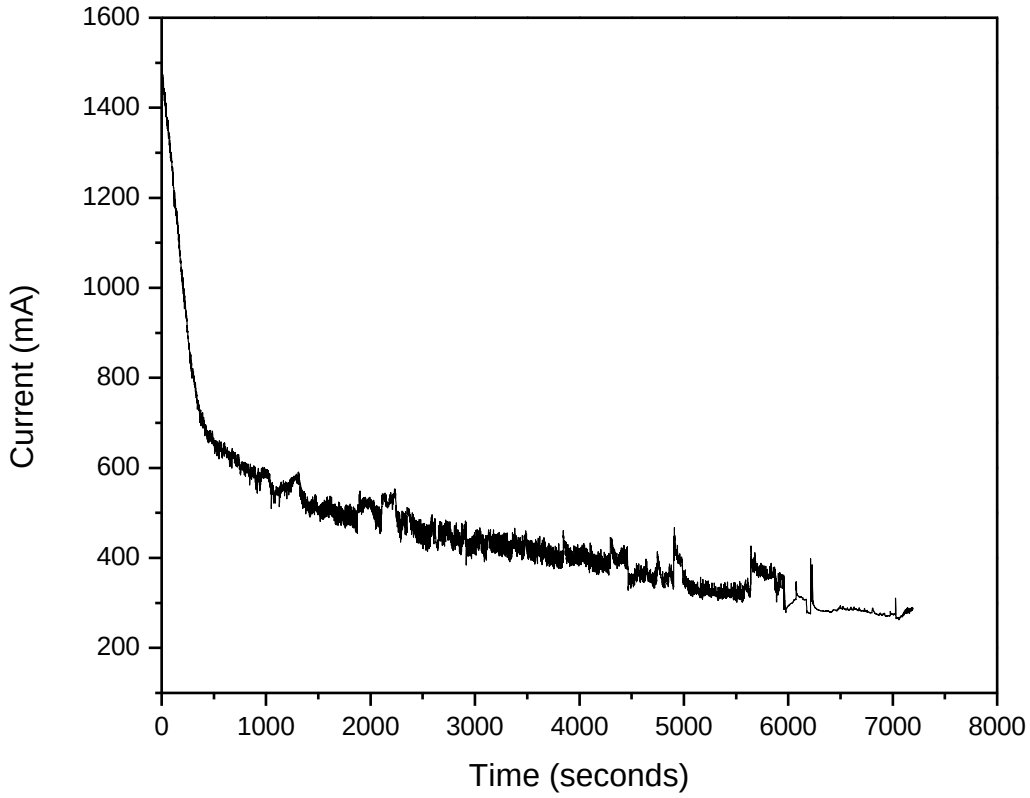

Figure 4.30. Current-Time response of the electrochemical reduction experiment at 800°C and 3.2 V in molten $CaCl_2$ containing 1wt% ScF_3 (Cathode: Stainless steel spoon involving a mini graphite crucible)

In the experiments above, due to thermodynamic limitations and slow mass transportation of scandium, the aluminum samples recovered from the salt did not contain scandium in the matrix. Instead, the electrochemically reduced scandium was deposited onto the stainless steel as can be seen from the results of XRF analysis in Table 4.7 taken from four selected points indicated in Figure 4.31.

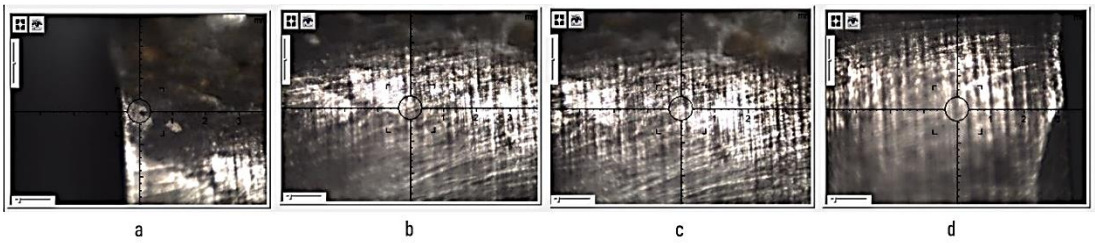

Figure 4.31. The selected regions of stainless steel for XRF analysis

Table 4.7. *The results of XRF analysis of locations shown in Figure 4.31*

Analyzed Region	*Fe (wt%)*	*Cr (wt%)*	*Ni (wt%)*	*Mn (wt%)*	*Ca (wt%)*	*Sc (wt%)*
a	61.78	18.01	12.39	1.24	4.83	1.75
b	66.93	17.70	9.48	1.47	-	4.42
c	67.32	18.38	9.96	1.35	-	3.00
d	62.85	13.14	16.17	1.40	1.11	5.33

When the experiments and their corresponding current-time responses given above are taken into account, the most useful cathode design seems to be the steel spoon with mini graphite crucible in terms of aluminum recovery. However, the utilization of this cathode design inhibits scandium diffusion into the aluminum due to the interaction between Fe and Sc. In addition to this, the increase in the scandium fluoride content of the electrolyte increases the time required for electrochemical reduction experiments which causes further disintegration of graphite due to the penetration of electrolyte into micro pores of graphite. Thus, it necessitates the use of an alternative cell setup, which enables aluminum recovery and involves equipment that does not interact with scandium and inhibits or decreases the graphite dust accumulation on the electrolyte surface. For this purpose, the cell setup given in Figure 3.1 was modified considering the problems encountered above. In this cell setup, the graphite anode was covered with a porous ceramic either mullite or alumina acting as a membrane for ion transportation while inhibiting the passage of graphite dust towards electrolyte.

An experiment was conducted at 800ºC in molten $CaCl_2$ containing 1wt% of ScF_3 by applying 3.0V between the graphite crucible and the graphite anode covered with mullite membrane. The scandium fluoride content of the electrolyte was kept the same as the experiments conducted with spoon cathodes to investigate the scandium recovery. The corresponding current-time diagram of this experiment is given in Figure 4.32.

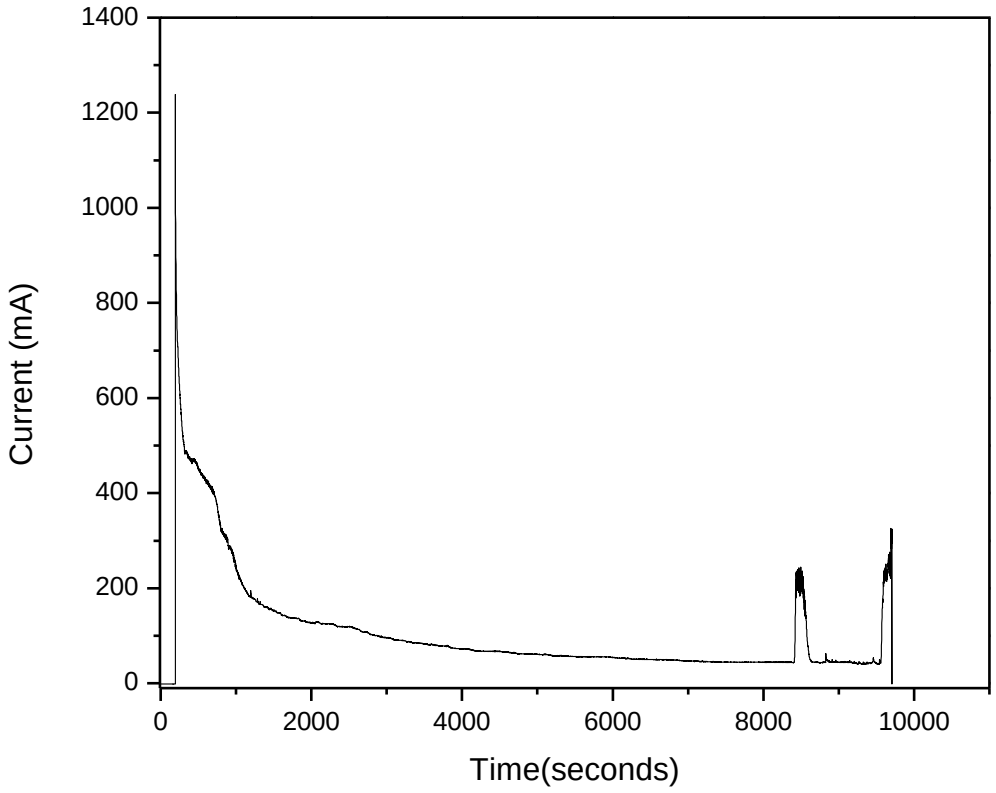

Figure 4.32. Current-Time response of the electrochemical reduction experiment at 800ºC and 3.0 V in molten $CaCl_2$ containing 1wt% ScF_3 (Cathode: Graphite crucible, Anode: Graphite rod covered with porous mullite)

The current increased from zero up to a certain current value, then decreased progressively and reached to very low values as the theoretical charge limit was attained. However, as the experiment goes further, current fluctuations occurred which could be due to the beginning of a new reaction. The reason of the slow increase in

the current at the beginning was due to the infiltration of electrolyte into the ceramic membrane. As soon as the electrolyte reached to the surface of the graphite anode, the electrochemical reduction started and current became decreasing. Aluminum sample was recovered easily at the end of the experiment. However, scandium was not found in the aluminum matrix due to the thermodynamic limitation mentioned before.

Another experiment was conducted at 800°C in molten $CaCl_2$-50wt% NaCl mixture containing 2 wt% ScF_3 under applied potential of 3.2 V. In this experiment, porous alumina was used as the ceramic membrane while the upper portion of the graphite was embedded in fused alumina sheath. As can be seen in current-time diagram in Figure 4.33, the current increased slowly up to a relatively low current value as compared to previous one, then decreased slowly and finished with a high background current. Current fluctuations was observed again at the end of the experiment.

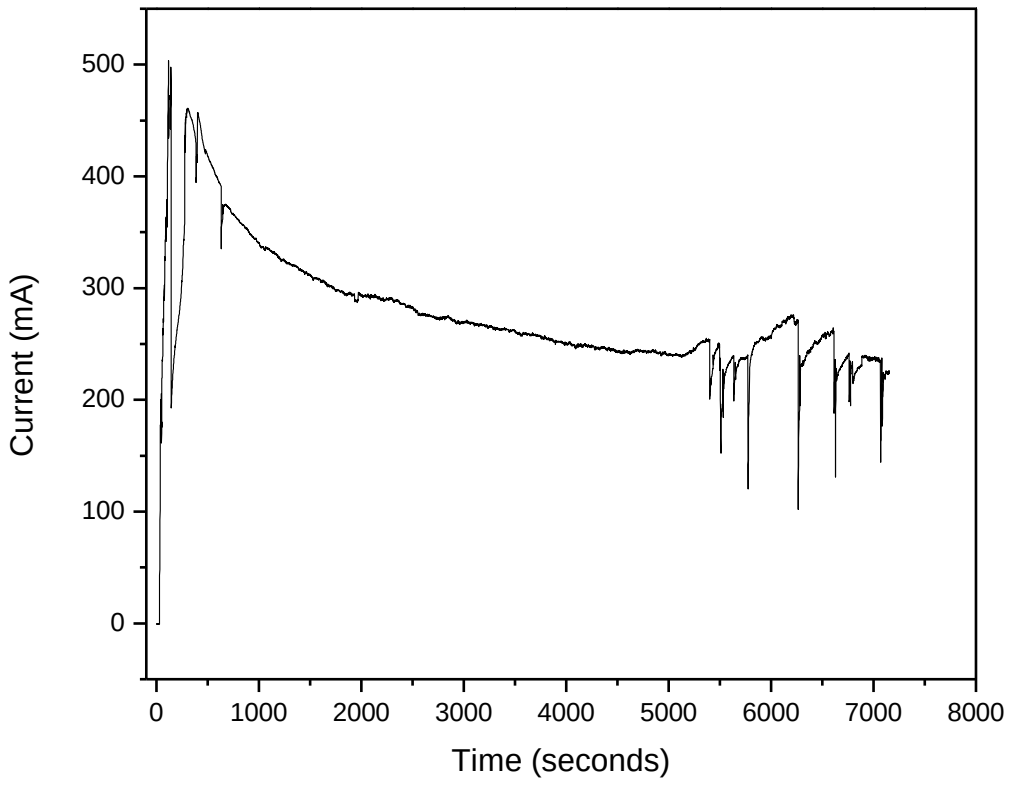

Figure 4.33. Current-Time response of the electrochemical reduction experiment at 800°C and 3.2 V in molten $CaCl_2$-50wt%NaCl containing 2wt% ScF_3 (Cathode: Graphite crucible, Anode: Graphite rod covered with porous alumina)

Unlike the previous experiment, scandium was alloyed with aluminum as a result of this experiment as shown in the optical micrographs given in Figure 4.34. As can be deduced from the microstructural examination, it could be stated that the practical limit of the content of ScF_3 in molten salt should be at least 2 wt% for making Al-Sc alloy.

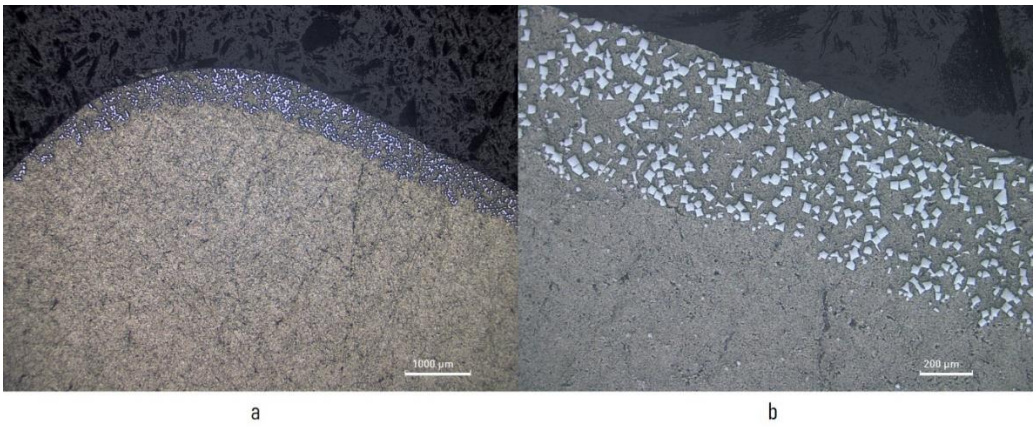

Figure 4.34. Optical micrographs of as polished Al-Sc alloy (Cathode: Graphite crucible, Anode: Graphite rod covered with porous alumina) a) 5x and b) 20x

On the other hand, when it comes to the performance of the porous alumina and mullite used as ceramic membranes in electrochemical reduction experiments, several consequences can be drawn. Both alumina and mullite ceramic membranes could be used only once due to corrosive environment of molten salt. This can be seen in Figure 4.35 which shows the appearance of the surface of the solidified salt after the electrochemical reduction experiments. In Figure 4.35a and b), the change in the surface appearance of the solidified salt upon using the same mullite membrane twice is seen. When the same membrane was used for the second time, it expanded due to infiltration of the salt into the open pores and several cracks formed upon solidification of the salt.

Therefore, the membrane could not inhibit the movement of graphite dust towards the molten salt as shown in Figure 4.35b. Furthermore, it could fracture and contaminate the electrolyte which may affect the electrochemical processing. However, their performance is quite well in terms of inhibition of graphite dust in their first usage as seen in Figure 4.35a and c.

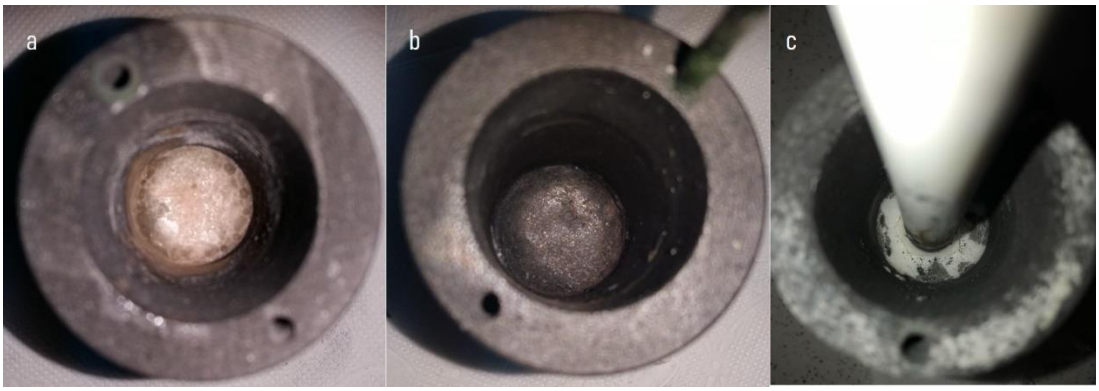

Figure 4.35. Appearance of the surface of solidified salt after electrochemical reduction when the ceramic membrane was a) and b) mullite, c) alumina

The performances of the ceramic membranes are also dependent on the operating temperature, the open porosity level, morphology of the pores, the wall thickness of the membrane which affect the ion transportation between anode and cathode and the structural stability. In the experiments with ceramic membranes, open porosity level, wall thickness and temperature were kept constant to see the effect of membrane on the electrochemical behavior of the system. Therefore, only the preliminary results were presented in the scope of this study. It necessitates to study further to find a combination of these parameters which improves Sc recovery rate and process efficiency.

CHAPTER 5

CONCLUSION

Electrochemical production of Al-Sc alloy was studied in pure molten $CaCl_2$ and $CaCl_2$-NaCl mixtures. Experiments involving molten $CaCl_2$ were carried out at 800^oC with applied voltages of 2.3, 3.0 and 3.2 V. While, experiments employing molten $CaCl_2$-NaCl mixtures were carried out at 800^oC under 3.2 V except for one experiment which was conducted at 850^oC and 3.0 V.

According to the results of the electrochemical reduction experiments conducted in pure molten $CaCl_2$, the following consequences could be drawn; i) Sc recovery rate increased with increasing voltage and the best result was obtained when 3.2 V was applied due to faster reaction kinetics. Thus, the applied potential in the experiments with $CaCl_2$-NaCl mixture was chosen as 3.2V to reach higher Sc recovery rate, ii) the hygroscopic nature of $CaCl_2$ caused the formation of calcium oxide which ended up with calcium contamination in Al-Sc alloy.

When $CaCl_2$-NaCl salt mixture was used as the electrolyte, calcium contamination problem was overcome by decreasing the activity of CaO. Sudden current increases were observed during the electrochemical reduction experiments. The instant of happening of sudden current increases was gradually postponed with the increase in the NaCl content of the electrolyte. The probable cause of such an unusual change was thought to be the interaction between freshly formed Al_3Sc intermetallic particles and the graphite anode.

Scandium fluoride (ScF_3) used as the scandium source was more likely to be soluble in $CaCl_2$-20wt%NaCl and $CaCl_2$-50wt%NaCl salt mixtures in comparison to pure $CaCl_2$ according to the XRD analysis of the salt samples taken after the electrochemical reduction experiments and the optical microcopy examination of the

Al-Sc alloy samples. Higher solvation capacity of the $CaCl_2$-NaCl salt mixture was thought to be due to the presence of free chloride ions whose concentration changed proportionally with the NaCl content of the electrolyte.

Al-Sc alloys produced electrochemically were hypereutectic alloys (i.e. wt %Sc > 0.55) exhibiting divorced eutectic behavior which caused separate nucleation and growth of Al-Sc intermetallic phase and α-Al matrix. According to SEM-EDS, elemental mapping and XRD analyses, the primary Al-Sc phase was found to be as Al_3Sc which appeared in the microstructure in the form of cuboid, star and triangular. Due to slow growth kinetics of Al_3Sc, the subsequent formation of Sc rich layer on liquid aluminum-molten salt interface and the length of the electron transport distance, surface segregation problem occurred which was independent on the electrolyte composition and the cooling rate.

The steel spoon cathode with mini graphite crucible was found to be efficient for recovery of aluminum. However, utilization of this cathode design was not very effective in terms of scandium recovery and decreasing the back ground current. On the other hand, ceramic membranes made up of porous alumina and mullite inhibited graphite dust accumulation and enabled decreasing the background current.

The practical limit for the scandium fluoride content of the electrolyte was found to be at least 2wt% in order for scandium to diffuse into aluminum to form Al-Sc alloy. When the electrolyte contains scandium fluoride less than 2wt%, the electrolyte becomes closer to the infinite dilution which increases the energy required to reduce ScF_3 electrochemically.

In conclusion, Al-Sc alloys were produced successfully by electrochemical reduction of domestic scandium bearing powder involving ScF_3, $NaScF_4$ and Na_3ScF_6 phases and alloying in-situ with liquid aluminum in both molten $CaCl_2$ and $CaCl_2$-NaCl salt mixtures according to the results of the optical microscopy, SEM-EDS and XRD analyses.

REFERENCES

[1] W. M. Haynes, D. R. Lide, and T. J. Bruno, *CRC Handbook of Chemistry and Physics, 97th Edition*. 2017.

[2] F. H. Spedding, "The Rare-Earth Metals," *Metall. Rev.*, vol. 5, no. 19, 1960.

[3] J. Lucas, P. Lucas, T. Le Mercier, A. Rollat, and W. Davenport, *Rare earths: science, technology, production and use*. Elsevier B.V., 2015.

[4] G. B. Haxel, J. B. Hedrick, G. J. Orris, P. H. Stauffer, and J. W. Hendley II, "Rare Earth Elements — Critical Resources for High Technology (No. 087-02)," 2002.

[5] "Mineral Commodity Summaries 2009," *U.S. Geol. Surv.*, p. 195, 2009.

[6] "Mineral Commodity Summaries 2010," *U.S. Geol. Surv.*, p. 193, 2010.

[7] "Mineral Commodity Summaries 2011," *U.S. Geol. Surv.*, p. 198, 2011.

[8] "Mineral Commodity Summaries 2012," *U.S. Geol. Surv.*, p. 198, 2012.

[9] "Mineral Commodity Summaires 2013," *U.S. Geol. Surv.*, p. 198, 2013.

[10] "Mineral Commodity Summaries 2014," *U.S. Geol. Surv.*, p. 196, 2014.

[11] "Mineral Commodity Summaries 2015," *U.S. Geol. Surv.*, p. 196, 2015.

[12] "Mineral Commodity Summaries 2016," *U.S. Geol. Surv.*, p. 202, 2016.

[13] "Mineral Commodity Summaries 2017," *U.S. Geol. Surv.*, p. 202, 2017.

[14] "Mineral Commodity Summaries 2018," *U.S. Geol. Surv.*, p. 200, 2018.

[15] D. Mendeleev, "On the Relationship of the Properties of the Elements to their Atomic Weights," *Zeitschrift für Chemie*, vol. 12, pp. 405–406, 1869.

[16] T. R. Thalen, "Spectral Analysis of a new earth," *C. R. Acad. Sci. Paris*, vol. 88, pp. 646–647, 1879.

[17] L. F. Nilson, "On scandium, a new element," *Over.Kgl.Svensk.Vet.Akad.Forh*, vol. 36, pp. 47–51, 1879.

[18] L. F. Nilson, "On scandium, a new element," *Ber.Dtsch.Chem.Ges*, vol. 12, pp.

554–557, 1879.

[19] L. F. Nilson, “On scandium, a new element,” *C.R.Acad.Sci. Paris*, vol. 88, pp. 645–648, 1879.

[20] P. . Cleve, “On Scandium,” *C.R.Acad.Sci. Paris*, vol. 89, no. 159, pp. 419–422, 1879.

[21] L. F. Nilson, “The atomic weight and some characteristic compounds of scandium,” *Ber.Dtsch.Chem.Ges*, vol. 13, pp. 1439–1450, 1880.

[22] W. Crookes, “On Scandium,” *Proc. Roy. Soc. Lond. A*, vol. 80, no. 541, pp. 516–518, 1908.

[23] W. Crookes, “II. On Scandium,” *Phil. Trans. Roy. Soc. Lond. A*, vol. 209, no. 441–458, pp. 15–46, 1909.

[24] W. Crookes, “On Scandium - Part II,” *Proc. Roy. Soc. Lond. A*, vol. 84, no. 568, pp. 79–85, 1910.

[25] G. Eberhard, “The wide distribution of scandium on the earth,” *Sitzb. Kgl. Preuss. Akad. Wiss. Berlin*, vol. 38, pp. 851–868, 1908.

[26] A. Fowler, “The spectrum of scandium and its relation to solar spectra,” *Proc. Roy. Soc. Lond. A*, vol. 81, no. 548, pp. 335–336, 1909.

[27] E. Artini, “Two minerals from Baveno with REE weibite and bazzite,” *Atti. Acad. Lincei*, vol. 24, pp. 313–319, 1915.

[28] R. J. Meyer, “Procedure for the production of scandium or scandium compounds from minerals. German Patent 202.523 (German). CA 3:530.,” 1908.

[29] J. Schetelig, “On thortveitite, a new mineral,” *Zbl. Miner. Geol. Palöontol.*, pp. 721–726, 1911.

[30] W. Fischer, K. Brunger, and H. Grieneisen, “On the metallic scandium,” *Z.Anorg.Allgem.Chem.*, vol. 231, pp. 54–62, 1937.

[31] V. W. Klemm and H. Bommer, “To the knowledge of rare earth metals,” *Zeitschrift für Anorg. und Allg. Chemie*, vol. 231, pp. 138–171, 1937.

[32] H. Bommer and E. Hohmann, “Thermochemistry of rare earths. I. Solution heats of rare earth metals,” *Zeitschrift für Anorg. und Allg. Chemie*, vol. 248, pp. 357–372, 1941.

[33] V. K. Iya, “Methods for Preparation of Pure Scandium,” *C. R. Acad. Sci. Paris*, vol. 236, pp. 608–610, 1953.

[34] F. Petru, B. Hajek, and V. Prochazka, “Preparation of Compact Metallic Scandium,” *Chem.listy*, vol. 50, p. 2025, 1956.

[35] F. Petru, V. Prochazka, and B. Hajek, “Contribution to the Chemistry of Rare Elements . 3. Presentation of Metallic Scandium in Compact Condition,” *Collect. Czechoslov. Chem. Commnications*, vol. 23, no. 3, pp. 367–371, 1958.

[36] F. H. Spedding, A. H. Daane, G. Wakefield, and D. H. Dennison, “Preparation and Properties of High Purity Scandium Metal,” *Trans. Met. Soc. AIME*, vol. 218, pp. 608–611, 1960.

[37] K. A. Gschneider, *Rare Earth Alloys: A Critical Review of the Alloy Systems of the Rare Earth, Scandium, and Yttrium Metals*. Van Nostrand, 1961.

[38] F. H. Spedding and J. J. Croat, “Magnetic properties of high purity scandium and the effect of impurities on these properties,” *J. Chem. Phys.*, vol. 58, no. 12, pp. 5514–5526, 1973.

[39] B. Y. Kotur, “Scandium Binary and Ternary Alloy Systems and Intermetallic Compounds,” *Croat. Chem. Acta*, vol. 71, no. 3, 1998.

[40] C. T. (ed. . Horovitz, *SCANDIUM: Its Occurence, Chemistry,Physics, Metallurgy, Biology and Technology*. Academic Press, 1975.

[41] W. Wang, Y. Pranolo, and C. Y. Cheng, “Metallurgical processes for scandium recovery from various resources: A review,” *Hydrometallurgy*, vol. 108, no. 1–2, pp. 100–108, 2011.

[42] C. Dittrich, F. Diekmann, and B. Yagmurlu, “Recovery of Rare Earth Elements and Scandium from European Deposits by Solvent Extraction,” in *ALTA 2016 Uranium-REE*, 2016, no. 636876.

[43] A. I. Journal, A. Akcil, N. Akhmadiyeva, and R. Abdulvaliyev, “Overview On Extraction and Separation of Rare Earth Elements from Red Mud : Focus on Scandium Overview On Extraction and Separation of Rare Earth Elements from Red Mud : Focus on Scandium,” *Miner. Process. Extr. Metall. Rev.*, vol. 39, no. 3, pp. 145–151, 2018.

[44] C. Dittrich and B. Yağmurlu, “SCALE: An Emerging Project for European Scandium Supply,” in *ALTA 2018 Uranium-REE-Lithium*, 2018, pp. 145–150.

[45] G. M. Mudd, “Nickel Sulfide Versus Laterite: The Hard Sustainability Challenge Remains,” in *48th Conference of Metallurgists*, 2009, August 2009, pp. 1–10.

[46] K. Akira, M. Kosuke, and Y. Hiromasa, “Processes for recovering scandium from nickel-containing oxide ore,” 1999.

[47] M. Haslam and B. Arnall, “An investigation into the feasibility of extracting scandium from nickel laterite ores,” in *ALTA 1999 Nickel-Cobalt Pressure Leaching & Hydrometallurgy Forum*, 1999.

[48] N. Ricketts and W. Duyvesteyn, “The Current Status of Scandium Supply Projects and Their Technical Challenges,” in *ALTA 2017*, 2017.

[49] M. Ali, R. Önal, and Y. A. Topkaya, “Pressure acid leaching of Çaldağ lateritic nickel ore : An alternative to heap leaching,” *Hydrometallurgy*, vol. 142, pp. 98–107, 2014.

[50] Ş. Kaya, C. Dittrich, S. Srecko, and B. Friedrich, “Concentration and Separation of Scandium from Ni Laterite Ore Processing Streams,” *Metals (Basel).*, vol. 7, no. 12, pp. 557–563, 2017.

[51] V. I. Yelagin, “Alloying of Wrought Aluminum Alloys with Transition Metals,” *Metallurgiya*, 1975.

[52] L. A. Willey, “Aluminum Scandium Alloy, U.S. Patent No: 3,619,181,” 1971.

[53] V. I. Elagin, V. V. Zakharov, and T. D. Rostova, “Scandium-alloyed aluminum alloys,” *Met. Sci. Heat Treat.*, vol. 34, no. 1, pp. 37–45, 1992.

[54] V. G. Davydov, T. D. Rostova, V. V. Zakharov, Y. A. Filatov, and V. I. Yelagin, “Scientific principles of making an alloying addition of scandium to aluminium alloys,” *Mater. Sci. Eng. A*, vol. 280, no. 1, pp. 30–36, 2000.

[55] W. T. Tack, “Aluminum Scandium Alloys, U.S. Patent No:5,597,529,” 1997.

[56] F. Palm, “Making aluminum sheet alloyed with scandium and zirconium and having high fracture resistance in e.g. aerospace applications, employs roller casting process and specified hot-working, DE 10248594A1,” 2003.

[57] T. Rosenqvist, *Principles of Extractive Metallurgy*. Tapir Academic Press, 2004.

[58] A. Allanore, “Contribution of Electricity to Materials Processing : Historical

and Current Perspectives," *JOM*, vol. 65, no. 2, pp. 130–135, 2013.

[59] D. Fray, "Molten salt electrolysis for sustainable metals extraction and materials processing—A review.," in *Electrolysis: Theory, Types and Applications*, S. Kuai and J. Meng, Eds. New York: Nova Science, 2010.

[60] H. Davy, "I. The Bakerian Lecture, on some new phenomena of chemical changes produced by electricity, particularly the decomposition of the fixed Alkalies, and the exhibition of the new substances which constitute their bases; and on the general nature of alkaline," *Philos. Trans. R. Soc. London*, vol. 98, pp. 1–44, 1807.

[61] H. Davy, "XXIII. Electro-chemical researches, on the decomposition of the earths; with observations on the metals obtained from the alkaline earths, and on the amalgam procured from ammonia," *Philos. Trans. R. Soc. London*, vol. 98, pp. 333–370, 1808.

[62] M. Faraday, "VI. Experimental researches in electricity.—Sixth series," *Philos. Trans. R. Soc. London*, vol. 124, pp. 77–122, 1834.

[63] C. M. Hall, "Process of Reducing Aluminium by Electrolysis, U.S. Patent No: 400,766," 1889.

[64] P. Héroult, "Process of Preparing Aluminum Bronze and Other Alloys, U.S. patent No: 387,876," 1888.

[65] D. R. Sadoway, "Metallurgical electrochemistry: the interface between materials science and molten salt chemistry," *Mater. Sci. Forum*, vol. 73–75, pp. 555–560, 1991.

[66] X. Y. Yan and D. J. Fray, "Production of niobium powder by direct electrochemical reduction of solid Nb2O5 in a eutectic CaCl2-NaCl melt," *Metall. Mater. Trans. B Process Metall. Mater. Process. Sci.*, vol. 33, no. 5, pp. 685–693, 2002.

[67] D. J. Fray and G. Z. Chen, "Reduction of titanium and other metal oxides using electrodeoxidation," *Mater. Sci. Technol.*, vol. 20, no. 3, pp. 295–300, 2004.

[68] G. Z. Chen, E. Gordo, and D. J. Fray, "Direct electrolytic preparation of chromium powder," *Metall. Mater. Trans. B Process Metall. Mater. Process. Sci.*, vol. 35, no. 2, pp. 223–233, 2004.

[69] R. Barnett, K. T. Kilby, and D. J. Fray, "Reduction of Tantalum Pentoxide

Using Graphite and Tin-Oxide-Based Anodes via the FFC-Cambridge Process," *Metall. Mater. Trans. B Process Metall. Mater. Process. Sci.*, vol. 40, no. 2, pp. 150–157, 2009.

[70] M. Erdoğan and İ. Karakaya, "Electrochemical reduction of tungsten compounds to produce tungsten powder," *Metall. Mater. Trans. B Process Metall. Mater. Process. Sci.*, vol. 41, no. 4, pp. 798–804, 2010.

[71] E. Ergül, İ. Karakaya, and M. Erdoğan, "Electrochemical decomposition of SiO2 pellets to form silicon in molten salts," *J. Alloys Compd.*, vol. 509, no. 3, pp. 899–903, 2011.

[72] X. Y. Yan and D. J. Fray, "Electrosynthesis of NbTi and Nb3Sn superconductors from oxide precursors in CaCl2-based melts," *Adv. Funct. Mater.*, vol. 15, no. 11, pp. 1757–1761, 2005.

[73] R. Bhagat, M. Jackson, D. Inman, and R. Dashwood, "Production of Ti–W Alloys from Mixed Oxide Precursors via the FFC Cambridge Process," *J. Electrochem. Soc.*, vol. 156, no. 1, p. E1, 2008.

[74] S. Tan, T. Örs, M. K. Aydinol, T. Öztürk, and İ. Karakaya, "Synthesis of FeTi from mixed oxide precursors," *J. Alloys Compd.*, vol. 475, no. 1–2, pp. 368–372, 2009.

[75] S. Tan, K. Aydinol, T. Öztürk, and İ. Karakaya, "Direct synthesis of Mg-Ni compounds from their oxides," *J. Alloys Compd.*, vol. 504, no. 1, pp. 134–140, 2010.

[76] M. Harata, K. Yasuda, H. Yakushiji, and T. H. Okabe, "Electrochemical production of Al-Sc alloy in CaCl2-Sc2O3molten salt," *J. Alloys Compd.*, vol. 474, no. 1–2, pp. 124–130, 2009.

[77] Z. Ahmad, "The properties and application of scandium-reinforced aluminum," *Jom*, vol. 55, no. 2, pp. 35–39, 2003.

[78] I. Barin, *Thermochemical Data For Pure Substances*, 3rd Editio. VCH Publisher Inc., 1995.

[79] F. H. Spedding and A. H. Daane, "Production of Rare Earth Metals In Quantity Allows Testing of Physical Properties," *JOM*, vol. 6, no. 5, pp. 504–510, 1954.

[80] G. P. Tarcy and P. A. F. Jr., "'Method for making a light metal-rare earth metal alloy.' U.S. Patent No. 5,037,608.," 1991.

[81] M. Harata, T. Nakamura, H. Yakushiji, and T. H. Okabe, “Production of scandium and Al–Sc alloy by metallothermic reduction,” *Miner. Process. Extr. Metall.*, vol. 117, no. 2, pp. 95–99, 2008.

[82] A. Vignes, *Extractive metallurgy 3: Processing Operations and Routes*. John Wiley & Sons, 2003.

[83] A. J. Bard, L. R. Faulkner, J. Leddy, and C. G. Zoski, *Electrochemical Methods: Fundamentals and Applications*, vol. 2. 1980.

[84] K. Mohandas and D. J. Fray, “FFC Cambridge process and removal of oxygen from metal-oxygen systems by molten salt electrolysis: an overview,” *Trans.Indian Inst.Met*, vol. 57, no. 6, pp. 579–592, 2004.

[85] G. Z. Chen and D. J. Fray, “Understanding The Electro-Reduction of Metal Oxides in Molten Salts,” in *Light Metals 2004*, 2004, pp. 881–886.

[86] B. S. Hopkins and L. F. Audrieth, “The Electrolysis of Rare Earth Metal Salts in Non-Aqueous Solvents,” *Trans. Electrochem. Soc.*, vol. 66, no. 1, pp. 135–142, 1934.

[87] A. V. Suzdaltsev, A. A. Filatov, A. Y. Nikolaev, A. A. Pankratov, N. G. Molchanova, and Y. P. Zaikov, “Extraction of Scandium and Zirconium from Their Oxides during the Electrolysis of Oxide–Fluoride Melts,” *Russ. Metall.*, vol. 2018, no. 2, pp. 133–138, 2018.

[88] A. V. Rudenko, O. Y. Tkacheva, A. A. Kataev, A. A. Red’kin, and Y. P. Zaikov, “The Effect of Sc2O3 on the Physicochemical Properties of Low-Melting Cryolite Melts KF–AlF3 and KF–NaF–AlF3,” *Russ. J. Electrochem.*, vol. 54, no. 9, pp. 683–689, 2018.

[89] C. Guan, J. Xue, J. Zhu, and Q. Liu, “Preparing Aluminum-Scandium Alloys Using Direct Hall Reduction Process,” in *3rd International Symposium on High-Temperature Metallurgical Processing*, 2012, pp. 243–250.

[90] Z. Wang, C. Guan, Q. Liu, and J. Xue, “Formation of Intermetallic Phases in Al-Sc Alloys Prepared by Molten Salt Electrolysis at Elevated Temperatures.,” in *6th International Symposium on High-Temperature Metallurgical Processing*, 2015, pp. 215–222.

[91] Q. Liu, J. Xue, J. Zhu, and C. Guan, “Preparing Aluminium-Scandium Inter-Alloys During Reduction Process in KF-ALF3 -SC2O3 Melts,” in *Light Metals 2012*, 2012, pp. 685–689.

[92] G. Cacciamani *et al.*, “Thermodynamic measurements and assessment of the Al–Sc system,” *Intermetallics*, vol. 7, no. 1, pp. 101–108, 1999.

[93] K. B. Hyde, A. F. Norman, and P. B. Prangnell, “The effect of cooling rate on the morphology of primary Al3Sc intermetallic particles in Al-Sc alloys,” *Acta Mater.*, vol. 49, no. 8, pp. 1327–1337, 2001.

[94] A. Rudenko, A. Kataev, I. D. Zakiryanova, and O. Y. Tkacheva, “Co-solubility of aluminium and scandium oxides in molten sodium cryolite.,” *Tsvetnye Met.*, vol. 4, no. 11, pp. 22–26, 2017.

[95] K. Grjotheim, *Introduction to Aluminium Electrolysis: Understanding the Hall-Héroult Process*. Aluminium-Verlag, 1993.

[96] E. W. Dewing, “The Chemistry of the Alumina Reduction Cell,” *Can. Metall. Q.*, vol. 30, no. 3, pp. 153–161, 1991.

[97] H. Zhu and D. R. Sadoway, “An electroanalytical study of electrode reactions on carbon anodes during electrolytic production of aluminum,” in *Light Metals 2000*, 2000, pp. 257–263.

[98] H. Zhu and D. R. Sadoway, “Towards elimination of anode effect and PFC emissions via current shunting,” in *Light Metals 2001*, 2001, pp. 303–307.

[99] K. M. Axler and G. L. DePoorter, “Solubility studies of the Ca-CaO-CaCl2 system,” *Mater. Sci. Forum*, vol. 73, pp. 19–24, 1991.

[100] L. Sweet, S. M. Zhu, S. X. Gao, J. A. Taylor, and M. A. Easton, “The effect of iron content on the iron-containing intermetallic phases in a cast 6060 aluminum alloy,” *Metall. Mater. Trans. A Phys. Metall. Mater. Sci.*, vol. 42, no. 7, pp. 1737–1749, 2011.

[101] İ. Karakaya, “Electrochemical Determination of Thermodynamic Properties of Magnesium Cell Electrolyte - The System MgCl2-NaCl-CaCl2, PhD Thesis,” 1985.

[102] F. G. Cottrell, “Time dependence of current under diffusion control at constant potential,” *Zeitschrift für Phys. Chemie*, vol. 42, p. 358, 1903.

[103] N. Eustathopoulos, J. C. Joud, P. Desre, and J. M. Hicter, “The wetting of carbon by aluminium and aluminium alloys,” *J. Mater. Sci.*, vol. 9, no. 8, pp. 1233–1242, 1974.

[104] D. A. Weirauch and W. J. Krafick, “The Effect of Carbon on Wetting of

Aluminum Oxide by Aluminum," *Metall. Trans. A*, vol. 21, no. 6, pp. 1745–1751, 1990.

[105] J. Ye and Y. Sahai, "Interfacial behavior and coalescence of aluminum drops in molten salts. Materials Transactions, JIM, 37(2), 175-180.," *Mater. Trans. JIM*, vol. 37, no. 2, pp. 175–180, 1996.

[106] R. R. Roy and Y. Sahai, "Coalescence behaviour of aluminium alloy drops in molten salts," *Materials Transactions, JIM*, vol. 38, no. 11. pp. 995–1003, 1997.

[107] T. A. Utigard, R. R. Roy, and K. Friesen, "The Roles of Molten Salts in the Treatment of Aluminum," *Can. Metall. Q.*, vol. 40, no. 3, pp. 327–334, 2001.

[108] G. Z. Chen and D. J. Fray, "Voltammetric Studies of the Oxygen-Titanium Binary System in Molten Calcium Chloride," *J. Electrochem. Soc.*, vol. 149, no. 11, p. E455, 2002.

[109] J. B. Story and J. T. Clarke, "Electrical Conductivity of Fused Sodium Chloride-Calcium Chloride Mixtures," *JOM*, vol. 9, no. 11, pp. 1449–1454, 1957.

[110] "FACTSAGE-Collection of Phase Diagrams." [Online]. Available: http://www.crct.polymtl.ca/fact/phase_diagram.php?file=CaCl2-NaCl.jpg&dir=FTsalt. [Accessed: 10-May-2019].

[111] G. Qiu, K. Jiang, M. Ma, D. Wang, X. Jin, and G. Z. Chen, "Roles of cationic and elemental calcium in the electro-reduction of solid metal oxides in molten calcium chloride," *Zeitschrift fur Naturforsch. - Sect. A J. Phys. Sci.*, vol. 62, no. 5–6, pp. 292–302, 2007.

[112] W. D. Kaplan, "Alumina—Aluminium Interfaces," in *Interfacial Science in Ceramic Joining*, 1998, pp. 153–160.

[113] Y. Castrillejo, P. Hernández, J. A. Rodriguez, M. Vega, and E. Barrado, "Electrochemistry of scandium in the eutectic LiCl-KCl," *Electrochim. Acta*, vol. 71, pp. 166–172, 2012.

[114] Y. Castrillejo, M. R. Bermejo, and E. Barrado, "Solubilization of rare earth oxides in the eutectic LiCl–KCl mixture at 450° C and in the equimolar CaCl2-NaCl melt at 550° C.," *J. Electroanal. Chem.*, vol. 545, no. 3, pp. 141–157, 2003.

[115] A. D. Pelton, “A Complex Ion Model for Molten Halides,” *Can. Metall. Q.*, vol. 49, no. 24, pp. 3919–3934, 1971.

[116] S. N. Flengas and A. S. Kucharski, “Theory of Enthalpy of Mixing in Reactive Charge Asymmetrical Molten Salt Systems . P a r t I . Binary Solutions,” *Can. J. Chem.*, vol. 49, no. 24, pp. 3971–3985, 1971.

[117] I. Karakaya and W. T. Thompson, “A Thermodynamic Study of the System MgCl2–NaCl–CaCl2. Canadian Metallurgical Quarterly, 25(4), 307-317.,” *Can. Metall. Q.*, vol. 25, no. 4, pp. 307–317, 1986.

[118] M. M. Metallinou, L. Nalbandian, G. N. Papatheodorou, W. Voigt, and H. H. Emons, “Thermal Analysis and Raman Spectroscopic Measurements Iodide-Cesium Iodide System the Scandium,” *Inorg. Chem.*, vol. 30, no. 22, pp. 4260–4264, 1991.

[119] G. D. Zissi and G. N. Papatheodorou, “Seven-coordinated scandium (iii) chloroions in ScCl3–CsCl molten mixtures at 600–900° C,” *J. Chem. Soc. Dalt. Trans.*, vol. 13, pp. 2599–2600, 2002.

[120] A. Kononov and E. Polyakov, “Cathodic process in halide melts containing scandium,” *Electrochim. Acta*, vol. 43, no. 16–17, pp. 2537–2542, 1998.

[121] A. F. Norman, P. B. Prangnell, and R. S. McEwen, “The solidification behaviour of dilute aluminium-scandium alloys,” *Acta Mater.*, vol. 46, no. 16, pp. 5715–5732, 1998.

[122] J. Royset, “Scandium in Aluminium alloys overview: Physical Metallurgy, Properties and applications,” *Metall. Sci. andTechnology*, vol. 25, no. 2, pp. 11–21, 2007.

[123] X. Liu, J. Xue, Z. Guo, and C. Zhang, “Segregation behaviors of Sc and unique primary Al3Sc in Al-Sc alloys prepared by molten salt electrolysis,” *J. Mater. Sci. Technol.*, vol. 35, no. 7, pp. 1422–1431, 2019.

[124] Y. Castrillejo, R. Bermejo, A. M. Martínez, E. Barrado, and P. D. Arocas, “Application of electrochemical techniques in pyrochemical processes – Electrochemical behaviour of rare earths at W , Cd , Bi and Al electrodes,” *J. Nucl. Mater.*, vol. 360, no. 1, pp. 32–42, 2007.

[125] Y. Castrillejo, A. Vega, M. Vega, P. Hernández, J. A. Rodriguez, and E. Barrado, “Electrochemical formation of Sc-Al intermetallic compounds in the eutectic LiCl-KCl. Determination of thermodynamic properties.,” *Electrochim.*

Acta, vol. 118, pp. 58–66, 2014.

[126] "FACTSAGE." [Online]. Available: http://www.crct.polymtl.ca/fact/. [Accessed: 10-May-2019].

[127] C. W. Bale *et al.*, "FactSage thermochemical software and databases," *Calphad*, vol. 26, no. 2, pp. 189–228, 2002.